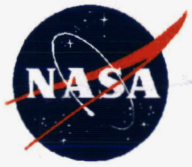

JPL Publication 05-9

SATURN RADIATION (SATRAD) MODEL

H. B. Garrett
J. M. Ratliff
Jet Propulsion Laboratory, California Institute of Technology
Pasadena, California

R. W. Evans
Gibbel Corp.
Montrose, California

National Aeronautics and Space Administration

Jet Propulsion Laboratory
California Institute of Technology
Pasadena, California

October 2005

JPL Publication 05-9

SATURN RADIATION (SATRAD) MODEL

H. B. Garrett
J. M. Ratliff
Jet Propulsion Laboratory, California Institute of Technology
Pasadena, California

R. W. Evans
Gibbel Corp.
Montrose, California

National Aeronautics and Space Administration

Jet Propulsion Laboratory
California Institute of Technology
Pasadena, California

October 2005

This research was carried out at the Jet Propulsion Laboratory, California Institute of Technology, under a contract with the National Aeronautics and Space Administration.

ABSTRACT

The Saturnian radiation belts have not received as much attention as the Jovian radiation belts because they are not nearly as intense—the famous Saturnian particle rings tend to deplete the belts near where their peak would occur. As a result, there has not been a systematic development of engineering models of the Saturnian radiation environment for mission design. A primary exception is that of Divine (1990). That study used published data from several charged particle experiments aboard the Pioneer 11, Voyager 1, and Voyager 2 spacecraft during their flybys at Saturn to generate numerical models for the electron and proton radiation belts between 2.3 and 13 Saturn radii. The Divine Saturn radiation model described the electron distributions at energies between 0.04 and 10 MeV and the proton distributions at energies between 0.14 and 80 MeV. The model was intended to predict particle intensity, flux, and fluence for the Cassini orbiter. Divine carried out hand calculations using the model but never formally developed a computer program that could be used for general mission analyses. This report seeks to fill that void by formally developing a FORTRAN version of the model that can be used as a computer design tool for missions to Saturn that require estimates of the radiation environment around the planet. The results of that effort and the program listings are presented here along with comparisons with the original estimates carried out by Divine. In addition, Pioneer and Voyager data were scanned in from the original references and compared with the FORTRAN model's predictions. The results were statistically analyzed in a manner consistent with Divine's approach to provide estimates of the ability of the model to reproduce the original data. Results of a formal review of the model by a panel of experts are also presented. Their recommendations for further tests, analyses, and extensions to the model are discussed

KEY WORDS: Saturn, Radiation Models, Radiation Belts, Cassini Spacecraft, High Energy Electrons, Trapped Particles, Space Radiation

EXECUTIVE SUMMARY

The primary objective of the Prometheus Saturnian Radiation Modeling task was to develop engineering models of the radiation environment near Saturn based on data from Pioneer 11 and from Voyagers 1 and 2 so that Prometheus mission planners could estimate the degree of radiation exposure for missions to the Saturnian system. This was accomplished by collecting and reviewing available high-energy electron and proton data relevant to the Saturnian system as originally done by Divine [1]. In that original study, Divine constructed models of the electron and proton fluxes as functions of pitch angle (α), magnetic field at the position (B), and magnetic field line passing through the location (L-shell). The current effort entailed encoding Divine's original algorithms and developing methods for estimating the Saturnian magnetic field components (B and L) needed to estimate the fluxes along a spacecraft trajectory. While originally used as an engineering tool to model Cassini spacecraft doses during its design, the current model implementation (called SATRAD) was used to estimate the doses for Prometheus missions to Saturn and will be used to compare with the Cassini measurements. To validate the SATRAD model, its fluxes have been compared by the authors to published Pioneer and Voyager data in the same manner as Divine. Those comparisons have been used to estimate the "accuracy" of the SATRAD model by calculating an "error range." Within the limits of the current study, the original estimates of Divine have been validated (e.g., to a factor of 2-3) and are well within current expectations for radiation modeling tools.

To independently validate the model and at the request of the Prometheus Program, a review was carried out by experts in the area of Saturnian magnetospheric modeling on 18 March 2005 to determine how well the model performs. While the Review Board found the model to be a useful baseline, the members provided a range of suggestions on how the model could be improved in the future. The Review Board comments on the model can be roughly divided into 4 groups:

1) Pioneer and Voyager particle data:
   a) Need to evaluate using data in the Planetary Data System (PDS).
   b) Need to re-evaluate detector background sources and calibrations in the light of current understanding of the instruments.
   c) Pioneer and Voyager data still of value because they cover energy ranges and locations not covered by Cassini.
   d) Potentially important local time (relative to Sun) and real-time "weather" variations are difficult to separate using only the Pioneer and Voyager data.
   e) Species identification requires more careful consideration—ions versus electrons; protons versus oxygen ions; etc.
   f) Some spurious features in model.
   g) Pitch angle distributions need to be reconsidered and a more flexible fitting scheme employed.

2) Cassini data:
   a) Need to incorporate latest Cassini data when it becomes available. Unfortunately, only data from the Saturn Orbit Insertion (SOI) orbit may be useful for critical pitch angle information as instruments may now be "stuck" in one position.

b) Cassini found an inner belt (see Figure 14) in a region that was previously unexplored, and thus not included in the model.

3) Magnetic Field:
   a) Uncertainties in magnetic field make field line tracing difficult as the field approaches 0 at ~10 Saturn radii (R_s)—magnetic field models of Saturn are still being developed.
   b) There are potentially important local-time (relative to Sun) and real-time ("space weather") variations that are difficult to separate in the data.
   c) Cassini found a 6 minute slowdown in Saturn rotation and a highly variable magnetic field in comparison to Pioneer and Voyager observations.
   d) Future magnetic field models will need to include effects of magnetopause and ring current in magnetic field model in outer magnetosphere (~10 R_s).

4) Overall model package:
   a) Need to standardize and have peer reviewed in literature.
   b) Recommend making code/engineering model available for Cassini and other programs outside JPL.

By way of summary, the Review Board found several areas that should be considered in both using the model and in updating it. These range from calibration/background issues with the original Pioneer and Voyager data to very real concerns over the apparent variability of the Saturnian magnetosphere. The reviewers stated that Cassini data should allow improvements in the SATRAD magnetic field model and flux estimates and should be actively pursued. Finally, the reviewers requested copies of the model for comparisons with the Cassini data and recommended that the model be standardized, made more readily available, and formally reviewed in the literature as soon as possible.

TABLE OF CONTENTS

FIGURES

TABLES

SATURN RADIATION (SATRAD) MODEL

H. B. Garrett,[a] J. M. Ratliff,[a] and R. W. Evans[b]

[a]*Jet Propulsion Laboratory, California Institute of Technology, 4800 Oak Grove Drive, Pasadena, California 91109*
[b]*Gibbel Corp., 2550 Honolulu Blvd., Montrose, California 91020*

INTRODUCTION

The SATRAD computer model of the Saturnian radiation environment is based on earlier work by Divine [1], who examined data from Pioneer 11 and from Voyagers 1 and 2, and used those data to develop an engineering model of the electron and proton fluxes over limited energy ranges between ~2 to 10 R_S (1 R_S = 1 Saturnian radius). In the present work, the "Divine model" has been used as a baseline for further development of the model and for implementing it into a formal computer code that can be used as a numerical tool for engineering calculations of the high-energy particle environment. The SATRAD model consists of two components: the original Divine formulation, which gives the electron and proton particle fluxes in terms of the so-called B-L coordinate system, and a second component which provides the magnetic field model used in determining the B-L coordinates necessary for evaluating the model fluxes. To demonstrate potential applications of the tool, Fig. 1 illustrates a mission dose/depth analysis prepared in support of a Prometheus Saturn mission study. Fig. 2 compares radiation estimates for Saturn with similar orbits at Jupiter. To evaluate the predictions of the tool, Pioneer and Voyager in situ data at Saturn have been digitized from original data plots for comparison with the model. Because much of those data are in count rates, count-rate-to-flux conversions were also developed. As an illustration of the process, Fig. 3 presents comparisons between Voyager data and the model. The agreement is quite good for these energies but other energy channels do not compare as well, implying that there are uncertainties in the Saturnian data (see later discussion and appendices). To independently evaluate the models and at the request of the Prometheus Project, a Review Board was asked to review the different model components, the validity of the data used to develop the model, and the ability of the model to predict the actual environment. This report details the materials presented to the Review Board and the Review Board findings relative to the overall SATRAD model. Finally, as requested by the Review Board, the SATRAD FORTRAN model listings are provided for use by the space science community.

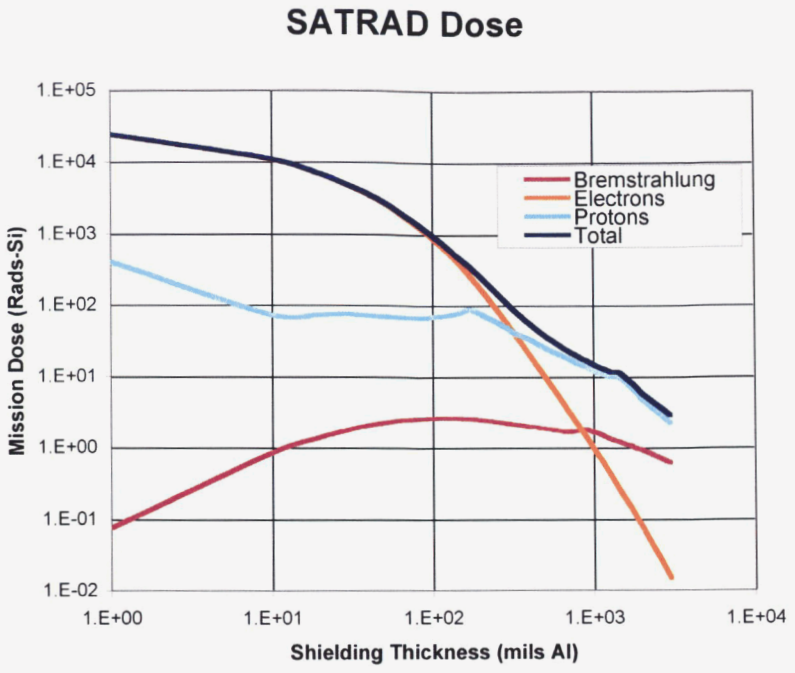

Fig. 1. Estimate of the dose for a potential Prometheus Saturn Moon Mission. The full Saturnian magnetic field was used in tracing the magnetic field lines.

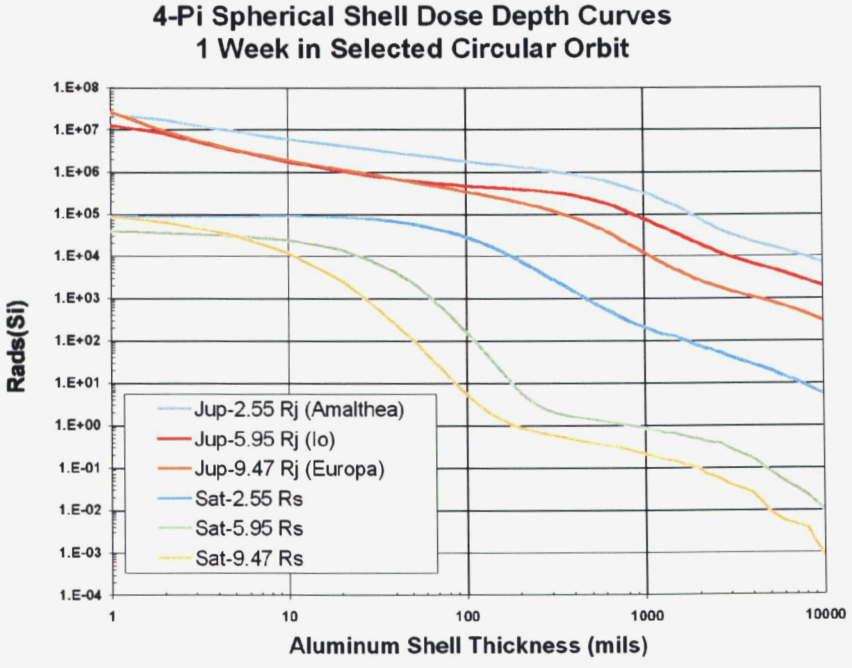

Fig. 2. Jovian and Saturnian radiation environments for a 1 week exposure. Distances are at 2.55 R, 5.95 R, and 9.47 R where R is one planetary radius (R_j = Jovian radii, R_s = Saturnian radii). Distances correspond to orbits of Amalthea, Io, and Europa at Jupiter. Dose in rad(Si) for 4π aluminum spherical shell.

(A)

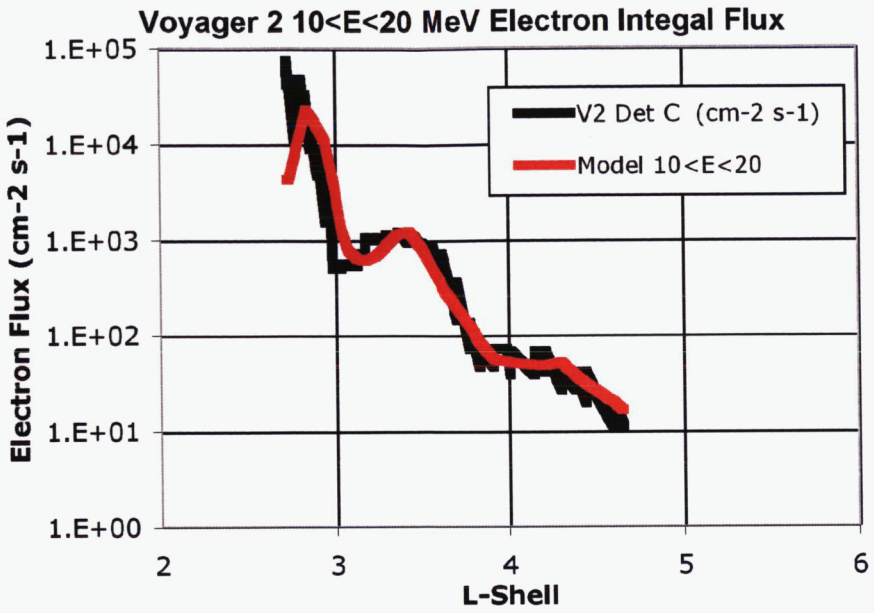

(B)

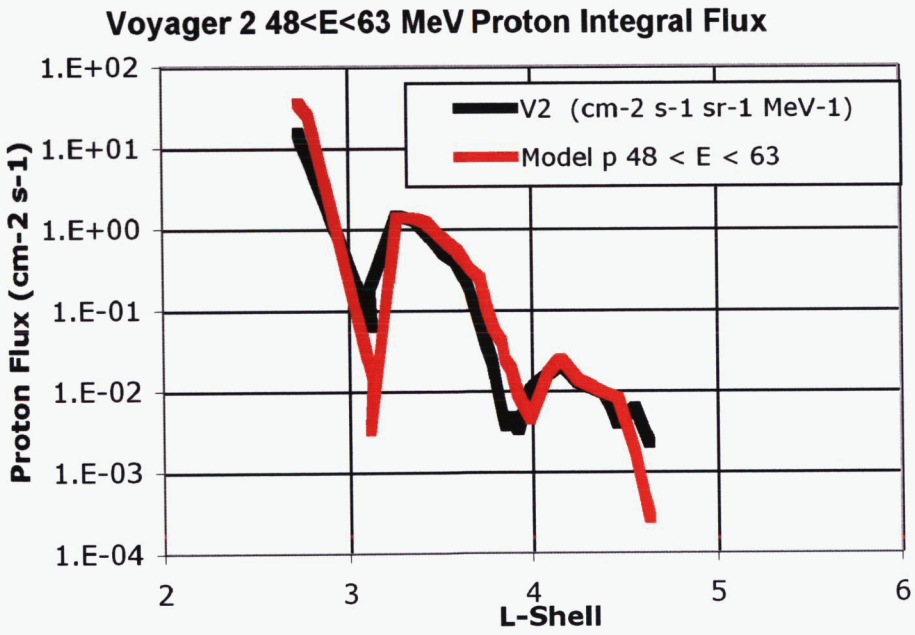

Fig. 3. Comparisons between the Saturn model and data from Voyager 2 fly-bys for (A) 10<E<20 MeV electron integral flux and (B) 48<E<63 MeV proton integral flux.

SATURN RADIATION MODEL DEVELOPMENT

THE DIVINE RADIATION MODEL

As a means for describing the development of the SATRAD model, the original particle model as discussed in Ref. 1 (N. Divine, JPL IOM-5217-90-029, Numerical Models for Electron and Proton Distributions in Saturn's Radiation Belts, 28 February 1990) will first be reviewed. Specifically, Ref. 1 is reviewed from the standpoint of Divine's original Saturn radiation modeling process and his methods for estimating residuals between the observations and the model predictions. To start, Divine's Saturn radiation model assumes these independent variables:

B = Magnetic Field strength (gauss)
L = L-shell [2.3<L<13.0]
α = pitch angle
E = Energy (MeV) [0.04<E_e<10 MeV; 0.14<E_p<80 MeV]

The following dependent variables are then estimated:

I = Integral Intensity ($cm^{-2}\ s^{-1}\ sr^{-1}$)
i = Differential Intensity ($cm^{-2}\ s^{-1}\ sr^{-1}\ MeV^{-1}$)

The algebraic form of the model to predict these variables becomes, in terms of the dependence of I on E,

$$\log I = A_0 - A_1 \log E + \left(\frac{A_1 - A_2}{2}\right)\log\left(\frac{E^2 + E_2^2}{1 + E_2^2}\right) + \left(\frac{A_2 - A_3}{3}\right)\log\left(\frac{E^3 + E_3^3}{1 + E_3^3}\right) \quad (1)$$

and

$$i = \frac{dI}{dE} = \frac{I}{E}\left[A_1 + \frac{A_2 - A_1}{1 + (E_2/E)^2} + \frac{A_3 - A_2}{1 + (E_3/E)^3}\right] \quad (2)$$

Dependence of I and i on α and B is given by:

$$A_n = \frac{B_e}{B}(\sin\alpha)^2(a_n - b_n) + b_n \quad (3)$$

where

n = 0, 1, 2, and 3
B_e = Magnetic Field strength at Magnetic Equator (gauss)
a_n, b_n, E_2, and E_3 are tabulated at selected values of L—they are to be linearly interpolated between the specified L values

Values for the various constants are presented in Tables 1 and 2 as taken from Divine (Ref. 1). The data and companion references that these parameters were derived from are listed in Appendices I, II, and III. Sample output from the model, namely the omnidirectional electron and proton fluxes at the equator and at high latitudes, are plotted in Figure 4. Also listed is the Saturnian magnetic field model assumed by Divine.

Table 1. Parameter values for the Saturn electron model (Divine, Ref. 1)

L	a_0	a_1	a_2	a_3	b_0	b_1	b_2	b_3	E_2	E_3
2.30	4.74	0.00	0.00	6.47	4.74	0.00	0.00	6.47	0.60	1.50
2.33	5.02	0.00	0.00	4.01	5.02	0.00	0.00	4.01	0.60	1.50
2.34	4.91	0.00	0.00	4.86	4.91	0.00	0.00	4.86	0.60	1.50
2.36	4.98	0.00	0.00	4.41	4.98	0.00	0.00	4.41	0.60	1.50
2.38	5.00	0.00	0.00	5.37	5.00	0.00	0.00	5.37	0.60	1.50
2.46	5.49	0.00	0.23	3.00	5.49	0.00	0.23	3.00	0.60	2.00
2.56	5.56	0.00	0.34	3.00	5.56	0.00	0.34	3.00	0.60	2.00
2.70	5.51	0.00	0.27	4.48	5.51	0.00	0.27	4.48	0.60	2.00
2.83	5.52	0.00	0.25	3.11	5.52	0.00	0.25	3.11	0.20	2.00
2.93	5.46	0.00	0.28	3.42	5.46	0.00	0.28	3.42	0.20	2.00
3.04	5.38	0.00	0.27	4.96	5.38	0.00	0.27	4.96	0.20	2.00
3.08	5.31	0.00	0.29	5.23	5.48	0.00	0.29	5.23	0.20	2.00
3.20	5.03	0.00	0.20	5.48	5.74	0.00	0.20	5.48	0.20	2.00
3.40	5.50	0.00	0.00	4.27	4.90	0.00	0.61	4.27	0.20	2.00
3.90	4.88	0.00	0.20	5.71	4.72	0.21	0.78	5.71	0.20	2.00
4.30	4.67	0.00	0.00	4.29	4.50	0.00	0.56	4.29	0.10	1.00
4.44	4.74	0.00	0.00	4.23	4.12	0.00	0.68	4.23	0.10	1.00
4.96	3.58	0.00	0.34	5.74	5.30	0.00	0.11	5.74	0.10	1.00
5.41	3.50	0.00	0.27	5.26	5.38	0.00	0.11	5.26	0.10	1.00
5.87	4.57	0.00	0.05	6.67	3.73	1.01	0.68	6.67	0.10	1.00
6.20	3.26	0.00	0.00	4.22	4.60	0.26	0.00	4.22	0.08	0.50
6.50	3.95	0.00	0.06	3.00	4.83	0.00	0.19	3.00	0.08	0.50
7.20	3.33	0.00	0.00	6.10	3.20	0.21	0.66	6.10	0.08	0.50
8.00	3.42	0.00	0.00	5.50	2.56	0.16	2.45	5.50	0.08	0.50
9.50	3.02	0.00	0.83	6.00	2.11	0.00	2.22	6.00	0.08	0.50
11.00	3.64	0.00	1.17	3.01	1.98	0.00	3.78	3.01	0.08	0.50
13.00	2.09	2.23	0.00	7.59	2.09	2.23	0.00	7.59	0.08	0.50

Table 2. Parameter values for the Saturn proton model (Divine, Ref. 1)

L	a_0	a_1	a_2	a_3	b_0	b_1	b_2	b_3	E_2	E_3
2.30	1.86	0.00	0.00	4.57	1.86	0.00	0.00	4.57	1.00	60.00
2.32	2.07	0.00	0.00	4.53	2.07	0.00	0.00	4.53	1.00	60.00
2.34	2.17	0.00	0.00	6.09	2.17	0.00	0.00	6.09	1.00	60.00
2.43	3.18	0.05	0.00	3.05	3.18	0.05	0.00	3.05	1.00	60.00
2.52	2.14	1.85	0.00	3.00	2.14	1.85	0.00	3.00	1.00	60.00
2.67	3.80	0.75	0.00	3.00	3.80	0.75	0.00	3.00	1.00	60.00
2.77	3.37	1.28	0.00	3.00	3.37	1.28	0.00	3.00	0.50	60.00
2.82	3.26	2.63	0.00	3.00	3.26	2.63	0.00	3.00	0.30	60.00
2.86	3.14	2.93	0.00	3.00	3.14	2.93	0.00	3.00	0.30	60.00
3.10	0.37	0.00	0.00	3.00	0.67	4.87	6.27	3.00	1.00	60.00
3.20	2.91	0.29	0.00	3.00	-0.25	6.63	0.00	3.00	1.00	60.00
3.31	2.86	0.02	0.02	3.00	0.29	8.30	0.00	3.00	0.50	60.00
3.44	2.80	0.98	0.00	3.00	0.46	7.41	0.00	3.00	0.50	60.00
3.71	2.16	1.77	0.00	3.00	0.40	7.10	0.00	3.00	0.50	60.00
3.99	-0.13	0.00	0.26	3.00	0.58	7.70	0.52	3.00	0.50	60.00
4.13	1.29	0.00	0.00	3.00	-0.10	9.00	0.15	3.00	0.50	60.00
4.27	0.63	0.46	0.29	3.22	0.16	8.55	0.00	3.22	0.50	60.00
4.38	0.61	5.05	0.20	3.12	-0.03	6.93	0.00	3.12	0.50	60.00
4.49	0.47	5.25	0.21	3.55	-0.06	7.15	0.00	3.55	0.50	60.00
5.01	0.68	1.45	0.00	4.41	-1.13	6.73	6.85	4.41	0.50	0.80
5.36	1.77	0.00	0.00	3.00	-0.98	6.78	8.25	3.00	0.50	0.80
6.20	2.32	3.32	0.00	3.08	0.10	5.51	2.99	3.08	0.50	0.80
6.45	2.40	3.34	0.00	3.00	0.06	5.81	2.66	3.00	0.50	0.80
6.70	2.46	2.59	0.52	4.72	0.30	5.83	0.12	4.72	0.50	0.80
7.63	2.46	3.55	0.25	3.85	0.81	4.90	0.61	3.85	0.50	0.80
8.40	2.31	6.28	1.73	3.35	1.07	0.48	1.73	3.35	0.30	0.80
10.30	1.90	6.52	1.81	4.11	0.74	0.00	0.85	4.11	0.30	0.80
12.00	1.24	0.00	6.35	3.94	1.24	0.00	6.35	3.94	0.30	0.80
13.00	1.22	0.00	6.72	3.31	1.22	0.00	6.72	3.31	0.30	0.80

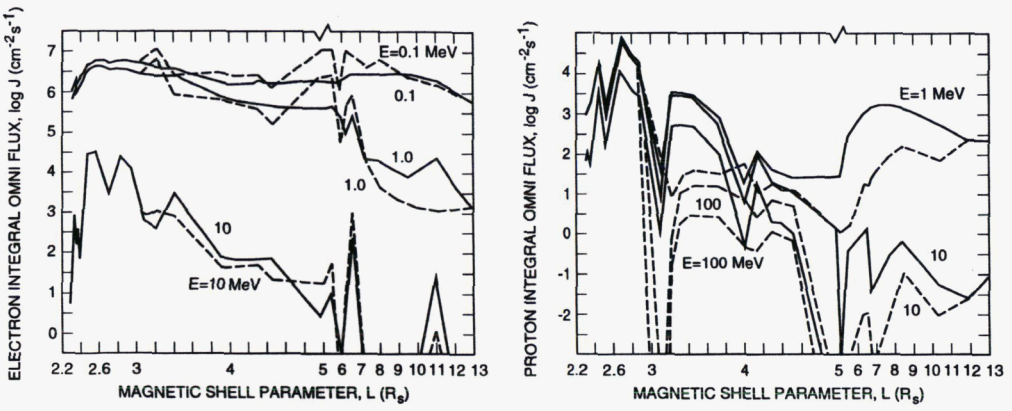

QUANTITY	VALUE	SOURCE
Radius	R_S=6.033×10⁷ m	CO84, p. 354
Gravitation	GM_S=3.794×10¹⁶ m³/s²	CE89
Rotation	ω=810.76 deg/day	CO84, p. 360
Magnetic field coefficients	g_1^1=0.21535 G	CO84,p. 363, Table II
	g_2^1=0.01642 G	
	g_3^1=0.02743 G	
	G_1^1=-0.0001 G	
	G_1^1=-0.00001 G	

Fig. 4. Basic representation of Divine's Saturn model illustrating the electron and proton omnidirectional fluxes and the magnetic field model.

DIVINE'S CALCULATIONS OF RESIDUALS METHODOLOGY

A critical step in the Divine model is determining how well it fits the data. Unfortunately this is not a straightforward step as the statistical distribution of the data is not well defined. Here we review the method used by Divine which assumes an approximate log-normal distribution for the fluxes. For each trio of data (observation R_D, model R_M, background R_B), he computed the following quantities Δ and Z:

$$\Delta = min[0, log(R_B/R_M)] \quad \text{for } R_D<R_B \qquad (4)$$
$$= log(R_D/R_M) \quad \text{for } R_D>R_B$$

and

$$Z = \Delta^2 \quad \text{for } |\Delta|\leq\Delta_0$$
$$= \Delta_o^2[2-(\Delta_0/\Delta)^2] \quad \text{for } |\Delta|\geq\Delta_0 \qquad (5)$$

Δ_0 was assumed to be 0.3 (giving a factor of ~2 in the ratio of data to model). He then computed Y, a modified root-mean-square (RMS) residual, using the weighting factor W:

$$Y = [(\Sigma WZ)/(\Sigma W)]^{1/2} \qquad (6)$$

W is a weighting value, normally assumed to be 1. The model is iterated until Y achieves a minimum value for the assumed database. This process was reviewed by the Board, and an alternative will be presented (see below).

LATITUDE AND FLUX VERSUS ENERGY VARIATIONS

In addition to the electron and proton omnidirectional fluxes, the model also provides the particle pitch-angle variations—that is, how the particle distributions change with angle relative to the magnetic field. As will be discussed shortly, the pitch-angle distributions assumed by Divine are very simple and may not adequately fit the observed distributions. Samples are provided in Figures 5 and 6 in the form of variations with magnetic field at the location divided into the magnetic field at the equator for that magnetic field line (for a location at the magnetic equator, $B = B_e$, so the ratio is unity; at high latitudes, $B >> B_e$, so the ratio is ~zero). These variations reflect the pitch-angle behavior of the model.

Particle flux variations with energy for the electrons and protons are presented in Figure 7 for various L-shell distances (L-shell is approximately the distance in Saturnian radii along its equator). As these are integral values, the observation that the flux is approximately constant from about 1 to 10 MeV for the protons implies that the model assumes little flux between these energies.

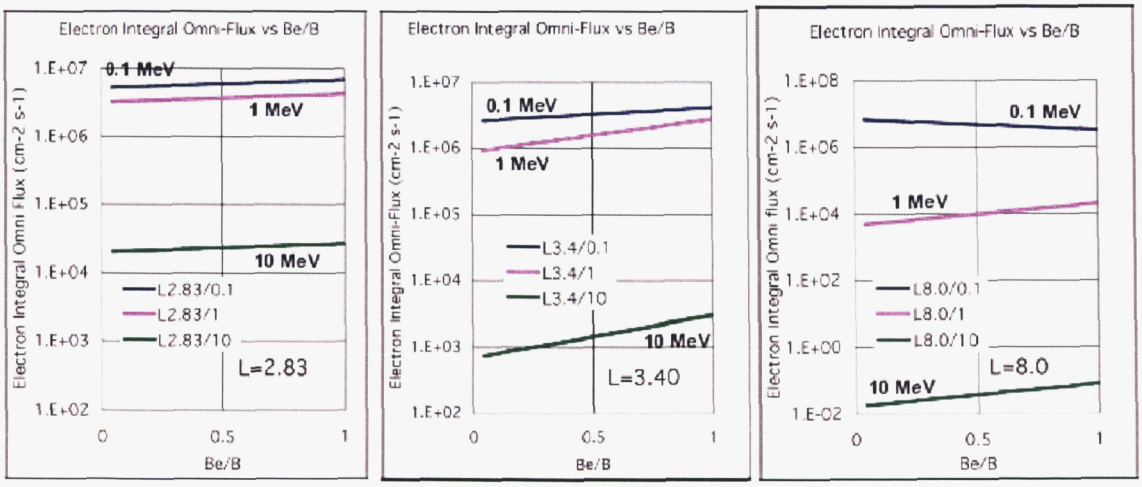

Fig. 5. Latitude variations of the electron omnidirectional integral flux predicted by the Divine model in terms of the ratio of the equatorial magnetic field to the observed magnetic field.

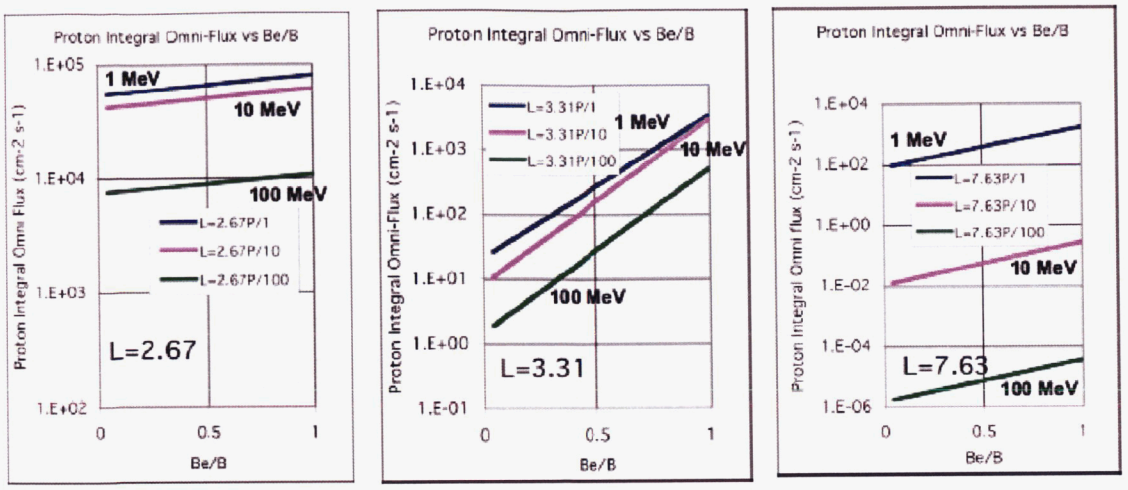

Fig. 6. Latitude variations of the proton omnidirectional integral flux predicted by the Divine model in terms of the ratio of the equatorial magnetic field to the observed magnetic field.

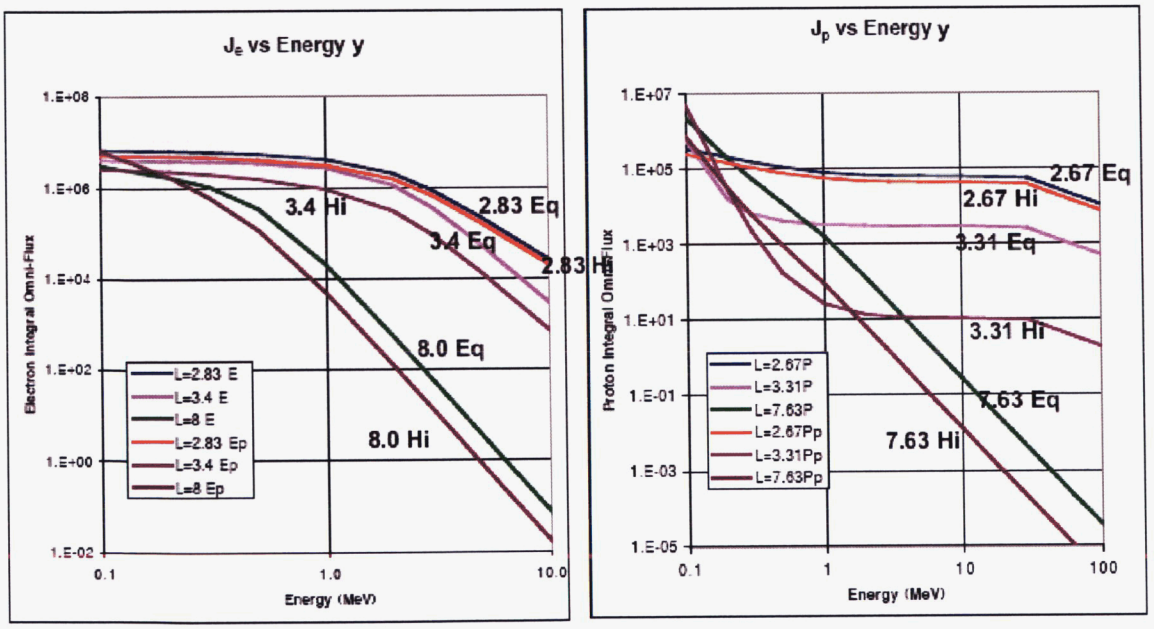

Fig. 7. Energy variations of the electron and proton omnidirectional integral fluxes predicted by the Divine model for various L-shell values at equatorial and high latitudes.

STEP #1: THE MAGNETIC FIELD AND L-SHELL MODEL

In order to implement Divine's algorithms, the B and L coordinates of the location must first be provided. As described by R.W. Evans,[1] the determination of the (B,L) coordinates can be quite complicated. We have, however, reduced it to a 3 step process. First, we define the multipole expansion of the magnetic field and compute the field vector and |B| at selected points. This can be quite involved depending on the formulation. Table 3 lists the magnetic field components for some of the Saturnian models considered. The second step is to trace the field line and integrate the quantity I along the field line using the magnetic field model (Ref. 2, Roederer, 1970, Eq. 2.38; see also Eq. 4.20):

$$I = \int_{s(B_{m0})}^{s(B_{m1})} \sqrt{1 - B(s)/B_m}\, ds \tag{7}$$

The third step requires inverting the I integral to get L corresponding to the point of interest. This is given by the following formula from Roederer (Eq. 4.21):

$$\frac{L^3 R^3 B_m}{k_0} = F\left(\frac{I^3 B_m}{k_0}\right) \tag{8}$$

Typical results in the form of various L-shell tracings are plotted in Figure 8 for several different magnetic field models. It should be noted that in several of the magnetic field models, when external field components are included, the magnetic field can go to zero or even reverse between 10 to 11 R_s, causing the field line tracing program to break down. This is a major problem for the radiation model outside ~10 R_s. Divine used the SZ3 magnetic model (see below) for which L-shells can successfully be traced beyond L = 10 R_s.

[1] JPL Interoffice Memorandum-5132-04-006, "Planetary Magnetic Field Models for Jupiter, Saturn, Uranus, and Neptune; with Field Line Tracing Algorithms (Computer Codes)," January 22, 2004 (JPL internal document).

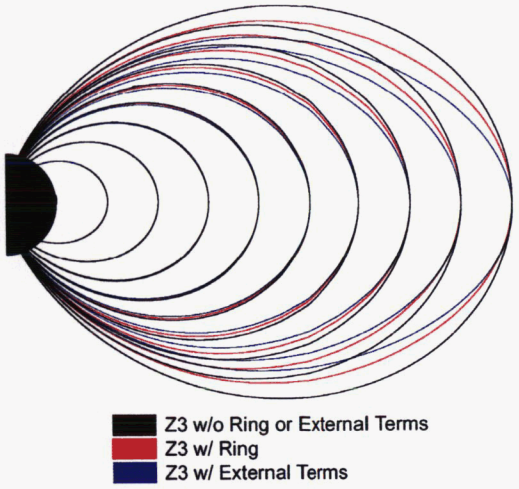

Fig. 8. Magnetic field lines (L-shell contours) for 3 Saturn magnetic field models. Field lines are drawn such that they meet at the equator; the lines do NOT represent the same L value for all three lines. (see Table 3 for the components for each model).

The models have been used to estimate the B and L values for the Pioneer and Voyager flyby trajectories. These are plotted in B-L space in Figure 9. Besides the observation that the field goes to ~0 near 10 R_s, it appears from these flybys and from the recent Cassini data that the Saturnian magnetic field varies in both UT and Local Time. The Saturnian rotation rate has also apparently varied between Pioneer and Voyager and Cassini (~6 minutes longer now). Further, the Saturnian field has been difficult to represent accurately and has several different representations: Internal, Internal + External, or Internal + Ring (we favor Internal + Ring for following field lines) and it is (as of this date) not clear which is correct.

Table 3. Magnetic field coefficients for various models of the Saturn magnetic field. (See legend below for abbreviations and acronyms.)

Coeff	SZ3	Z3e	SP1	SP2	SWE	Z3R		Coeff	Ring
g_1^0	0.21535	0.21535	0.21160	0.21160	0.21160	0.21535		a	8.0
g_2^0	0.01642	0.01642	0.01560	0.01560	0.01560	0.01642		b	15.5
g_3^0	0.02743	0.02743	0.02320	0.02320	0.02320	0.02743		D	3.0
G_1^0		-0.00010	-0.000075	-0.00012	-0.00010			$\mu_0 I_0$	10*
G_1^1		-0.00001			-0.00001				

Legend
SZ3: Saturn Zonal Harmonic model 3rd Order
Z3e: Saturn Zonal Harmonic model with 3rd Order_External Terms
SP1: Saturn (Parallel to Earth Sun Line) Voyager model 1
SP2: Saturn (Perpendicular to Earth Sun Line) Voyager model 2
SWE: SP1 or 2 with Z3e External Terms
Z3R: Z3 with Ring
G_m^n and g_m^n are coefficients of zonal spherical harmonic functions.
The ring model is that of Connerney (Ref. 3).

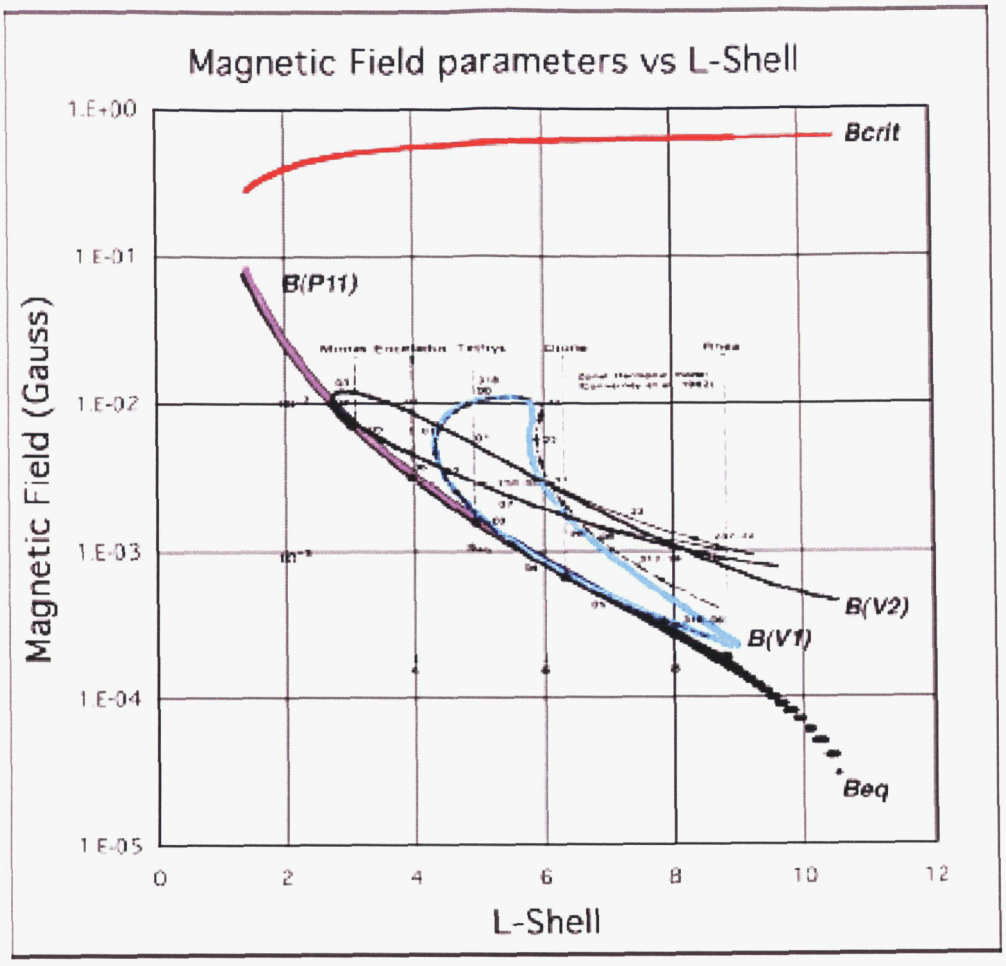

Fig. 9. Trajectories for the Saturn flybys in magnetic coordinates. Note that Pioneer 11 closely follows the $|B_{eq}|$ contour in to L = 1.43.

STEP #2: (B,L) FLUX MODEL IMPLEMENTATION

The next step in developing the SATRAD model[2] is to implement the model in FORTRAN. The process is as follows:

1: Look up the coefficients (a_n, b_n, E_2, and E_3) at discrete L values—linearly interpolate to get values at a specific L-shell

2: Calculate the A_n's as functions of B, B_e, and pitch angle α

3: Calculate $I(\alpha,E)$ and $i(\alpha,E)$ at (B,L) for the A_n's and E_2, E_3

[2] H. B. Garrett, Jet Propulsion Laboratory Interoffice Memorandum 5130-04-007, "Draft version of the Divine Saturn radiation model code," April 6, 2004 (JPL internal document).

4: Integrate between the pitch angle α's corresponding to B_m and $B_{crit}(L)$ at the specified position to get the omnidirectional flux.

The results of the FORTRAN implementation (in color) are overlayed on Divine's original estimates in Figures 10 and 11. Note that there are slight differences for the high-latitude components, as we computed the values at the actual B_{crit} location rather than at the extreme value $B_e/B=0$ assumed by Divine.

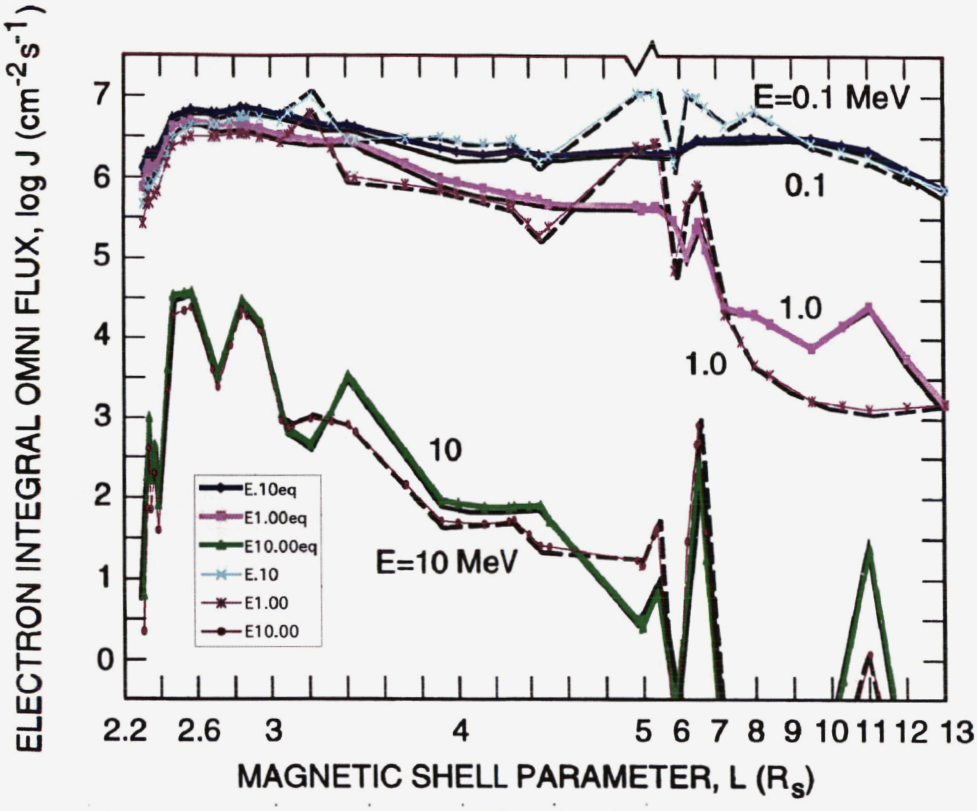

Fig. 10. The FORTRAN modeled omnidirectional fluxes for electrons (solid, colored curves) as functions of L for various energies overlaid with Divine's original hand-calculated estimates. For the hand-calculations, solid lines correspond to the equator and dashed lines to high latitudes-see Fig. 4.

To test the SATRAD model, it was next used to plot integral flux contours for the electrons and protons at 1 MeV and 10 MeV, respectively, in Figure 12. Note the complex, multiple belts that appear.

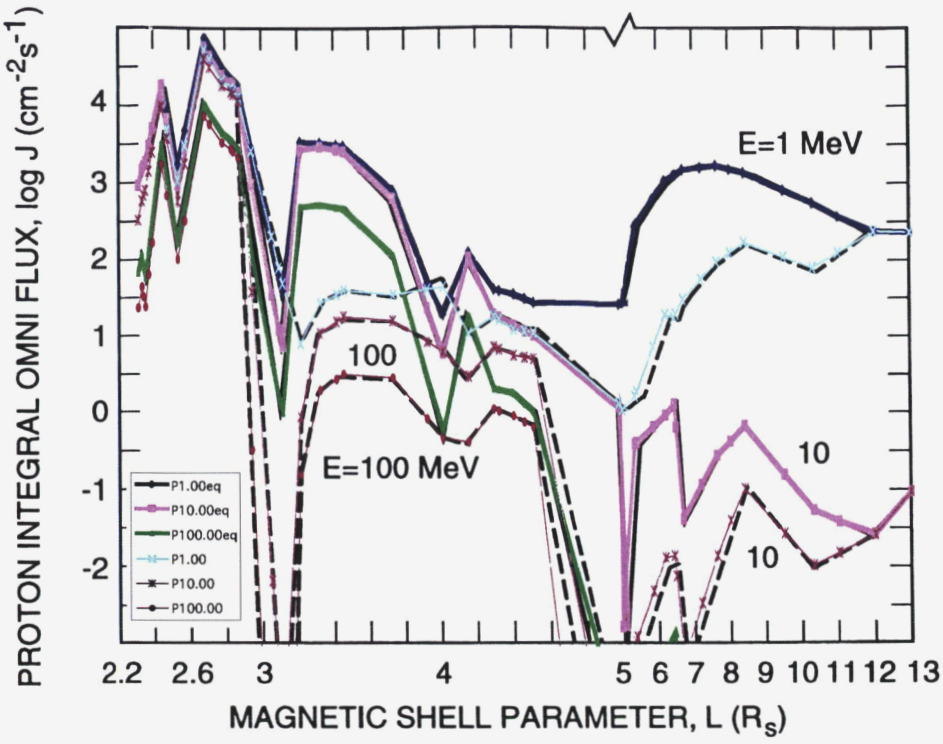

Fig. 11. The FORTRAN modeled omnidirectional fluxes for protons (solid, colored curves) as functions of L for various energies overlaid with Divine's original hand-calculations. For the hand-calculations, solid lines correspond to the equator and dashed lines to high latitudes-see Fig. 4.

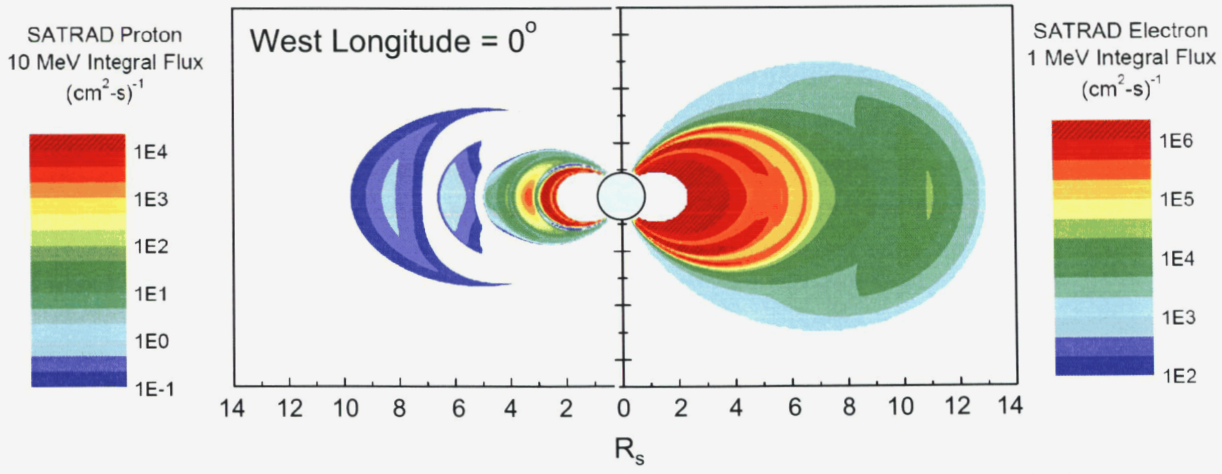

Fig. 12. Integral flux contours for the electrons and protons at 1 MeV and 10 MeV, respectively, based on the SATRAD computer model (courtesy of I. Jun, JPL).

STEP #3: COMPARISONS WITH P11, V1, V2 DATA

The final step in the SATRAD model development and its review was to compare it with the actual data. This is accomplished by computing the residuals between the observations and the data. The data sources and instruments and their energy ranges for each spacecraft employed in this study are listed in Table 4. The references are listed in

the appendices along with additional data references used by Divine. Comparison plots for the scanned data and the model predictions are also presented in the appendices (note: the data sources used in Divine's original study are discussed in Ref. 1, which is included in the appendices as well).

Table 4. References, spacecraft, instruments, and energy ranges used in evaluating the SATRAD model.

		Electrons	(MeV)			Protons	(MeV)
REF	S/C	Instrument	Energy Range	REF	S/C	Instrument	Energy Range
VA84	V02	LECP	0.252-0.48	BC80	P11	CPT	.5-1.8
PD04	V02	LECP	>0.48	VA84	P11	GTT	0.6-3.41
VA84	V02	LECP	0.48-.853	CS80	P11	CPT-FCD	>35
VA84	P11	GTT	>0.56	SM83	V02	CRS	48-63
VA84	V02	LECP	0.853-1.2	KR82	V02	LECP	54-87
KR82	V02	LECP	>1.5	SM83	V02	CRS	63-160
SB03	V02	LECP	>3.24	VA80b	P11	GTT	>80
BC80	P11	CPT-ECD	>3.4	CS80	P11	LET	>80
BC80	P11	CPT-MT	7-17	FM80	P11	TRD M3	>80
KR82	V02	LECP	10-20				

Acronyms:
CPT: Charged Particle Telescope (APL)
-ECD Electron Current Detector
-MT Main Telescope
-FCD Fission Cell Detector
CRS: Cosmic Ray Subsystem
GTT: Geiger Tube Telescope (U of Chicago)
LECP: Low Energy Charged Particle Experiment (U of Iowa)
LET: Low Energy Telescope (U of Chicago)
TRD M3: Trapped Radiation Detector, channel M3 (UC San Diego)

RESIDUALS

To estimate how well the SATRAD model fits the observations, published Voyager and Pioneer data were scanned and digitized. Following determination of the appropriate geometric factors, the data were next converted to fluxes that could be compared to the model predictions. Background values were eliminated from the data set. The data and the model comparison plots are presented in the appendices. Based on those plots, residuals were estimated using the equations below.

First assume that the data are distributed log-normally:

$$\rho(r) = \frac{1}{\sigma\sqrt{2\pi}} e^{-\frac{1}{2}\left(\frac{r_i-\mu}{\sigma}\right)^2} \tag{9}$$

where

$$r_i = \log_{10}\left(\frac{I_{fit}}{I_{obs}}\right)_i \tag{10}$$

and

$$\sigma^2 = \sum_{i=1}^{N} \frac{r_i^2}{N-1} \tag{11}$$

We then define a "standard deviation" or error range:

$$STD = 10^{\sigma} \tag{12}$$

The latter quantity approximates the error range factor we would expect for a true log-normal distribution. It is normally used to define the "error range" for Earth's radiation belt models. Figure 13 is a plot of the resulting residuals defined above for the data plots considered in this study. The error range is about 2-5.5 (i.e., the typical model/observation ratio is inside a range of $2^{\pm 1}$) for all the values considered. If the few points with residuals outside a range of $10^{\pm 1}$ (colored blue or dark in Fig.13) are excluded as not being realistic, the overall error range is reduced to a factor of 2.2 (electrons) to 2.77 (protons)—similar to the factor of 2-3 accepted for Earth trapped-radiation models. This method is somewhat different than Divine's, which limited the residuals above a set value of the ratio or below instrument background (see Eqs. 4, 5, and 6). Even so, it yields similar results—namely that the SATRAD predictions are typically within acceptable limits for a radiation model.

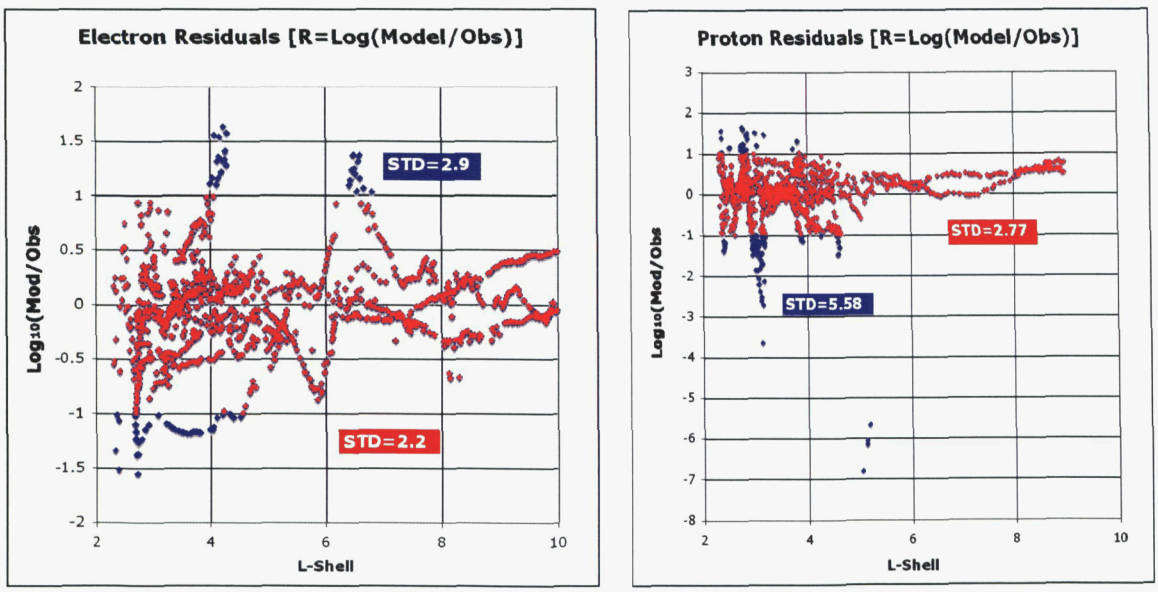

Fig. 13. The electron and proton residuals calculated for the selected data and the SATRAD model are plotted. The total set of data is represented by Blue + Red. The Blue points correspond to residual ratios outside the range $10^{\pm 1}$.

REVIEW BOARD FINDINGS

The Review Board met on 18 March 2005 at JPL. Table 5 lists the attendees. The primary purpose of the board was to determine the suitability of the radiation model for evaluating radiation shielding designs for future Saturnian missions. The Board determined that SATRAD was currently the best available engineering model for this purpose. The secondary purpose was to identify improvements that could enhance its value as an engineering tool. Specific questions concerning the model put to the board participants are listed in Table 6. To aid in evaluating the Prometheus Saturnian Radiation model, reviewers' responses were requested in the form of "Request for Action" sheets. Their responses are presented in Appendix VII.

Table 5. Saturn Radiation Model Review Board.

Participant	In-Person or Call-In	Institution
John Cooper	Call-In	NASA GSFC
Joseph Minow	Call-In	NASA MSFC
Giacomo Giampieri	In-person	ESA/JPL
Tom Armstrong	In-person	Fundamental Technology, Inc.
David Edwards	In-person	NASA MSFC
David Brinza	In-person	JPL
Insoo Jun	In-person	JPL
J. Martin Ratliff	In-person	JPL
Robin W Evans	In-person	JPL
Kent Tobiska	In-person	Space Environment Technologies
Chris Paranicas	Call-In	APL
Charles Barnes	In-person	JPL

Table 6. Specific questions for the Review Board.

Answer the following questions:

- Are the high-energy fluxes produced by the model reasonable?
  - Over what energy ranges are Divine's estimates applicable?
  - Is time-dependence an issue (UT and Local)?
  - What are the problems with the pitch-angle distributions?
- Are there shortcomings in the magnetic field model?
  - Should external terms be included?
  - Is a ring model more appropriate?
  - How variable is the magnetic field (UT and Local)?
- Does the particle model adequately represent the Pioneer and Voyager data?
  - At the end of the day, does it fit the data?
  - Is the method used to evaluate the ability of the model to fit the spacecraft data reasonable?
- Is the model a useful engineering design tool as formulated?

MODELING ISSUES

Although the review brought to light concerns with the original model and its current implementation, Divine was well aware of various problems in fitting the original Pioneer and Voyager data and in the fitting process itself. These can be listed as follows:

- Actual data points versus lines (or fits)
- Inbound/Outbound observations mismatch
- Raw versus corrected count rates (i.e., dead-time corrections)
- Omni versus spin-modulated responses
- Species confusion and alternation
- Detector response functions
- Time-averaged versus spin-averaged count rates
- Background count-rate levels
- Mistakes in computing the differential spectra (e.g., $\Delta I/\Delta E$ replacing i)
- Logarithmic versus linear scales
- L-shell (a magnetic field coordinate) versus R (radial distance) scales
- Left- versus right-hand scales (often not clear which goes with which)
- Factors used to spread the profiles
- Pitch-angle versus latitude distributions (see Figures 5 and 6 for example)

In an attempt to address these issues, the original model developed by Divine was reviewed immediately after its initial issuance in March 1990 (almost exactly 15 years ago) by outside reviewers. As their comments (based on written correspondence to the Project) closely follow those at the March meeting, they are summarized here.

Richard Selesnick of the California Institute of Technology, for example, noted that the pitch-angle data he was aware of changes its dependence to isotropic near 4 R_s—this implies the model is too anisotropic outside this distance. He suggested that there was a need to model each encounter separately to test if there are any significant time variations.

S. M. Krimigis of the Applied Physics Laboratory (APL), who was principal investigator for the Low-Energy Charge Particle (LECP) [experiment] instrument (a main source of data for the model), also reviewed the data. He indicated that the pitch-angle dependences were not in agreement with the APL observations of protons at L~2.67 and electrons at L~4.5-5. He believed that the "protons only" assumption that Divine made in interpreting ion flux data was dubious at energies <1 MeV (e.g., oxygen ions may be present). Although Divine ignored the LECP ion data at various locations, Krimigis believed that the LECP ion spectra at L = 7.15 R_s in the inner magnetosphere were reliable and should be included in the model. He also indicated that he felt that two instrument detectors (the S 180B and MD 80 detectors) used by Divine were contaminated by electrons and may have had high proton fluxes which made these data unreliable.

The most extensive review was carried out by John Cooper, one of the current reviewers (see Table 5). He wrote that there were background contamination concerns in several data sets. Sub-MeV data should only be used with caution inwards of the Tethys orbit (4.88 R_s) as penetrating trapped radiation in the inner magnetosphere mimics the response to sub-MeV particles. Electrons and the 100 MeV proton-induced background overwhelms the 0.5-10 MeV proton data in the Saturnian proton belt. The Voyager 2 LECP responded to background from higher-energy electrons while the radial profiles for sub-MeV electrons were similarly affected by high-energy background. Only the 100 Mev proton curves were good inside 5 R_s. Lower energies were contaminated and represented only an upper limit. Cooper also had various concerns with the pitch-angle distributions—he has since suggested that the model needs to use the more flexible pitch-angle distributions of the Divine-Garrett Jupiter radiation model that treat the loss cone better. It should be possible to include more Pioneer 11 (unpublished) data to determine the electron anisotropies. Likewise, the model needs to improve its description of the proton anisotropies. In fact, the model requires $B_c = 0$ for $A_n = b_n$ and allows only isotropic fluxes at high latitudes—it needs to be updated with Cassini data.

The pitch angles are more complex than isotropic inside ~4 R_s (probably not important for radiation modeling). The 63-160 MeV proton anisotropies have strong radial variations so that the uniform isotropy assumed by the model in the inner region is incorrect (as a specific concern, what is source of 100 MeV anisotropy profile at 7.63 R_s?). There is probably real-time variability in the MeV electrons that the static Divine model does not account for. There are a few specific glitches in the model—namely the 10 MeV peak at 2.5 R_s and the notch at 2.65 R_s are in error (see Figure 4)—need to review the Northrop and Fillius Pioneer 11 data. Finally, the model needs to show that electrons dominate in satellite regions—protons elsewhere. The 0-20 MeV electrons determined from the profile in Krimigis et al., 1982 (see Ref. KR82 in appendices) may be an order of magnitude too high at 2.7 R_s in the model.

REVIEW BOARD COMMENTS

In addition to the above. the Review Board comments on the SATRAD model can be roughly divided into 4 groups:

1) Pioneer and Voyager particle data (Note: these data are still of value as they cover energy ranges and locations not covered by Cassini):

- a) Need to re-evaluate using data now in the Planetary Data System (PDS).
- b) Need to re-evaluate detector background sources and calibrations in the light of current understanding of the instruments.
- c) Potentially important local-time (relative to Sun) and real-time "weather" variations—difficult to separate!
- d) Species identification requires more careful consideration—ions versus electrons, protons versus oxygen ions; etc.
- e) Some spurious features in model (see J. Cooper comments).
- f) Pitch-angle distributions in particular need to be reconsidered and a more flexible fitting scheme employed.

2) Cassini data:
    a) Need to incorporate latest Cassini data. Unfortunately, only data from the Saturn Orbit Insertion (SOI) orbit may be useful for critical pitch-angle information as instrument may now be "stuck" in one position.
    b) Cassini found an inner belt (see Figure 14) in a region that was previously unexplored, and thus not currently included in the model.
3) Magnetic field:
    a) Uncertainties in magnetic field make field line tracing difficult at ~10 R_s as field approaches zero there.
    b) As for particles, potentially important local time (relative to Sun) and real time ("weather") variations that are difficult to separate!
    c) Cassini found 6 minute slowdown in Saturn rotation and a highly variable magnetic field.
    d) Need to include effects of magnetopause and ring current in magnetic field model in outer magnetosphere (~10 R_s).
4) Overall model package
    a) Need to standardize and have peer-reviewed in literature.
    b) Need to make code/engineering model available for Cassini and other programs outside JPL.

REVIEW BOARD RECOMMENDATIONS

Based on the preceding, the Review Board recommendations as to areas that should be considered in both using the model and in updating it in the future can be concisely summarized as follows:

- Calibration/background issues with the original Pioneer and Voyager data need to be taken into account.
- The pitch-angle distributions need to be reconsidered.
- There are concerns over the apparent variability of the Saturnian magnetosphere with respects to local solar time and absolute time.
- Cassini data should be actively pursued to improve the SATRAD magnetic field model and flux estimates.
- The model should be standardized, made available to the general community, and formally reviewed in the literature.

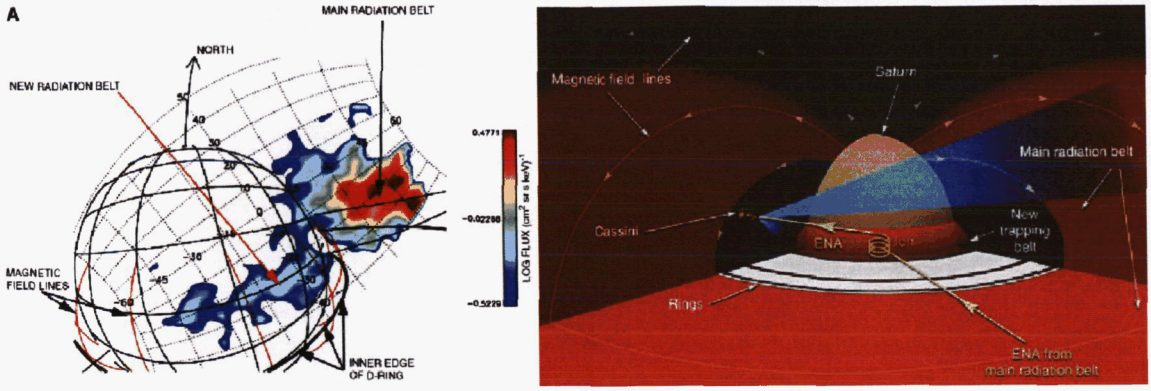

Fig. 14. Energetic neutral atom (ENA) image obtained during Cassini's passage over the rings showing an inner radiation belt not included in the current model (A) Ion and Neutral Camera (INCA) image for 20-to 50-keV/nucleon ENAs. Bright region above Saturn's limb is caused by ENAs produced by charge-exchange collisions between main radiation belt ions and near-equatorial gas. The band of emission above equator on disk is produced by the same ENAs from the main belt being stripped in Saturn's exosphere between the inner edge of the D ring and the cloud tops, trapped there temporarily as energetic ions and then reemitted as ENAs that INCA can image. The image is bounded by the limits of the INCA field of view (dotted arcs). (B) Schematic of charge exchange/stripping process that begins as ENA emission from the main belt and produces ENA emission from Saturn's exosphere. (Reprinted with permission from Krimigis et al., "Dynamics of Saturn's Magnetosphere from MIMI during Cassini's Orbital Insertion," *Science*, Vol. 307, pp. 1270–1273, February 25, 2005. Copyright 2005 AAAS).

CONCLUSIONS

In the early 1990's, Neil Divine developed a Saturn proton/electron radiation model based on data from Pioneer 11, Voyager 1, and Voyager 2. That model has been turned into a FORTRAN computer code for analyzing the radiation environment at Saturn. The code, SATRAD, uses Divine's formulation to compute the electron and proton fluxes at a specified B and L coordinate. A separate model of the Saturnian magnetic field is used to compute the B and L coordinates along a spacecraft trajectory. While originally intended as an engineering tool to model radiation doses to Cassini during its design, the current model implementation was used to estimate the doses for Prometheus missions to Saturn and will be used to compare with the Cassini measurements when they become available. To validate the SATRAD model, its flux predictions have been compared by the authors with published Pioneer and Voyager data. Those comparisons allow an estimate of the "accuracy" of the SATRAD model by providing an error range. Within the limits of the current study, the original estimate of Divine has been validated to a factor of 2-3 and is within current expectations for radiation modeling. While agreeing to the general usefulness and validity of SATRAD for radiation modeling, the Review Board found several areas that should be considered in both using the model and in updating it. These ranged from calibration/background issues with the original Pioneer and Voyager data to very real concerns over the apparent

variability of the Saturnian magnetosphere. Finally, Cassini data, when they become available, should allow improvements in the SATRAD magnetic field model and flux estimates and should be actively pursued. The reviewers requested copies of the current model for comparisons with the Cassini data and recommended that the model be standardized, made more readily available, and formally reviewed in the literature. This document was written to address those issues.

TEXT REFERENCE

1. Divine, Neil, JPL Interoffice Memorandum-5217-90-029, Numerical Models for Electron and Proton Distributions in Saturn's Radiation Belts, Jet Propulsion Laboratory, Pasadena, California, 28 February 1990.

2. Roederer, J. G., *Dynamics of Geodynamically Trapped Radiation*, Springer-Verlag, Berlin, 1970.

3. Connerney, J. E. P., M. H. Acuna, and N. F. Ness, "Currents in Saturn's magnetosphere", *J. Geophys. Res.*, V88, A11, pp. 8779-8789, 1983.

4. Krimigis, S. M., D. G. Mitchell, D. C. Hamilton, N. Krupp, S. Livi, E. C. Roelof, J. Dandouras, T. P. Armstrong, B. H. Mauk, C. Paranicas, P. C. Brandt, S. Bolton, A. F. Cheng, T. Choo, G. Gloeckler, J. Hayes, K. C. Hsieh, W.-H. Ip, S. Jaskulek, E. P. Keath, E. Kirsch, M. Kusterer, A. Lagg, L. J. Lanzerotti, D. LaVallee, J. Manweiler, R. W. McEntire, W. Rasmuss, J. Saur, F. S. Turner, D. J. Williams, J. Woch, "Dynamics of Saturn's Magnetosphere from MIMI During Cassini's Orbital Insertion", *Science*, Vol. 307, pp. 1270-1273, February 25, 2005.

APPENDICES

APPENDIX I. Table A1. Electron Model Data Sources (Divine, Ref. 1)

SPACECRAFT, SUBSYSTEM [a]	REFERENCE, PAGE	FIGURE, LINE [b]	CHANNEL	ENERGIES E_a, E_b (MeV) [c]	CONVERSION R/J (cm^{-2}) [d]	BACK-GROUND Log R_B [e]	NOTES
V02 LECP	KR82, 573	2C, 2	EAB10	10, 20	1.03(-3)	-2.0	[f]
P11 CPT	SI80b, 5749	21c, 1	ECD	3.4	1.00	4.2	[g]
	SI80b, 5742	13, 4	ECD	3.4	1.00	4.2	[g]
P11 TRD	FM80, 5804	1ab, 4	CDC	2.0	6.3(-15)	0.0	[h]
P11 CPT	SI80b, 5740	11, 2	MT	2.0, 7.0	3.42(-2)	-1.6	[i]
V02 LECP	KR82, 573	2C, 1	ESA0	1.5	9.55(-4)	0.0	[j]
P11 CRT	MD80, 5824	18, 4		1.1, 2.0	0.088	1.0	[k]
	TR80, 422	2, 3		1.1, 2.0	0.088	1.0	[k]
V02 LECP	VA84, 307	20, 5	Eγ08-Eγ09	0.853, 1.2	1.35(-5)	-1.5	[l]
P11 CRT	MD80, 5824	18, 3		0.8, 1.1	0.265	2.0	[k]
	TR80, 422	2, 2		0.8, 1.1	0.265	2.0	[k]
P11 GTT	VA80a, 419	5,2	B	0.56, 21	1.27(-3)	-0.4	[m]
	VA80c, 5710	1, 2	B	0.56, 21	1.27(-3)	-0 4	[m]
	VA84, 300	14, 2	B	0.56, 21	0.08	2.0	[n]
V02 LECP	VA84, 307	20, 4	Eγ07-Eγ08	0.48, 0.853	2.79(-4)	1.0	[l]
P11 TRD	FI80, 429	5,1	E1	0.45	1.64(-3)	0.2	[o]
	FM80, 5804	1ab, 3	E3	0.46	4.54(-4)	0.0	[p]
P11 CRT	MD80, 5824	18, 2		0.43, 0.8	0.215	2.0	[k]
V02 LECP	VA84, 307	20, 3	Eγ06-Eγ07	0.252, 0.48	6.45(-4)	1.7	[l]
	AR83, 8899	12, 1	Eγ06-Eγ07	0.252, 0.48	6.45(-4)	0.5	[f]
V01 LECP	KR81, 226	1A, 2	Eβ05	0.2, 0.5	1.59(-4)	-1.0	[f]
P11 CRT	MD80, 5824	18, 1		0.16, 0.43	0.295	3 0	[k]
	TR80, 422	2, 1		0.1, 0.43	0.241	3 0	[k]
P11 TRD	FI80, 427	2C, 2	E1-1.25E2	0.16, 0.25	0.856	4.0	[q]
V01 LECP	CH85, 508	2, 384	Eβ04	0.14, 0.2	4.77(-4)	-0.5	[f]
	KR83, 8877	6, 5	Eβ04	0.13, 0.2	4.77(-4)	-1.0	[f]
V02 LECP	VA84, 307	20, 2	Eβ04	0.112, 0.183	3.1(-4)	1.0	[l]
	AR83, 8899	11, 2	Eβ04	0.112, 0.183	3.1(-4)	1.0	[f]
P11 GTT	VA80a, 419	5, 1	A	0.04, 21	1.37(-3)	-0.3	[m]
	VA80c, 5710	1, 1	A	0.04, 21	1.37(-3)	-0.3	[m]
	VA84, 300	13, 1&2	A	0.04, 21	0.08	2.7	[n]

NOTES TO TABLE A1

[a] The profiles appear in order of decreasing threshold energy E_a (see column 5 above and note [c], below); a profile lacking an entry in column 1 is used in the model only for trajectory points at which no value for count rate R (see note [d]) is available from the profile identified on the line immediately above.

[b] Second entry in this column is the curve placement, counting down from the top of the figure cited.

[c] Where two entries appear, the response (next column) is assumed constant between them, and zero elsewhere; a single entry represents the smaller (threshold E_a) of these two energies, and the other (E_b) is assumed infinite.

[d] Units cm^{-2} assumes R is a count rate (units s^{-1}); exceptions are cited in the notes, and the entry in this column is always the ratio of the profile quantity R (count rate, intensity, flux, etc.) to the local omni flux J (see text following Eq. 7). Parentheses enclose powers of 10.

[e] This entry is estimated from the noise or limit of the profile in the figure, in the same units as R in the preceding column (see note [d]).

[f] Energies from profile label; conversion is εG in cm^2sr (KR83, p. 8874, Table 1) divided by 4π sr.

[g] Energy from figure label, profile is flux J, no conversion needed.

[h] Energy from source (FM80, p. 5805, Table 1), profile is current; conversion is as discussed in Appendix B (last paragraph).

[i] Energies from profile label, conversion is 0.43 cm^2sr (SI80b, p. 5757, Table A1) divided by 4π sr.

[j] Energy from profile label, conversion is εG=0.12 cm^2sr (KR83, p. 8874, Table 1) divided by 4π sr and by an additional factor 10 to secure agreement with a corresponding profile (KA82, p. 1144, Fig. 2, curve 3 from top) and with Pioneer 11 detectors at nearby energies.

[k] Energies from figure caption (or label), profile is differential intensity i, conversion is $(4\pi\ sr)^{-1}\ (E_b\text{-}E_a)^{-1}$.

[l] Same as note [f], but conversion also confirmed by comparison with spectrum at L = 9.56, as discussed in Appendix B (paragraph 4).

[m] Energies from source (VA80a, p. 416, Table 1), conversion is Q from same table.

[n] Energies as in note [m], profile is integral intensity I, conversion is $(4\pi\ sr)^{-1}$.

[o] Energy from profile label, conversion is $(R/J)_3(R_1/R_3)$, where subscript 1 is for channel E1, subscript 3 is for channel E3, R_1 and R_3 are the peak count rates at L = 2.7, and conversion $(R/J)_3$ is derived in note [p].

[p] Energy from source (FM80, p. 5805, Table 1), conversion is 0.0057 cm^2sr (same table) divided by 4π sr.

[q] Energies from source (Fl80, p. 426, Table 1), profile is differential intensity i, conversion is $(4\pi\ sr)^{-1}(E_b—E_a)^{-1}$.

APPENDIX II. Table A2. Proton Model Data Sources (Divine, Ref. 1)

SPACECRAFT, SUBSYSTEM [a]	REFERENCE, PAGE	FIGURE, LINE [b]	CHANNEL	ENERGIES E_a, E_b (MeV) [c]	CONVERSION R/J (cm^{-2}) [d]	BACK-GROUND Log R_B [e]	NOTES
P11 TRD	FI80, 429	5, 3	M1	80	0.038	0.0	[f]
	FM80, 5804	1ab, 5	M3	80	0.012	-1.0	[g]
P11 GTT	VA80a, 418	4, 2&4	D	80	0.043	-0 5	[h]
	VA80c, 5710	1, 4	D	80	0.043	-0 5	[i]
	VA80a, 417	3, 2&4	D	80	0.043	-0.5	[h]
P11 GTT	VA80a,419	5, 3	C	80	0.122	-0.3	[h]
	VA80a, 418	4, 1&3	C	80	0.122	0.0	[h]
	VA83, 6913	4, 1	C	80	0.122	0.0	[j]
	VA83, 6913	5, 1	C	80	0.122	0.0	[j]
	VA80c, 5710	1, 3	C	80	0.122	-0.3	[i]
	VA80a, 417	3, 1&3	C	80	0.122	0.0	[h]
V02 CRS	SM83, 8925	3, 2		63, 160	8.2(-4)	-3 0	[k]
V02 LECP	KR82, 573	2C, 3	PAB12	54, 87	0.004	-2.0	[l]
V02 CRS	SM83, 8925	3, 1		48, 63	5.31(-3)	-2.5	[k]
	SM83, 8924	2, 1		48, 63	1.85	0.0	[m]
P11 CPT	SI80b, 5742	14, 2	FCD	35	2.5(-5)	-1 5	[n]
V02 CRS	VO82, 579	3, 1	A	27, 160	0.08	-0.8	[o]
P11 CRT	MD80, 5815	3, 4		2.1, 3.1	0.08	-2.0	[k]
P11 CRT	MD80, 5824	19, 1		1.56, 5.1	0.08	-2.0	[o]
P11 CRT	TR80, 422	1, 3		1.1, 2.15	0.076	0.0	[p]
P11 CRT	TR80,422	1, 2		0.75, 1.2	0.177	1.0	[p]
P11 GTT	VA80a, 417	2,1	G	0.61, 3.41	3.5(-3)	-0.8	[h]
	VA84, 290	5, 1&2	G	0.61, 3.41	0.08	0.2	[o]
V02 LECP	VA84, 296	10, 2	PL06	0.54, 0.99	0.009	-3.0	[l]
P11 CRT	MD80, 5815	3, 2		0.53, 0.74	0.379	1.0	[p]
P11 CPT	SI80b, 5748	20A2, 1	L1~~L2~~	0.5, 1.8	0.039	0.3	[q]
	SI80b, 5748	20C2, 1	L1~~L2~~	0.5, 1.8	0.039	0.3	[q]
	SI80b, 5742	14, 1	L1~~L2~~	0.5, 1.8	0.039	0.3	[q]
	SI80b, 5743	15, 1&2	L1~~L2~~	0.5,1.8	0.039	0.3	[q]
P11 CRT	TR80, 422	1, 1		0.2, 0.75	0.145	2.0	[k]
V01 LECP	CH85, 508	1, 3&4	PL04	0.139, 0.22	3.2(-3)	-0.5	[l]
V02 LECP	AR83, 8895	3, 2	PL04	0.137, 0.215	0.009	2.0	[l]

NOTES TO TABLE A2

[a] The profiles appear in order of decreasing threshold energy E_a (see column 5 above, note [c] below); a profile lacking an entry in column 1 is used in the model only for trajectory points at which no value for count rate R (note [d]) is available from the profile immediately above.

[b] Second entry in this column is the curve placement, counting down from the top of the figure cited.

[c] Where two entries appear, the response (next column) is assumed constant between them, and zero elsewhere; a single entry represents the smaller (threshold E_a) of these two energies, and the other (E_b) is assumed infinite.

[d] Units cm^{-2} assumes R is a count rate (units s^{-1}); exceptions are cited in the notes, and the entry in this column is always the ratio of the profile quantity R (count rate, intensity, flux, etc.) to the local omni flux J (see text following Eq. 7). Parentheses enclose powers of 10.

[e] This entry is estimated from the noise or limit of the profile in the figure, in the same units as R in the preceding column (see note [d]).

[f] Energy from profile label, conversion is geometric factor in cm^2 (FI80, p. 426, Table 1).

[g] Energy from source (FM80, p. 5805, Table 1), conversion is geometric factor in cm^2 (same table; note disagreement with FI80, p. 426, Table 1).

[h] Energy from source (VA80a, p. 416, Table 1), conversion is Q from same table.

[i] Energy from source (VA80b, p. 5682, Table 2), conversion is Q from same table.

[j] Energy as in note [h], conversion from source (VA83, p. 6912, Eq. 1).

[k] Energies from figure caption (or label), profile is differential intensity i, conversion is $(47\sim \text{sr})^{-1}$ $(E_b-E_a)^{-1}$.

[l] Energies from profile label, conversion is εG in cm^2sr (KR83, p. 8874, Table 1) divided by 4π sr.

[m] Energies as for preceding profile, conversion is $(4\pi \text{ sr})^{-1}$ $(E_b-E_a)^{-1}$ (R_3/i_3) where $\log R_3=3.75$ and $\log i_3=1.21$ are peak rates from this and the preceding profile.

[n] Energy from profile label, conversion from source (SI80b, p. 5757, Table A1), weight is 2.0 to compensate for indistinguishability of the inbound and outbound profiles.

[o] Energies from figure caption, profile is integral intensity I, conversion is $(4\pi \text{ sr})^{-1}$.

[p] Same as note [k], but conversion also confirmed by comparison with spectrum at 7.81 R_s, as discussed in Appendix B (paragraph 4).

[q] Energies from profile label, conversion is geometric factor in cm^2sr (SI80b, p. 5757, Table A1) divided by 4π sr.

APPENDIX III. Saturn Data References

This appendix lists the original sources of data that Divine (1990) used to construct the Saturnian radiation model. These were also the sources of the data used herein to re-evaluate the SATRAD model.

AR83 Armstrong, T. P., et al., 1983 Nov. 1: "Voyager Observations of Saturnian Ion and Electron Phase Space Densities," *J. Geophys. Res.*, Vol. 88, No. A11, pp. 8893-8904.

BC80 Bastian, T. S., D. L. Chenette, and J. A. Simpson, "Charged particle anisotropies in Saturn's magnetosphere," *J. Geophys. Res.*, V85, A11, 5763-5771. Nov, 1980.

CE80 Cesarone, R. J., et al., 1980 Oct. 9: "Voyager 1 Saturn Encounter Trajectory Information," JPL IOM Voyager-NAV-80-196 (JPL internal document).

CE89 Cesarone, R. J., 1989 (private communication).

CH85 Cheng, A. F., et al., 1985 Oct. 10: "Does Saturn Have Rings Outside 10 R_S?", *Nature*, Vol. 317, pp. 508-509.

C084 Connerney, J. E. P., et al., 1984: "Magnetic Field Models," in *Saturn* (T. Gehrels and M. S. Matthews, Editors, Univ. of Arizona Press, Tucson), pp. 354-377.

C089 Cooper, J. F., 1989 Oct. 10: "A Critical Review of Charged Particle Astronomy at Saturn: The Evidence for Co-Orbiting Material in the Inner Satellite System", pp. 5-C-1 to 5-C-35 in Vol. Xlll: *Physical Models, Cassini Mission: Saturn Orbiter Proposal Information Package*, JPL D-6464.

CS80 Cooper, J. F., and J. A. Simpson, "Sources of high-energy protons in Saturn's magnetosphere", *JGR*, V85, No. A11, 5793-5802, Nov, 1980.

DI80 Divine, Neil, 1980 May 8: "Saturn Radiation Belt Models and Predicted Electron Flux and Fluence for Voyager," JPL IOM 3576-80-93 (internal document).

DI90 Divine, Neil, 1990 Feb. 12: "Saturn Energetic Electron and Proton Spectra for Cassini," JPL IOM 5217-90-023 (internal document).

DG83 Divine, N., and H. B. Garrett, 1983 Sept. 1: "Charged Particle Distributions in Jupiter's Magnetosphere," *J. Geophys. Res.*, Vol. 88, No. A9, pp. 6889-6903.

EV87a Evans, R., 1987 Jan. 22: "Saturn Proton Radiation Hazard for a Mariner Mark II Spacecraft," JPL IOM 5137-87-20 (internal document).

EV87b Evans, R., 1987 Feb 6: "Jupiter and Saturn Single Event Upset Hazard for a Mariner Mark ll Spacecraft," JPL IOM 5137-87-35 (internal document).

FI80 Fillius, W., et al., 1980 Jan. 25: "Trapped Radiation Belts of Saturn: First Look," *Science*, Vol. 207, No. 4429, pp. 425-431.

FM80 Fillius, W., and C. McIlwain, 1980 Nov. 1: "Very Energetic Protons in Saturn's Radiation Belt," *J. Geophys. Res.*, Vol. 85, No. A11, pp. 5803-5811.

HA83 Hamilton, D. C., et al., 1983 Nov. 1: "Energetic Atomic and Molecular Ions in Saturn's Magnetosphere", *J. Geophys. Res.*, Vol. 88, No. A11, pp. 8905-8922.

HO89 Hood, L. L., 1989 Oct. 10: "Investigation of the Saturn Dust Environment from the Analysis of Energetic Charged Particle Measurements," pp. 5-D-1 to 5-D-30 in *Vol.XIII: Physical Models, Cassini Mission: Saturn Orbiter Proposal Information Package*, JPL D-6464 (internal document).

KA82 Krimigis, S. M., and T. P. Armstrong, 1982 Oct.: "Two-Component Proton Spectra in the Inner Saturnian Magnetosphere," *Geophys. Res. Letters*, Vol. 9, No. 10, pp. 1143-1146.

KR81 Krimigis, S. M., et al., 1981 April 10: "Low-Energy Charged Particles in Saturn's Magnetosphere: Results from Voyager 1," *Science*, Vol. 212, No. 4491, pp. 225-231.

KR82 Krimigis, S. M., et al., 1982 Jan. 29: "Low-Energy Hot Plasma and Particles in Saturn's Magnetosphere," *Science*, Vol. 215, No. 4532, pp. 571-577.

KR83 Krimigis, S. M., et al., 1983 Nov. 1: "General Characteristics of Hot Plasma and Energetic Particles in the Saturnian Magnetosphere: Results from the Voyager Spacecraft," *J. Geophys. Res.*, Vol. 88, No. A11, pp. 8871-8892.

MD80 McDonald, F. B., et al., 1980 Nov. 1: "If You've Seen One Magnetosphere, You Haven't Seen Them All: Energetic Particle Observations in the Saturn Magnetosphere," *J. Geophys. Res.*, Vol. 85, No. A11, pp. 5813-5830.

MS80 McKibben, R. B., and J. A. Simpson, 1980 Nov. 1: "Charged Particle Diffusion and Acceleration in Saturn's Radiation Belts," *J. Geophys. Res.*, Vol. 85, No. A11, pp. 5773-5783.

PD04 Paranicas, C., R. B. Decker, B. H. Mauk, and S. M. Krimigis, GRL, V31, L04810, doi:10.1029/2003GL018899, 2004.

RO70 Roederer, J. G., 1970: *Dynamics of Geomagnetically Trapped Radiation*, Springer-Verlag, Berlin, 166 pp.

SB03 Santos-Costa, D., M. Blanc, S. Maurice, and S. J. Bolton, "Modeling the electron and proton radiation belts of Saturn," GRL, V30, N20, 2059, doi:10.1029/2003GL017972, 2003.

SL74 Schulz, M., and L. J. Lanzerotti, 1974: *Particle Diffusion in the Radiation Belts*, Springer-Verlag, Berlin, 215 pp.

SM83 Schardt, A. W., and F. B. McDonald, 1983 Nov. 1: "The Flux and Source of Energetic Protons in Saturn's Inner Magnetosphere," *J. Geophys. Res.*, Vol. 88, No.A11, pp. 8923-8935.

Sl80a Simpson, J. A., et al., 1980 Jan. 25: "Saturnian Trapped Radiation and Its Absorption by Satellites and Rings: The First Results from Pioneer 11," *Science*, Vol. 207, No. 4429, pp. 411-415.

Sl80b Simpson, J. A., et al., 1980 Nov. 1: "The Trapped Radiations of Saturn and Their Absorption by Satellites and Rings," *J. Geophys. Res.*, Vol. 85, No. A11, pp. 5731-5762.

TR80 Trainor, J. H., et al., 1980 Jan. 25: "Observations of Energetic Ions and Electrons in Saturn's Magnetosphere," *Science*, Vol. 207, No. 4429, pp. 421-425.

VA80a Van Allen, J. A., et al., 1980 Jan. 25: "Saturn's Magnetosphere, Rings, and Inner Satellites," *Science*, Vol. 207, No. 4429, pp. 415-421.

VA80b Van Allen, J. A., et al., 1980 Nov. 1: "Sources and Sinks of Energetic Electrons and Protons in Saturn's Magnetosphere," *J. Geophys. Res.*, Vol. 85, No. A11, pp. pp. 5679-5694.

VA80c Van Allen, J. A., et al., 1980 Nov. 1: "The Energetic Charged Particle Absorption Signature of Mimas," *J. Geophys. Res.*, Vol. 85, No. A11, pp. 5709-5718.

VA83 Van Allen, J. A., 1983 Sept. 1: "Absorption of Energetic Protons by Saturn's Ring G," *J. Geophys.* Res., Vol. 88, No. A9, pp. 6911-6918.

VA84 Van Allen, J. A., 1984: "Energetic Particles in the Inner Magnetosphere of Saturn," in Saturn (T. Gehrels and M. S. Matthews, Editors, Univ. of Arizona Press, Tucson), pp. 281-317.

V082 Vogt, R. E., et al. 1982 Jan. 29: "Energetic Charged Particles in Saturn's Magnetosphere: Voyager 2 Results," *Science*, Vol. 215, No. 4532, pp. 577-582.

W081 Wolff, D. M., et al., 1981 June 23: "Voyager 2 Saturn Encounter Trajectory Information", JPL IOM Voyager-NAV-81-118 (internal document).

APPENDIX IV. Data Comparisons between SATRAD and P11, V1, AND V2

Fig. A1 (next page and following) SATRAD model predictions versus P11, V1, and V2 data. Specific frame, reference (see Appendix III), and figure number for each reference are as follows:

Fig. A1 Subfig. #	Ref. Doc. ID	Fig. # in Ref. Doc.	Comment
1	VA84	20	6.45E-04 cm^2
2	PD04	2	1.59E-04 cm^2
3	VA84	20	2.79E-04 cm^2
4	VA84	14	original in flux units
5	VA84	20	1.35E-05 cm^2
6	KR82	2C	9.55E-03 cm^2
7	SB03	4	original in flux units
8	BC80	6	original in flux units
9	BC80	6	1.27E-03 cm^2
10	KR82	2	1.035E-03 cm2
11	KR82	2	1.035E-03 cm^2
12	BC80	5	0.039 cm^2
13	VA84	5	0.224 cm^2
14	VA84	5	0.224 cm^2
15	CS80	1	2.50E-05 cm^2
16	SM83	3	original in flux units
17	SM83	3	original in flux units
18	KR82	2C	0.003979 cm^2
19	KR82	2C	0.003979 cm^2
20	SM83	3	original in flux units
21	SM83	3	original in flux units
22	VA80b	18	original in flux units with paper corrections
23	FM80	1ab	0.012 cm^2
24	CS80	1	0.012 cm^2

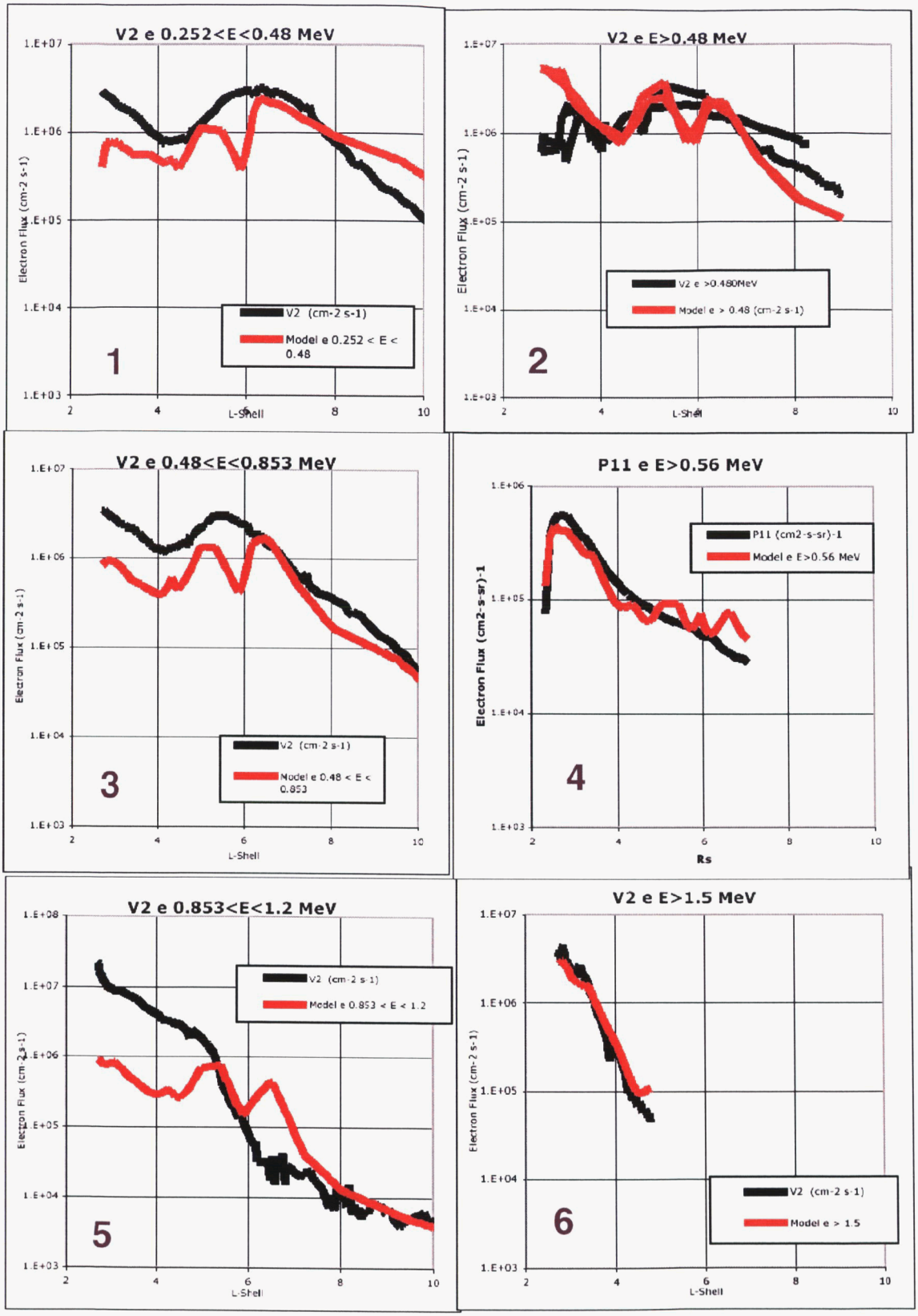
V2 e 0.252<E<0.48 MeV
Electron Flux (cm-2 s-1)
L-Shell
V2 (cm-2 s-1)
Model e 0.252 < E < 0.48
1
V2 e E>0.48 MeV
V2 e >0.480MeV
Model e > 0.48 (cm-2 s-1)
2
V2 e 0.48<E<0.853 MeV
V2 (cm-2 s-1)
Model e 0.48 < E < 0.853
3
P11 e E>0.56 MeV
Electron Flux (cm2-s-sr)-1
P11 (cm2-s-sr)-1
Model e E>0.56 MeV
Rs
4
V2 e 0.853<E<1.2 MeV
V2 (cm-2 s-1)
Model e 0.853 < E < 1.2
5
V2 e E>1.5 MeV
V2 (cm-2 s-1)
Model e > 1.5
6

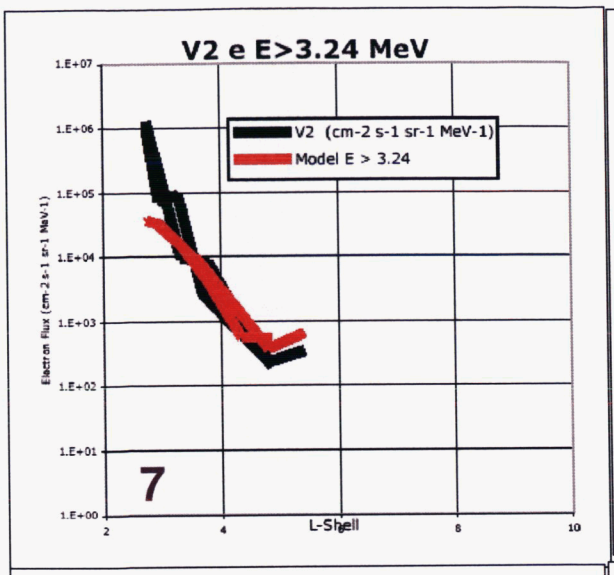
V2 e E>3.24 MeV
V2 (cm-2 s-1 sr-1 MeV-1)
Model E > 3.24
Electron Flux (cm-2 s-1 sr-1 MeV-1)
L-Shell
7

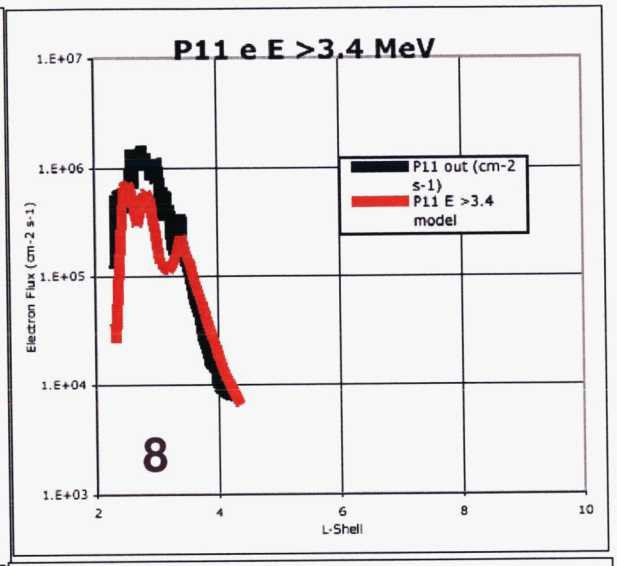
P11 e E >3.4 MeV
P11 out (cm-2 s-1)
P11 E >3.4 model
Electron Flux (cm-2 s-1)
L-Shell
8

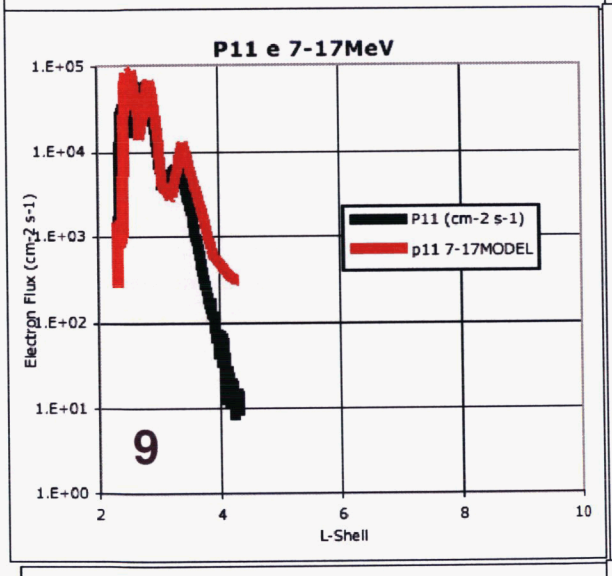
P11 e 7-17MeV
P11 (cm-2 s-1)
p11 7-17MODEL
Electron Flux (cm-2 s-1)
L-Shell
9

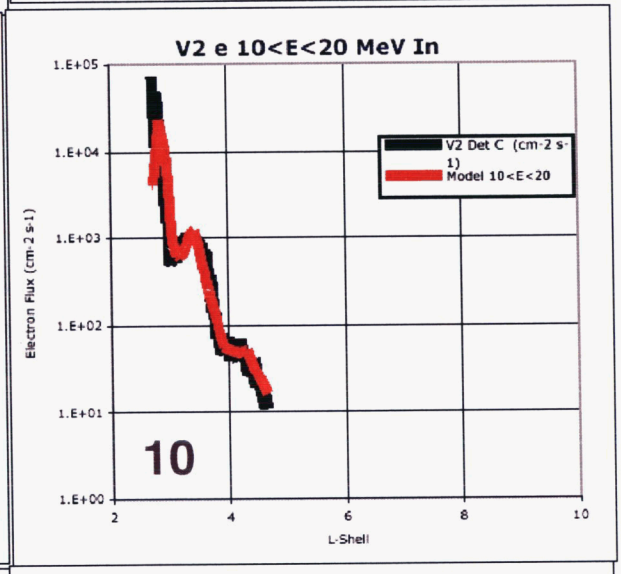
V2 e 10<E<20 MeV In
V2 Det C (cm-2 s-1)
Model 10<E<20
Electron Flux (cm-2 s-1)
L-Shell
10

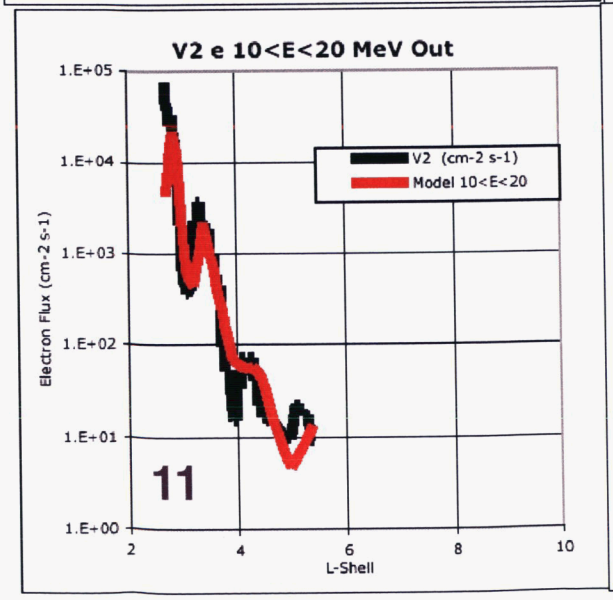
V2 e 10<E<20 MeV Out
V2 (cm-2 s-1)
Model 10<E<20
Electron Flux (cm-2 s-1)
L-Shell
11

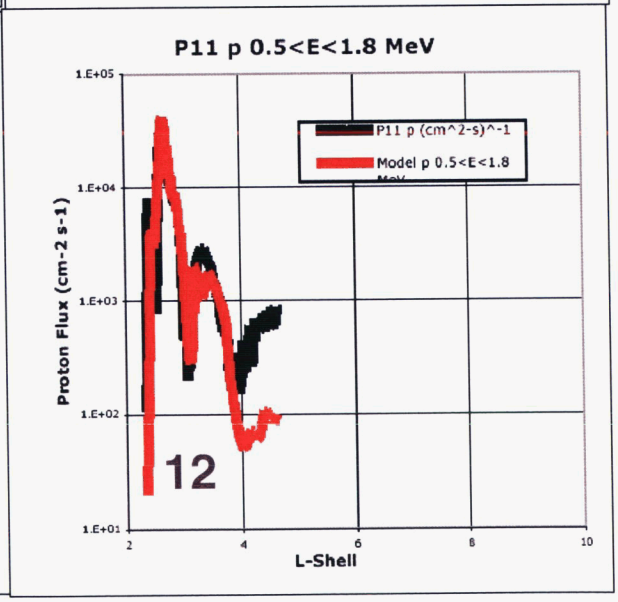
P11 p 0.5<E<1.8 MeV
P11 p (cm^2-s)^-1
Model p 0.5<E<1.8
Proton Flux (cm-2 s-1)
L-Shell
12

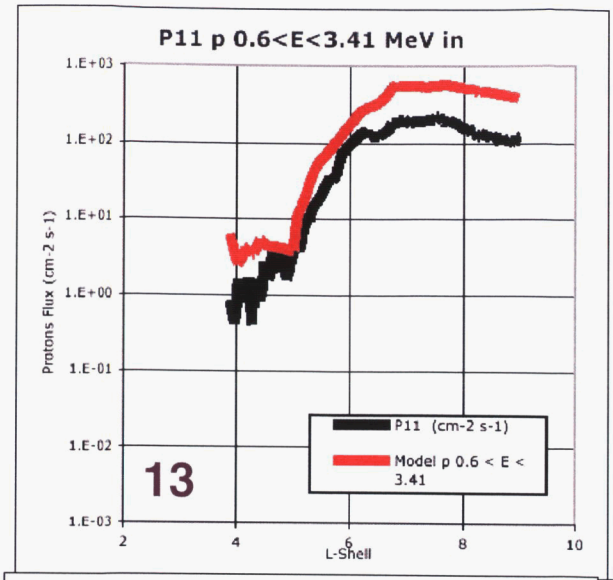
P11 p 0.6<E<3.41 MeV in
Protons Flux (cm-2 s-1)
1.E+03
1.E+02
1.E+01
1.E+00
1.E-01
1.E-02
1.E-03
2
4
6
8
10
L-Shell
P11 (cm-2 s-1)
Model p 0.6 < E < 3.41
13

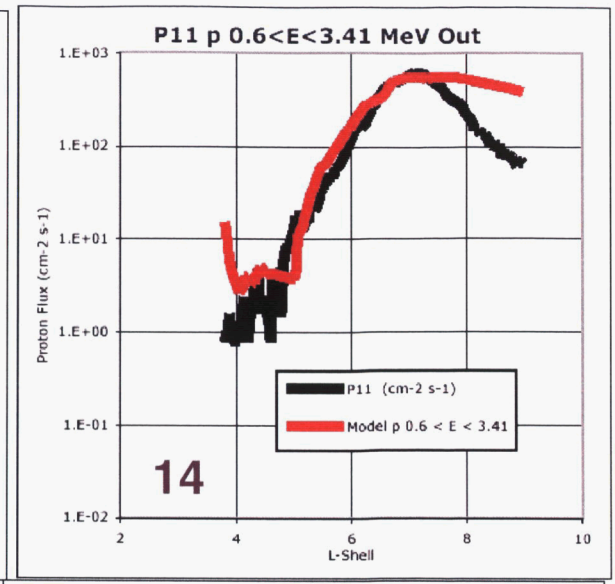
P11 p 0.6<E<3.41 MeV Out
Proton Flux (cm-2 s-1)
1.E+03
1.E+02
1.E+01
1.E+00
1.E-01
1.E-02
2
4
6
8
10
L-Shell
P11 (cm-2 s-1)
Model p 0.6 < E < 3.41
14

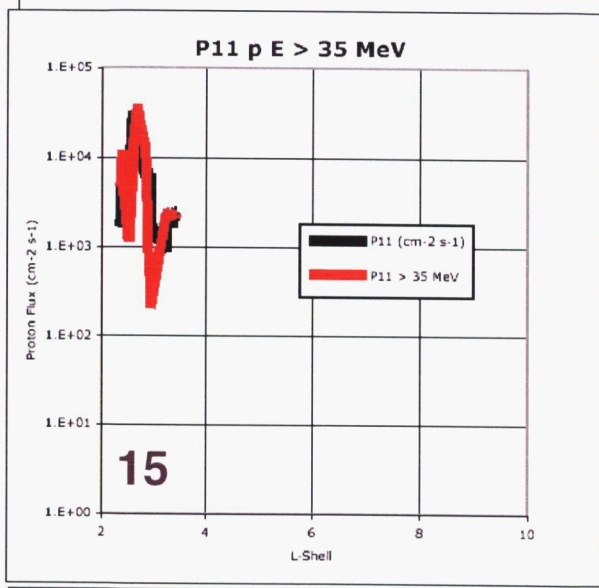
P11 p E > 35 MeV
Proton Flux (cm-2 s-1)
1.E+05
1.E+04
1.E+03
1.E+02
1.E+01
1.E+00
2
4
6
8
10
L-Shell
P11 (cm-2 s-1)
P11 > 35 MeV
15

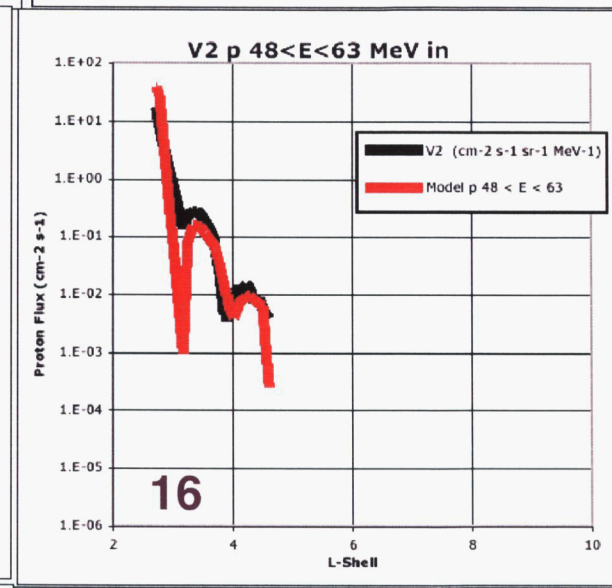
V2 p 48<E<63 MeV in
Proton Flux (cm-2 s-1)
1.E+02
1.E+01
1.E+00
1.E-01
1.E-02
1.E-03
1.E-04
1.E-05
1.E-06
2
4
6
8
10
L-Shell
V2 (cm-2 s-1 sr-1 MeV-1)
Model p 48 < E < 63
16

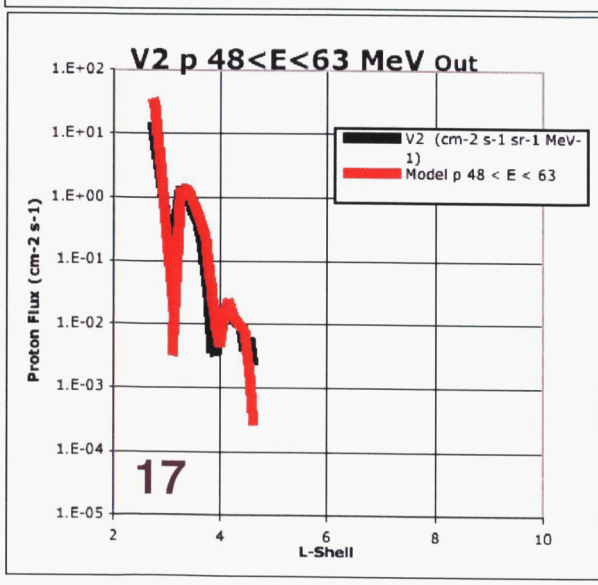
V2 p 48<E<63 MeV Out
Proton Flux (cm-2 s-1)
1.E+02
1.E+01
1.E+00
1.E-01
1.E-02
1.E-03
1.E-04
1.E-05
2
4
6
8
10
L-Shell
V2 (cm-2 s-1 sr-1 MeV-1)
Model p 48 < E < 63
17

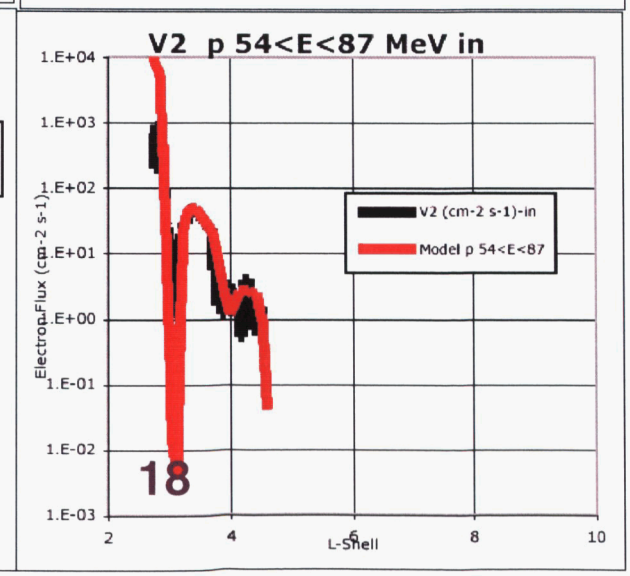
V2 p 54<E<87 MeV in
Electrop.Flux (cm-2 s-1)
1.E+04
1.E+03
1.E+02
1.E+01
1.E+00
1.E-01
1.E-02
1.E-03
2
4
6
8
10
L-Shell
V2 (cm-2 s-1)-in
Model p 54<E<87
18

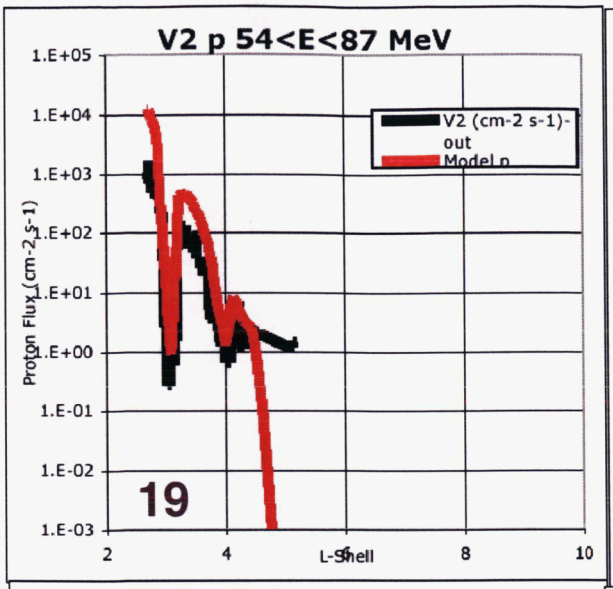
V2 p 54<E<87 MeV
Proton Flux (cm-2 s-1)
L-Shell
V2 (cm-2 s-1)-out
Model p
19

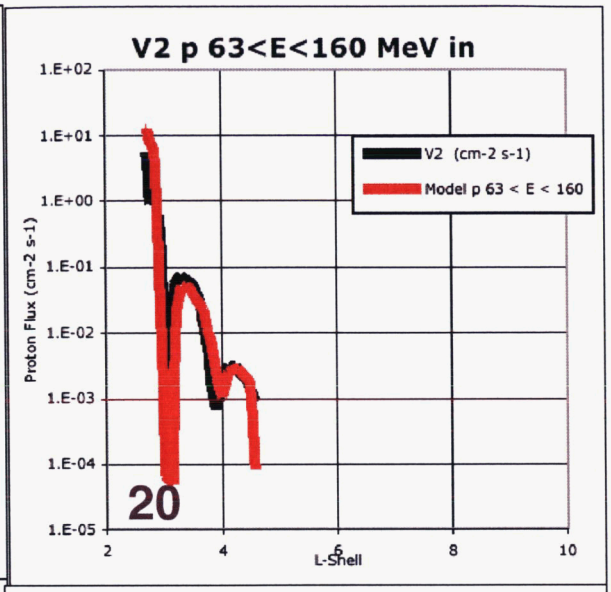
V2 p 63<E<160 MeV in
Proton Flux (cm-2 s-1)
L-Shell
V2 (cm-2 s-1)
Model p 63 < E < 160
20

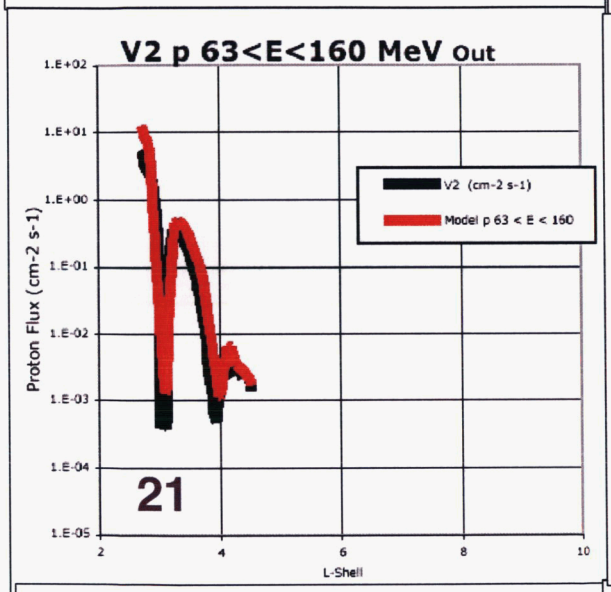
V2 p 63<E<160 MeV Out
Proton Flux (cm-2 s-1)
L-Shell
V2 (cm-2 s-1)
Model p 63 < E < 160
21

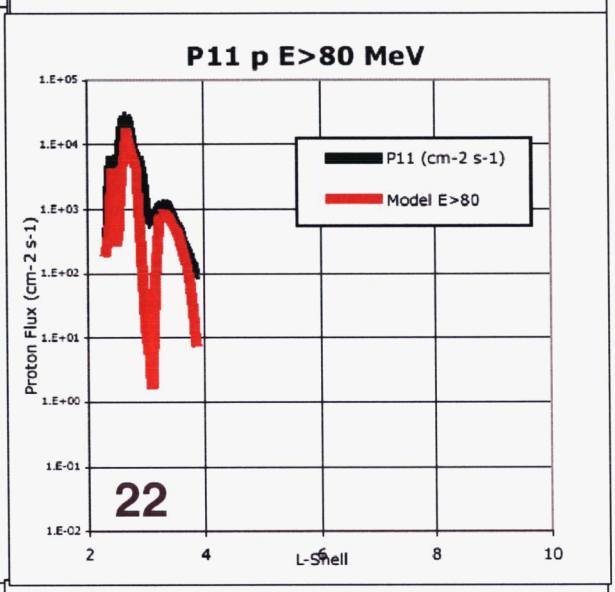
P11 p E>80 MeV
Proton Flux (cm-2 s-1)
L-Shell
P11 (cm-2 s-1)
Model E>80
22

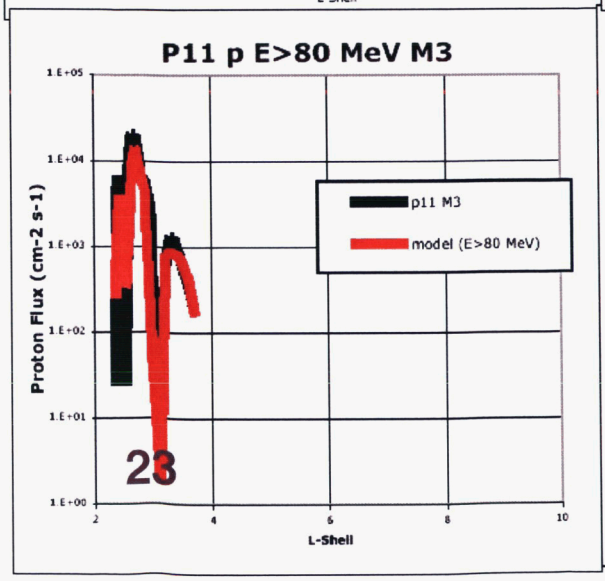
P11 p E>80 MeV M3
Proton Flux (cm-2 s-1)
L-Shell
p11 M3
model (E>80 MeV)
23

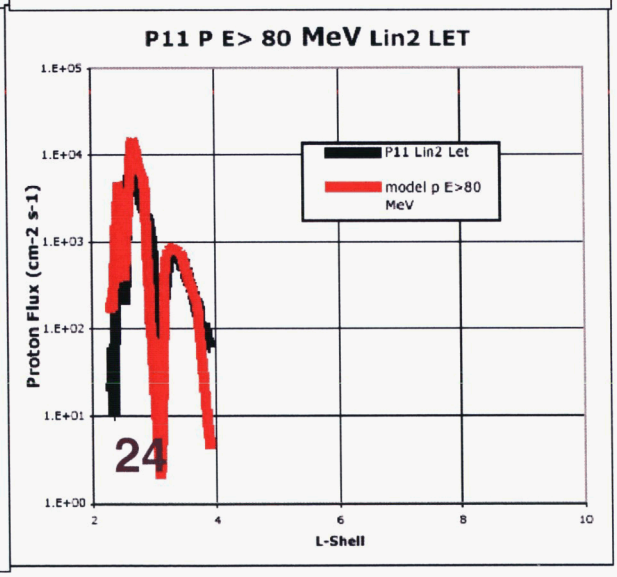
P11 P E> 80 MeV Lin2 LET
Proton Flux (cm-2 s-1)
L-Shell
P11 Lin2 Let
model p E>80 MeV
24

APPENDIX V. SATRAD Listings

Saturn Radiation Program

The following is a FORTRAN listing of the SATRAD model. It consists of a main calling program, "Smainrxx," which reads in the trajectory and magnetic field data along the trajectory (see "traj.in") and prepares various output files. It also establishes the energy channels to be analyzed. This program can be easily modified to handle a variety of input formats. The second primary component is subroutine SATRADxx and its subsidiary subroutines. This component should be kept as is.

```
      Program Smainrxx
c     Smainrxx.f is an example of a main calling program for
c     SATRAD.f  SATRAD.f calculates the Saturnian electron and proton fluxes.
c
c     The SATRAD Program is documented in JPL Publication 05-9, October 2005,
c     "Saturn Radiation (Satrad) Model", H.B. Garrett, J.M. Ratliff,
c     and R.W. Evans  Algorithms are those of Neil Divine, as documented in
c     N. Divine, "Numerical Models for Electron and Proton Distributions
c     in Saturn's Radiation Belts", JPL IOM-5217-90-029, 28 February, 1990.
c     Final coding by Garrett and Evans, based on subroutines created by Ratliff
c     ca. 1992, with I/O changes and some restructuring courtesy of Janet
c     Luhmann, UC Berkeley, ca. 1994.
c                                          H. Garrett

c     Smainr is an example of how to provide the set up variables
c necessary for the Saturnian radiation model in the "Satrad" package.  The
c inputs and common variables are listed below.  Note that the primary
c input is observer position, species (electron or proton), and energy.
c The Satrad package returns the electron and proton differential
c and integral omindirectional energy flux.

c Variables:
c [variable names are enclosed in single quotes...  'variable'.]

c       INPUTS:
c      'EE(n)'   = Vector of energies at which fluxes are to be
c               estimated; "n" is the number of energies to be computed.
c                      Units are MeV.
c      'E'              = Input energy at which fluxes are to be
c                      estimated by Satrad.  Units are MeV.

c      'N'              =      Number of integration steps in Eq. 10, Ref. 1
c                      (typically, N = 7)

c Coordinate System:
c      'ALAT'        = Input latitude at which fluxes are to be
c               estimated by Satrad.  Units are degrees
c               (north is positive, south negative).
c      'RS'          = Input radial distance at which fluxes are to be
c               estimated by Satrad.  Units are Saturnian radii
c               (1 Rj = 60,330 km).
c      'WLONG'       = Input longitude at which fluxes are to be
c               estimated by Satrad.  Units are degrees
c                      (longitude is positive westward).

c      OUTPUTS:
c      'OFLX(4)' = Output vector from Satrad (Note: all values are
c               log base 10):
c                           OFLX(1)=J(CM**2-S)**-1              for electrons
c                           OFLX(2)=DJ/DE(CM**2-S-MEV)**-1  for electrons
c                           OFLX(3)=J(CM**2-S)**-1              for protons
c                           OFLX(4)=DJ/DE(CM**2-S-MEV)**-1  for protons
c                     where:
c                           J = omnidirectional integral flux as given by
c                                 Eq. 4, Ref. 1
```

```
c                              DJ/DE = omnidirectional differential flux
c      'OOF(4,n)' = Output matrix of (10**OFLX) values at energies 1,...,n.
c      'VX'       = Output vector such that:
c                           V(1)  = Bx component of magnetic field (units of G)
c                           V(2)  = By component of magnetic field (units of G)
c                           V(3)  = Bz component of magnetic field (units of G)
c                           V(4)  = B magnitude of magnetic field (units of G)
c                           V(5)  = L value of field line through point
c                           V(6)  = Cutoff latitude of field line through point
c                                   (cutoff means top of atmosphere)
c                           V(7)  = Be, amplitude of field line at equator
c                           V(8)  = Bc, cutoff field strength along field line
c                           V(9)  = B, amplitude at mirror point for given pitch
c                                   angle
c                           V(10) = theta, magnetic co-latitude (in degrees) of
c                                   point
c                           V(11) = OFLX(1)
c                           V(12) = OFLX(2)
c                           V(13) = OFLX(3)
c                           V(14) = OFLX(4)

c   'ALE(21)'    =      L shell values for electron model (Table 5, Ref. 1).
c   'AAE(14,21)' =      Parameter values for electron model (Table 5, Ref. 1).
c   'ALP(28)'    =      L shell values for proton model (Table 6, Ref. 1).
c   'AAP(14,28)' =      Parameter values for proton model (Table 6, Ref. 1).
c   'BB(14,19)'  =      Matrix of critical latitude and B field and of B at
c                       the magnetic equator such that (note: BB(4-14,19) are
c                            not used!!):
c     BB(1,1-19) = Equatorial field strength at L values
c                       given in vector AL0 (see Satrad)
c     BB(2,1-19) = Cufoff field strength at L values
c                       given in vector AL0 (see Satrad)
c     BB(3,1-19) = Cufoff latitude at L values given in vector
c                       AL0 (see Satrad)



      DIMENSION EE(13),OFLX(4),OOF(4,13),OOFT(4,13),VX(14)
            character*80 aa
      COMMON/RADAT/VX

c      Input array values for energy steps (EE)

      DATA EE/.1,.2,.3,.5,1.0,2.0,3.0,5.0,10.0,30.,100.,300.,1000.0/

c      Default values for west longitude (WLONG = 0; the magnetic and
c       spin axes are assumed to be aligned) and the number of
c      angular integration steps (can be as high as ~98).

      DATA WLONG,N/0.0,14/

c      Main output data files

c      For this exercise, we will use TIME = 1 minute = 60 s
c      e.g., time = 60.
c      Here we will read time from input file...

      DO 10 J=1,4
        DO 10 IE=1,13
   10     OOFT(J,IE)= 0

      OPEN(2,FILE='SOrbitfluence.dat')
      write(2,*)'Divine, IOM 5217-90-029, 02/28/90'
        write(2,*)' '
      write(2,*)'FLUENCE SPECTRA'

      OPEN(5,FILE='Sfluence.dat')
      write(5,*)'Divine IOM 5217-90-029, 02/28/90'
        write(5,*)' '
      write(5,*)'FLUENCE SPECTRA'
      write(5,*)'                    Electrons
     x  Protons'
```

```
      write(5,*)'Energy       Integral     Differential            Integ
     xral     Differential'
      write(5,*)'(MeV)        (cm**-2)     (cm**2 MeV)**-1         (cm**
     x-2)     (cm**2 MeV)**-1'

      OPEN(4,FILE='Sfluxint.dat')
      write(4,*)'Divine IOM 5217-90-029, 02/28/90'
      write(4,*)'Energy (MeV) levels E(1) to E(13) are:'
      write(4,103) (EE(i), i=1,13)
      write(4,*) ' '
      write(4,*)'INTEGRAL FLUX SPECTRA'
      write(4,*)'Each line contains the following sequence of informatio
     xn:'
      write(4,104)
      write(4,*)'Time(JD)   Range(Rs)  Lat(deg) WLong(deg) B(gauss) Beq(
     xgauss)  L-shell  Blat(deg)  Se(E(1)   Se(E(2))  Se(E(3))  Se(E(4))
     xSe(E(5))  Se(E(6))  Se(E(7))  Se(E(8))  Se(E(9))  Se(E(10)) Se(E(1
     x1)) Se(E(12)) Se(E(13)) Sp(E(1)   Sp(E(2))  Sp(E(3))  Sp(E(4))  Sp
     x(E(5))  Sp(E(6))  Sp(E(7))  Sp(E(8))  Sp(E(9))  Sp(E(10)) Sp(E(11)
     x) Sp(E(12)) Sp(E(13))'

      write(4,*)' '

      OPEN(3,FILE='Sfluxdiff.dat')
      write(3,*)'Divine IOM 5217-90-029, 02/28/90'
      write(3,*)'Energy (MeV) levels E(1) to E(13) are:'
      write(3,103) (EE(i), i=1,13)
      write(3,*) ' '
      write(3,*)'DIFFERENTIAL FLUX SPECTRA'
      write(3,*)'Each line contains the following sequence of informatio
     xn:'
      write(3,105)
      write(3,*)'Time(JD)   Range(Rs)  Lat(deg) WLong(deg) B(gauss) Beq(
     xgauss)  L-shell  Blat(deg)  Se(E(1)   Se(E(2))  Se(E(3))  Se(E(4))
     xSe(E(5))  Se(E(6))  Se(E(7))  Se(E(8))  Se(E(9))  Se(E(10)) Se(E(1
     x1)) Se(E(12)) Se(E(13)) Sp(E(1)   Sp(E(2))  Sp(E(3))  Sp(E(4))  Sp
     x(E(5))  Sp(E(6))  Sp(E(7))  Sp(E(8))  Sp(E(9))  Sp(E(10)) Sp(E(11)
     x) Sp(E(12)) Sp(E(13))'

      write(3,*)' '

c   Loop to setup position (rs,lat,wlong)
c   Read from file traj.in. Format is julian date, radial distance
c   in Rs, latitude (deg), and west longitude (deg).

      open(8,file='traj.in')

c   Header files
      read(8,101)aa
      write(*,*)aa
      read(8,101)aa
      write(*,*)aa
      read(8,101)aa
      write(*,*)aa

c   Lines of data
      read(8,*)NN,time
      write(*,*)NN,time
      read(8,101)aa
      write(*,*)aa

      do 2 irj =1,1000

      read(8,*)date,rs,alat,wlong,al,B,Be,Bc

c   Check for end of orbital segment
      if (date.eq. 1.0) go to 22
c   Check for end of data
      if (date.eq. 2.0) go to 3

c    Loop to setup energy channel
```

```
      DO 1 IE=1,13
      E=EE(IE)

c     Main call to Satrad library

c      CALL SATRAD(E,ALAT,Rs,WLONG,N,OFLX)
       Call Satradxx(E,B,Bc,Be,AL,ALAT,Rs,WLNG,N,OFLX)

c     Check loop to catch "-999" zero value flags (actually the
c     -999 represents 0.0 value as all OFLX values are log base 10 and
c     10**-999=0 is valid...).  Note that OFLX and OOF are log base 10.

      DO 1 J=1,4
      IF(OFLX(J).EQ.-999.) OOF(J,IE)=0.0
      IF(OFLX(J).EQ.-999.) GO TO 1
      OOF(J,IE)=10.**OFLX(J)
      OOFT(J,IE)=OOFT(J,IE)+OOF(J,IE)*TIME
    1 CONTINUE

c     Output:

      b=vx(4)
      be=vx(7)
      AL=vx(5)
      BLAT=90.-VX(10)

      WRITE(4,100)date,rs,alat,wlong,b,be,al,blat,(oof(1,ie),
     x  ie=1,13),(oof(3,ie),ie=1,13)
      WRITE(3,100)date,rs,alat,wlong,b,be,al,blat,(oof(2,ie),
     x  ie=1,13),(oof(4,ie),ie=1,13)
      dater=date
      go to 2

   22 CONTINUE
      write(2,*)dater
      write(2,*)'      Electrons'
      write(2,*)'Energy       Integral'
      write(2,*)'(MeV)        (cm**-2)'
      do 5 ie = 1,13
    5 write(2,102)ee(ie),ooft(1,ie)
      write(2,*)'      Protons'
      write(2,*)'Energy       Integral'
      write(2,*)'(MeV)        (cm**-2)'
      do 6 ie = 1,13
    6 write(2,102)ee(ie),ooft(3,ie)
      write(2,*)' '
    2 continue

    3 CONTINUE

      do 4 ie = 1,13
    4 write(5,102)ee(ie),(ooft(j,ie),j=1,4)

  100 format(f10.4,7(1x,e9.3),13(1x,e9.3),13(1x,e9.3))
  101 format(1a80)
  102 format(f9.2,4x,e9.3,3x,e9.3,15x,e9.3,4x,e9.3)
  103 format(13(f10.2))
  104 format(140x,'Electron_Flux (cm^2-s)^-1',120x,
     x'Proton_Flux (cm^2-s)^-1)')
  105 format(140x,'Electron_Flux (cm^2-s-MeV)^-1',115x,
     x'Proton_Flux (cm^2-s-MeV)^-1)')
      CLOSE(2,STATUS='KEEP')
      CLOSE(3,STATUS='KEEP')
      CLOSE(4,STATUS='KEEP')
      CLOSE(5,STATUS='KEEP')

      pause

      STOP
      END

c      'VX'          = Output vector such that:
```

```
c             V(1)  = Brad radial component of magnetic field (units of G)
c             V(2)  = Btheta component of magnetic field (units of G)
c             V(3)  = Bphi component of magnetic field (units of G)
c             V(4)  = B magnitude of magnetic field (units of G)
c             V(5)  = L value of field line through point
c             V(6)  = Cutoff latitude of field line through point
c                     (cutoff means top of atmosphere)
c             V(7)  = Be, amplitude of field line at equator
c             V(8)  = Bc, cutoff field strength along field line
c             V(9)  = B, amplitude at mirror point for given pitch
c                     angle
c             V(10) = theta, magnetic co-latitude (in degrees) of point
c             V(11) = OFLX(1)
c             V(12) = OFLX(2)
c             V(13) = OFLX(3)
c             V(14) = OFLX(4)

C *************************
C     Contains RDD/DMU corrections.

      SUBROUTINE SATRADxx(E,B,Bc,Beq,AL,ALAT,RS,WLONG,N,OFLX)

      DIMENSION VX(14),XX(100),CUR(4,100),CUR1(100),OFLX(4)
      COMMON/RADAT/VX
C** Corrected 09/2000 (more accurate) HBG
      RDD=.017453292

      ALPHA=0
      Vx(1)=0
      Vx(2)=0
      Vx(3)=0
      Vx(6)=0
      Vx(4)=B
      Vx(5)=AL
      Vx(7)=Beq
      VX(8)=BC

      BM=B/(SIN(ALPHA*RDD)**2)
      Vx(9)=Bm

      Theta=90.-alat
      Vx(10)=Theta

c  If the L shell is less than 2.3 or greater than 13, then
c  the model gives 0 values.  As the data are log base 10, a
c  common value of -999 is assumed to indicate "0".

      IF(AL.LT.2.3 .or. AL.GT.13.) GO TO 55

c  If the magnetic field amplitude  B is greater than BC, then
c  the particle is in the loss cone and its flux is set to "0".

      IF(B.GE.BC)GO TO 55

c  'dMu' = differential step in pitch angle used in the integral.
c  It is given by dividing the critical pitch angle by N-1 intervals.

      BMUC=SQRT(1.-B/BC)
      DMU=BMUC/(N-1)

c** Corrected for numerical inaccuracy 09/2000 HBG
      dmu=dmu-.000001*dmu

c  This is the main loop to set up the pitch angle integrations.

      DO 1 IA=1,N
        XX(IA)=FLOAT(IA-1)*DMU
        ALPHA=ACOS(FLOAT(IA-1)*DMU)/RDD

c  'ALPHA' = pitch angle of particle.

      CALL SRADBL(B,Bc,Beq,AL,ALAT,RS,WLONG,ALPHA,E)
```

```
      CUR(1,IA)=VX(11)
      CUR(2,IA)=VX(12)
      CUR(3,IA)=VX(13)
      CUR(4,IA)=VX(14)
    1 CONTINUE

c  (Carry out actual integral....)
      DO 3 IFF=1,4
       IF (CUR(IFF,1).EQ.0.0) OFLX(IFF)=-999
       IF (CUR(IFF,1).EQ.0.0) GO TO 3
      DO 4 IA=1,N
4      CUR1(IA)=CUR(IFF,IA)
      CALL INTEG(CUR1,XX,N,OF)
       OFLX(IFF)=ALOG10(OF*4.*3.14159)
    3 CONTINUE
      RETURN

c  As stated this is the section when L is outside range

   55 DO 56 I=1,4
   56 OFLX(I)=-999
      RETURN
      END

      SUBROUTINE SRADBL(B,Bcc,Bee,AL,ALAT,RS,WLONG,ALPHA,E)

C     PROGRAM TO FIND HIGH ENERGY FLUXES OF ELECTRONS AND PROTONS
C     FIE=I(CM**2-S-SR)**-1 FOR ELECTRONS
C     FDE=DI/DE(CM**2-S-SR-MEV)**-1 FOR ELECTRONS
C     FIP=I(CM**2-S-SR)**-1 FOR PROTONS
C     FDP=DI/DE(CM**2-S-SR-MEV)**-1 FOR PROTONS

      COMMON /RADAT/Brad,Btheta,Bphi,Bt,AL1,ALATC,
     1       BE,BC,BM,THETA,FIE,FDE,FIP,FDP

C** Corrected 09/2000 (more accurate) HBG
      RDD=.017453292

      be=bee
      bc=bcc

c     Is ALPHA along the field line?  If so, flux = 0.

      IF (ALPHA.EQ.0.0) GO TO 49
      IF (ALPHA.EQ.180.) GO TO 49

C     Is BM<=BC?  If not, then flux = 0.

      BM=B/(SIN(ALPHA*RDD)**2)
      IF (BM.GT.BC) GO TO 49

C    FIND ELECTRON INTEGRAL/DIFFERENTIAL INTENSITIES
      call eIntensity(alpha,E,Be,B,AL,FIE,FDE)
      call pIntensity(alpha,E,Be,B,AL,FIP,FDP)

      GO TO 50

c      Zero flux trap....
   49 FIE=0
      FDE=0
      FIP=0
      FDP=0
      BM=999.

   50 CONTINUE

      RETURN
      END


      Subroutine eIntensity(pitch,Energy,Beqmag,Bmag,Lvalue,
```

```
     %                        eiintst,edintst)
c         Calculate the Intensity for a specified pitch angle
c         and (r,colat,elong) geographic position.
      real E2x, E3x, Energy, pitch, AA(4), Lvalue

c      Get A coefficients:
      eiintst=0.0
      edintst=0.0
      call eAcoeff(pitch,AA,E2x,E3x,Beqmag,Bmag,Lvalue,iflagout)
        if(iflagout.ne.0)return

      x1= AA(1) - AA(2)*alog10(Energy)
      x2=.5*(AA(2)-AA(3))*alog10((Energy**2+E2x**2)/(1.+ E2x**2))
      x3=(AA(3)-AA(4))*alog10((Energy**3+E3x**3)/(1.+E3x**3))/3.
      eiintst = 10.**(x1+x2+x3)

      edintst=(eiintst/Energy)*(AA(2)+(AA(3)-AA(2))/
     %       (1.+(E2x/Energy)**2)+(AA(4)-AA(3))/(1.+(E3x/Energy)**3))

      Return
      End

      Subroutine eAcoeff(pitch,AA,E2x,E3x,Beqmag,Bmag,Lvalue,iflagout)
      real Lvalue
      real AA(4), An(4,27), Bn(4,27), pitch, Ax(4), Bx(4)
      real E2(27), E3(27), E2x, E3x, Ltable(27)
      data (An(i,1), i=1,4) /4.74, 0.00, 0.00, 6.47/
      data (An(i,2), i=1,4) /5.02, 0.00, 0.00, 4.01/
      data (An(i,3), i=1,4) /4.91, 0.00, 0.00, 4.86/
      data (An(i,4), i=1,4) /4.98, 0.00, 0.00, 4.41/
      data (An(i,5), i=1,4) /5.00, 0.00, 0.00, 5.37/
      data (An(i,6), i=1,4) /5.49, 0.00, 0.23, 3.00/
      data (An(i,7), i=1,4) /5.56, 0.00, 0.34, 3.00/
      data (An(i,8), i=1,4) /5.51, 0.00, 0.27, 4.48/
      data (An(i,9), i=1,4) /5.52, 0.00, 0.25, 3.11/
      data (An(i,10), i=1,4)/5.46, 0.00, 0.28, 3.42/
      data (An(i,11), i=1,4)/5.38, 0.00, 0.27, 4.96/
      data (An(i,12), i=1,4)/5.31, 0.00, 0.29, 5.23/
      data (An(i,13), i=1,4)/5.03, 0.00, 0.20, 5.48/
      data (An(i,14), i=1,4)/5.50, 0.00, 0.00, 4.27/
      data (An(i,15), i=1,4)/4.88, 0.00, 0.20, 5.71/
      data (An(i,16), i=1,4)/4.67, 0.00, 0.00, 4.29/
      data (An(i,17), i=1,4)/4.74, 0.00, 0.00, 4.23/
      data (An(i,18), i=1,4)/3.58, 0.00, 0.34, 5.74/
      data (An(i,19), i=1,4)/3.50, 0.00, 0.27, 5.26/
      data (An(i,20), i=1,4)/4.57, 0.00, 0.05, 6.67/
      data (An(i,21), i=1,4)/3.26, 0.00, 0.00, 4.22/
      data (An(i,22), i=1,4)/3.95, 0.00, 0.06, 3.00/
      data (An(i,23), i=1,4)/3.33, 0.00, 0.00, 6.10/
      data (An(i,24), i=1,4)/3.42, 0.00, 0.00, 5.50/
      data (An(i,25), i=1,4)/3.02, 0.00, 0.83, 6.00/
      data (An(i,26), i=1,4)/3.64, 0.00, 1.17, 3.01/
      data (An(i,27), i=1,4)/2.09, 2.23, 0.00, 7.59/

      data (Bn(i,1), i=1,4) /4.74, 0.00, 0.00, 6.47/
      data (Bn(i,2), i=1,4) /5.02, 0.00, 0.00, 4.01/
      data (Bn(i,3), i=1,4) /4.91, 0.00, 0.00, 4.86/
      data (Bn(i,4), i=1,4) /4.98, 0.00, 0.00, 4.41/
      data (Bn(i,5), i=1,4) /5.00, 0.00, 0.00, 5.37/
      data (Bn(i,6), i=1,4) /5.49, 0.00, 0.23, 3.00/
      data (Bn(i,7), i=1,4) /5.56, 0.00, 0.34, 3.00/
      data (Bn(i,8), i=1,4) /5.51, 0.00, 0.27, 4.48/
      data (Bn(i,9), i=1,4) /5.52, 0.00, 0.25, 3.11/
      data (Bn(i,10), i=1,4)/5.46, 0.00, 0.28, 3.42/
      data (Bn(i,11), i=1,4)/5.38, 0.00, 0.27, 4.96/
      data (Bn(i,12), i=1,4)/5.48, 0.00, 0.29, 5.23/
      data (Bn(i,13), i=1,4)/5.74, 0.00, 0.20, 5.48/
      data (Bn(i,14), i=1,4)/4.90, 0.00, 0.61, 4.27/
      data (Bn(i,15), i=1,4)/4.72, 0.21, 0.78, 5.71/
      data (Bn(i,16), i=1,4)/4.50, 0.00, 0.56, 4.29/
      data (Bn(i,17), i=1,4)/4.12, 0.00, 0.68, 4.23/
      data (Bn(i,18), i=1,4)/5.30, 0.00, 0.11, 5.74/
```

```
      data (Bn(i,19), i=1,4)/5.38, 0.00, 0.11, 5.26/
      data (Bn(i,20), i=1,4)/3.73, 1.01, 0.68, 6.67/
      data (Bn(i,21), i=1,4)/4.60, 0.26, 0.00, 4.22/
      data (Bn(i,22), i=1,4)/4.83, 0.00, 0.19, 3.00/
      data (Bn(i,23), i=1,4)/3.20, 0.21, 0.66, 6.10/
      data (Bn(i,24), i=1,4)/2.56, 0.16, 2.45, 5.50/
      data (Bn(i,25), i=1,4)/2.11, 0.00, 2.22, 6.00/
      data (Bn(i,26), i=1,4)/1.98, 0.00, 3.78, 3.01/
      data (Bn(i,27), i=1,4)/2.09, 2.23, 0.00, 7.59/

      data Ltable/2.30,2.33,2.34,2.36,2.38,2.46,2.56,2.70,2.83,
     •      2.93,3.04,3.08,3.20,3.40,3.90,4.30,4.44,4.96,5.41,5.87,
     *      6.20,6.50,7.20,8.00,9.50,11.00,13.00/

      data E2/.6,.6,.6,.6,.6,.6,.6,.6,.2,.2,.2,.2,.2,.2,.2,.1,
     *      .1,.1,.1,.1,0.08,0.08,0.08,0.08,0.08,0.08,0.08/
      data E3/1.5,1.5,1.5,1.5,1.5,2.,2.,2.,2.,2.,2.,2.,
     •      2.,2.,1.,1.,1.,1.,1.,0.5,0.5,0.5,0.5,0.5,0.5,0.5/

        iflagout=0
              if (Lvalue.gt.Ltable(27).or.Lvalue.lt.Ltable(1)) then
            iflagout = 1
            goto 520
            end if
c      Interpolate coeffs.
      if(Lvalue .GE. Ltable(27)) then
            nmin=26
            goto 501
            end if
      if(Lvalue .LT. Ltable(7))  then
            nmin=1
            end if
      if(Lvalue.GE.Ltable(7).and.Lvalue.LT.Ltable(13))  then
            nmin=7
            end if
      if(Lvalue.GE.Ltable(13).and.Lvalue.LT.Ltable(20)) then
            nmin=13
            end if
      if(Lvalue.GE.Ltable(20).and.Lvalue.LE.Ltable(27)) then
            nmin=20
            end if
      do 500, j=nmin,26
            if(Lvalue .LT. Ltable(j+1)) then
            nmin=j
            Goto 501
            end if
 500      continue
 501      continue
      scale=(Lvalue-Ltable(nmin))/(Ltable(nmin+1)-Ltable(nmin))
      do 510, I=1,4
      Ax(I) = An(I,nmin) + scale*(An(I,nmin+1)-An(I,nmin))
      Bx(I) = Bn(I,nmin) + scale*(Bn(I,nmin+1)-Bn(I,nmin))
51      continue
 510      continue
      E2x= E2(nmin) + scale*(E2(nmin+1)-E2(nmin))
      E3x= E3(nmin) + scale*(E3(nmin+1)-E3(nmin))

c      Calculate AA
      rp=pitch *3.14159/180.
      do 520, J=1,4
      AA(J) = ((Beqmag/Bmag)*(Ax(J) - Bx(J))*(sin(rp))**2.)+Bx(J)
 520      continue
      Return
      End

      Subroutine pIntensity(pitch, Energy,Beqmag,Bmag,Lvalue,
     %                      piintst,pdintst)

c           Calculate the log of the Intensity for a specified pitch angle
c           and (r, lat) geographic position.
      real E2x, E3x, Energy, pitch, AA(4), Lvalue
```

```
c      Get A coefficients:
       piintst=0.0
       pdintst=0.0

       call pAcoeff(pitch,AA,E2x,E3x,Beqmag,Bmag,Lvalue,iflagout)
         if(iflagout.ne.0)return
       x1 = AA(1) - AA(2)*alog10(Energy)
       x2=0.5*(AA(2)-AA(3))*alog10((Energy**2 + E2x**2)/(1 + E2x**2))
       x3=(1./3.)*(AA(3)-AA(4))*alog10((Energy**3+E3x**3)/(1 + E3x**3))
       piintst =10.**(x1+x2+x3)

       pdintst=(piintst/Energy)*(AA(2)+(AA(3)-AA(2))/
      %(1.+(E2x/Energy)**2)+(AA(4)-AA(3))/(1.+(E3x/Energy)**3))

       Return
       End

       Subroutine pAcoeff(pitch,AA,E2x,E3x,Beqmag,Bmag,Lvalue,iflagout)
       real Lvalue
       real AA(4), An(4,29), Bn(4,29), pitch, Ax(4), Bx(4)
       real E2(29), E3(29), E2x, E3x, Ltable(29)
       data (An(i,1), i=1,4) /1.86, 0.00, 0.00, 4.57/
       data (An(i,2), i=1,4) /2.07, 0.00, 0.00, 4.53/
       data (An(i,3), i=1,4) /2.17, 0.00, 0.00, 6.09/
       data (An(i,4), i=1,4) /3.18, 0.05, 0.00, 3.05/
       data (An(i,5), i=1,4) /2.14, 1.85, 0.00, 3.00/
       data (An(i,6), i=1,4) /3.80, 0.75, 0.00, 3.00/
       data (An(i,7), i=1,4) /3.37, 1.28, 0.00, 3.00/
       data (An(i,8), i=1,4) /3.26, 2.63, 0.00, 3.00/
       data (An(i,9), i=1,4) /3.14, 2.93, 0.00, 3.00/
       data (An(i,10), i=1,4)/0.37, 0.00, 0.00, 3.00/
       data (An(i,11), i=1,4)/2.91, 0.29, 0.00, 3.00/
       data (An(i,12), i=1,4)/2.86, 0.02, 0.02, 3.00/
       data (An(i,13), i=1,4)/2.80, 0.98, 0.00, 3.00/
       data (An(i,14), i=1,4)/2.16, 1.77, 0.00, 3.00/
       data (An(i,15), i=1,4)/-0.13, 0.00, 0.26, 3.00/
       data (An(i,16), i=1,4)/1.29, 0.00, 0.00, 3.00/
       data (An(i,17), i=1,4)/0.63, 0.46, 0.29, 3.22/
       data (An(i,18), i=1,4)/0.61, 5.05, 0.20, 3.12/
       data (An(i,19), i=1,4)/0.47, 5.25, 0.21, 3.55/
       data (An(i,20), i=1,4)/0.68, 1.45, 0.00, 4.41/
       data (An(i,21), i=1,4)/1.77, 0.00, 0.00, 3.00/
       data (An(i,22), i=1,4)/2.32, 3.32, 0.00, 3.08/
       data (An(i,23), i=1,4)/2.40, 3.34, 0.00, 3.00/
       data (An(i,24), i=1,4)/2.46, 2.59, 0.52, 4.72/
       data (An(i,25), i=1,4)/2.46, 3.55, 0.25, 3.85/
       data (An(i,26), i=1,4)/2.31, 6.28, 1.73, 3.35/
       data (An(i,27), i=1,4)/1.90, 6.52, 1.81, 4.11/
       data (An(i,28), i=1,4)/1.24, 0.00, 6.35, 3.94/
       data (An(i,29), i=1,4)/1.22, 0.00, 6.72, 3.31/

       data (Bn(i,1), i=1,4) /1.86, 0.00, 0.00, 4.57/
       data (Bn(i,2), i=1,4) /2.07, 0.00, 0.00, 4.53/
       data (Bn(i,3), i=1,4) /2.17, 0.00, 0.00, 6.09/
       data (Bn(i,4), i=1,4) /3.18, 0.05, 0.00, 3.05/
       data (Bn(i,5), i=1,4) /2.14, 1.85, 0.00, 3.00/
       data (Bn(i,6), i=1,4) /3.80, 0.75, 0.00, 3.00/
       data (Bn(i,7), i=1,4) /3.37, 1.28, 0.00, 3.00/
       data (Bn(i,8), i=1,4) /3.26, 2.63, 0.00, 3.00/
       data (Bn(i,9), i=1,4) /3.14, 2.93, 0.00, 3.00/
       data (Bn(i,10), i=1,4)/0.67, 4.87, 6.27, 3.00/
       data (Bn(i,11), i=1,4)/-0.25, 6.63, 0.00, 3.00/
       data (Bn(i,12), i=1,4)/0.29, 8.30, 0.00, 3.00/
       data (Bn(i,13), i=1,4)/0.46, 7.41, 0.00, 3.00/
       data (Bn(i,14), i=1,4)/0.40, 7.10, 0.00, 3.00/
       data (Bn(i,15), i=1,4)/0.58, 7.70, 0.52, 3.00/
       data (Bn(i,16), i=1,4)/-0.10, 9.00, 0.15, 3.00/
       data (Bn(i,17), i=1,4)/0.16, 8.55, 0.00, 3.22/
       data (Bn(i,18), i=1,4)/-0.03, 6.93, 0.00, 3.12/
       data (Bn(i,19), i=1,4)/-0.06, 7.15, 0.00, 3.55/
       data (Bn(i,20), i=1,4)/-1.13, 6.73, 6.85, 4.41/
       data (Bn(i,21), i=1,4)/-0.98, 6.78, 8.25, 3.00/
```

```
      data (Bn(i,22), i=1,4)/0.10, 5.51, 2.99, 3.08/
      data (Bn(i,23), i=1,4)/0.06, 5.81, 2.66, 3.00/
      data (Bn(i,24), i=1,4)/0.30, 5.83, 0.12, 4.72/
      data (Bn(i,25), i=1,4)/0.81, 4.90, 0.61, 3.85/
      data (Bn(i,26), i=1,4)/1.07, 0.48, 1.73, 3.35/
      data (Bn(i,27), i=1,4)/0.74, 0.00, 0.85, 4.11/
      data (Bn(i,28), i=1,4)/1.24, 0.00, 6.35, 3.94/
      data (Bn(i,29), i=1,4)/1.22, 0.00, 6.72, 3.31/

      data Ltable/2.30,2.32,2.34,2.43,2.52,2.67,2.77,2.82,2.86,
     *      3.10,3.20,3.31,3.44,3.71,3.99,4.13,4.27,4.38,4.49,5.01,5.36,
     *      6.20,6.45,6.70,7.63,8.40,10.30,12.00,13.00/

      data E2/1.,1.,1.,1.,1.,1.,0.5,0.3,0.3,1.,1.,0.5,0.5,0.5,0.5,0.5,
     *      0.5,0.5,0.5,0.5,0.5,0.5,0.5,0.5,0.5,0.3,0.3,0.3,0.3/
      data E3/60.,60.,60.,60.,60.,60.,60.,60.,60.,60.,60.,60.,
     *  60.,60.,60.,60.,60.,60.,0.8,0.8,0.8,0.8,0.8,0.8,0.8,0.8,0.8,0.8/

        iflagout=0
        if(Lvalue.gt.Ltable(29) .or. Lvalue .lt. Ltable(1)) then
            iflagout = 1
            goto 520
            end if
c      Interpolate coeffs.
      if(Lvalue .GE. Ltable(29)) then
            nmin=28
            goto 501
            end if
      if(Lvalue .LT. Ltable(7)) then
            nmin=1
            end if
      if(Lvalue.GE.Ltable(7).and.Lvalue.LT.Ltable(13)) then
            nmin=7
            end if
      if(Lvalue.GE.Ltable(13).and.Lvalue.LT.Ltable(20)) then
            nmin=13
            end if
      if(Lvalue.GE.Ltable(20).and.Lvalue.LE.Ltable(29)) then
            nmin=20
            end if
      do 500, j=nmin,28
            if(Lvalue .LT. Ltable(j+1)) then
            nmin=j
            Goto 501
            end if
 500      continue
 501      continue
      scale=(Lvalue-Ltable(nmin))/(Ltable(nmin+1)-Ltable(nmin))
      do 510, I=1,4
      Ax(I) = An(I,nmin) + scale*(An(I,nmin+1)-An(I,nmin))
      Bx(I) = Bn(I,nmin) + scale*(Bn(I,nmin+1)-Bn(I,nmin))
51      continue
 510      continue
      E2x= E2(nmin) + scale*(E2(nmin+1)-E2(nmin))
      E3x= E3(nmin) + scale*(E3(nmin+1)-E3(nmin))
c      Calculate AA

      rp=pitch *3.14159/180
      do 520, J=1,4
      AA(J) = ((Beqmag/Bmag)*(Ax(J) - Bx(J))*(sin(rp))**2)+Bx(J)
 520      continue
      Return
      End

      SUBROUTINE INTEG(YY,XX,N,AINT)
      DIMENSION YY(1),XX(1)
      AINT =0
      DO 1 I=1,N
    1 AINT=YY(I)+AINT
      AINT=(AINT-(YY(1)+YY(N))*.5)*(XX(2)-XX(1))
      RETURN
      END
```

Input file—"traj.in"

The input file provides the time, trajectory (rs = radial distance in R_s, alat = latitude in degrees, wlong = west longitude in degrees), and magnetic field components (ali = L-shell, bsc = magnetic field amplitude in gauss at spacecraft, beq = magnetic field amplitude in gauss at magnetic equator, bcrit = critical or cut-off magnetic field amplitude at top of atmosphere). "51" is the number of points and "60" is the time step in seconds required to calculate the fluence. The last two rows are for program control.

```
Test Case2 for Saturn--equator
---
---
51        60
  time        rs          alat       wlong     ali          bsc        beq        bcrit      bm
  60.00000    2.30000     .00000     .00000    2.30000      .01708     .01706     .43054     .21536
 120.00000    2.32000     .00000     .00000    2.32000      .01666     .01663     .43272     .21536
 180.00000    2.33000     .00000     .00000    2.33000      .01645     .01643     .43381     .21536
 240.00000    2.34000     .00000     .00000    2.34000      .01624     .01622     .43488     .21536
 300.00000    2.36000     .00000     .00000    2.36000      .01584     .01582     .43701     .21536
 360.00000    2.38000     .00000     .00000    2.38000      .01545     .01544     .43911     .21536
 420.00000    2.43000     .00000     .00000    2.43000      .01454     .01452     .44423     .21536
 480.00000    2.46000     .00000     .00000    2.46000      .01403     .01401     .44723     .21536
 540.00000    2.52000     .00000     .00000    2.52000      .01307     .01305     .45305     .21536
 600.00000    2.56000     .00000     .00000    2.56000      .01247     .01246     .45680     .21536
 660.00000    2.67000     .00000     .00000    2.67000      .01102     .01101     .46666     .21536
 720.00000    2.70000     .00000     .00000    2.70000      .01066     .01065     .46923     .21536
 780.00000    2.77000     .00000     .00000    2.77000      .00989     .00988     .47505     .21536
 840.00000    2.82000     .00000     .00000    2.82000      .00938     .00937     .47906     .21536
 900.00000    2.83000     .00000     .00000    2.83000      .00928     .00928     .47985     .21536
 960.00000    2.86000     .00000     .00000    2.86000      .00900     .00899     .48218     .21536
1020.00000    2.93000     .00000     .00000    2.93000      .00838     .00837     .48747     .21536
1080.00000    3.04000     .00000     .00000    3.04000      .00751     .00751     .49536     .21536
1140.00000    3.08000     .00000     .00000    3.08000      .00723     .00722     .49811     .21536
1200.00000    3.10000     .00000     .00000    3.10000      .00709     .00709     .49946     .21536
1260.00000    3.20000     .00000     .00000    3.20000      .00645     .00645     .50599     .21536
1320.00000    3.31000     .00000     .00000    3.31000      .00584     .00583     .51277     .21536
1380.00000    3.40000     .00000     .00000    3.40000      .00539     .00539     .51802     .21536
1440.00000    3.44000     .00000     .00000    3.44000      .00521     .00520     .52028     .21536
1500.00000    3.71000     .00000     .00000    3.71000      .00416     .00416     .53432     .21536
1560.00000    3.90000     .00000     .00000    3.90000      .00359     .00358     .54310     .21536
1620.00000    3.99000     .00000     .00000    3.99000      .00335     .00335     .54697     .21536
1680.00000    4.13000     .00000     .00000    4.13000      .00302     .00302     .55268     .21536
1740.00000    4.27000     .00000     .00000    4.27000      .00274     .00274     .55800     .21536
1800.00000    4.30000     .00000     .00000    4.30000      .00268     .00268     .55910     .21536
1860.00000    4.38000     .00000     .00000    4.38000      .00254     .00254     .56195     .21536
1920.00000    4.44000     .00000     .00000    4.44000      .00244     .00244     .56402     .21536
1980.00000    4.49000     .00000     .00000    4.49000      .00236     .00236     .56569     .21536
2040.00000    4.96000     .00000     .00000    4.96000      .00175     .00175     .57971     .21536
2100.00000    5.01000     .00000     .00000    5.01000      .00170     .00170     .58103     .21536
2160.00000    5.36000     .00000     .00000    5.36000      .00139     .00139     .58951     .21536
2220.00000    5.41000     .00000     .00000    5.41000      .00135     .00135     .59061     .21536
2280.00000    5.87000     .00000     .00000    5.87000      .00106     .00106     .59972     .21536
2340.00000    6.20000     .00000     .00000    6.20000      .00090     .00090     .60521     .21536
2400.00000    6.45000     .00000     .00000    6.45000      .00080     .00080     .60887     .21536
2460.00000    6.50000     .00000     .00000    6.50000      .00078     .00078     .60956     .21536
2520.00000    6.70000     .00000     .00000    6.70000      .00071     .00071     .61215     .21536
2580.00000    7.20000     .00000     .00000    7.20000      .00057     .00057     .61768     .21536
2640.00000    7.63000     .00000     .00000    7.63000      .00048     .00048     .62152     .21536
2700.00000    8.00000     .00000     .00000    8.00000      .00042     .00042     .62423     .21536
2760.00000    8.40000     .00000     .00000    8.40000      .00036     .00036     .62664     .21536
2820.00000    9.50000     .00000     .00000    9.50000      .00025     .00025     .63108     .21536
2880.00000   10.30000     .00000     .00000   10.30000      .00020     .00020     .63598     .21536
2940.00000   11.00000     .00000     .00000   11.00000      .00016     .00016     .63975     .21536
3000.00000   12.00000     .00000     .00000   12.00000      .00012     .00012     .64447     .21536
3060.00000   13.00000     .00000     .00000   13.00000      .00010     .00010     .64852     .21536
         1          0           0          0          0            0          0          0
         2          0           0          0          0            0          0          0
```

Sample Output Data—Sfluence.dat

Electron and proton integral and differential fluences at specified energies.

```
Divine IOM 5217-90-029, 02/28/90

 FLUENCE SPECTRA
                        Electrons                                Protons
 Energy          Integral      Differential              Integral      Differential
 (MeV)           (cm**-2)     (cm**2 MeV)**-1            (cm*•-2)     (cm**2 MeV)**-1
      .10     0.987E+10    0.143E+11                 0.315E+10     0.157E+12
      .20     0.882E+10    0.837E+10                 0.191E+09     0.291E+10
      .30     0.806E+10    0.702E+10                 0.685E+08     0.468E+09
      .50     0.682E+10    0.541E+10                 0.309E+08     0.701E+08
     1.00     0.463E+10    0.380E+10                 0.183E+08     0.807E+07
     2.00     0.175E+10    0.188E+10                 0.154E+08     0.945E+06
     3.00     0.616E+09    0.603E+09                 0.149E+08     0.278E+06
     5.00     0.123E+09    0.804E+08                 0.146E+08     0.665E+05
    10.00     0.126E+08    0.410E+07                 0.144E+08     0.295E+05
    30.00     0.382E+06    0.400E+05                 0.128E+08     0.148E+06
   100.00     0.908E+04    0.280E+03                 0.245E+07     0.613E+05
   300.00     0.310E+03    0.317E+01                 0.107E+06     0.107E+04
  1000.00     0.783E+01    0.239E-01                 0.289E+04     0.869E+01
```

Sample Output Data—SOrbitfluence.dat

Electron and proton integral fluences for input into a typical radiation program

```
Divine, IOM 5217-90-029, 02/28/90

 FLUENCE SPECTRA
   3060.00
        Electrons
 Energy        Integral
 (MeV)         (cm**-2)
      .10     0.987E+10
      .20     0.882E+10
      .30     0.806E+10
      .50     0.682E+10
     1.00     0.463E+10
     2.00     0.175E+10
     3.00     0.616E+09
     5.00     0.123E+09
    10.00     0.126E+08
    30.00     0.382E+06
   100.00     0.908E+04
   300.00     0.310E+03
  1000.00     0.783E+01
        Protons
 Energy        Integral
 (MeV)         (cm**-2)
      .10     0.315E+10
      .20     0.191E+09
      .30     0.685E+08
      .50     0.309E+08
     1.00     0.183E+08
     2.00     0.154E+08
     3.00     0.149E+08
     5.00     0.146E+08
    10.00     0.144E+08
    30.00     0.128E+08
   100.00     0.245E+07
   300.00     0.107E+06
  1000.00     0.289E+04
```

Sample Output Data—Sfluxdiff.dat

Detailed step-by-step electron and proton differential fluxes at indicated energies.

```
Divine IOM 5217-90-029, 02/28/90
 Energy (MeV) levels E(1) to E(13) are:
      .10       .20       .30       .50      1.00      2.00      3.00      5.00     10.00     30.00    100.00    300.00   1000.00

 DIFFERENTIAL FLUX SPECTRA
 Each line contains the following sequence of information:
                                                                                                                                   Electron_Flux
(cm^2-s-MeV)^-1                                                                                                          Proton_Flux (cm^2-s-
MeV)^-1)
 Time(JD)   Range(Rs)  Lat(deg) WLong(deg) B(gauss) Beq(gauss)  L-shell  Blat(deg)  Se(E(1)   Se(E(2))  Se(E(3))  Se(E(4))Se(E(5))  Se(E(6))  Se(E(7))
Se(E(8))  Se(E(9))  Se(E(10)) Se(E(11)) Se(E(12)) Se(E(13)) Sp(E(1)   Sp(E(2))  Sp(E(3))  Sp(E(4))  Sp(E(5))  Sp(E(6))  Sp(E(7))  Sp(E(8))  Sp(E(9))
Sp(E(10)) Sp(E(11)) Sp(E(12)) Sp(E(13))

   60.0000 0.230E+01 0.000E+00 0.000E+00 0.171E-01 0.171E-01 0.230E+01 0.000E+00 0.227E+05 0.901E+05 0.199E+06 0.506E+06 0.100E+07 0.196E+06 0.199E+05
0.583E+03 0.354E+01 0.976E-03 0.121E-06 0.331E-10 0.411E-14 0.189E-03 0.755E-03 0.170E-02 0.472E-02 0.189E-01 0.755E-01 0.170E+00 0.471E+00 0.187E+01
0.126E+02 0.241E+01 0.852E-02 0.106E-04
  120.0000 0.232E+01 0.000E+00 0.000E+00 0.167E-01 0.166E-01 0.232E+01 0.000E+00 0.226E+05 0.899E+05 0.199E+06 0.514E+06 0.115E+07 0.380E+06 0.658E+05
0.425E+04 0.793E+02 0.132E+00 0.118E-03 0.196E-06 0.175E-09 0.304E-03 0.121E-02 0.273E-02 0.759E-02 0.304E-01 0.121E+00 0.273E+00 0.758E+00 0.300E+01
0.203E+02 0.397E+01 0.146E-01 0.191E-04
  180.0000 0.233E+01 0.000E+00 0.000E+00 0.165E-01 0.164E-01 0.233E+01 0.000E+00 0.217E+05 0.863E+05 0.192E+06 0.498E+06 0.118E+07 0.507E+06 0.115E+06
0.110E+05 0.361E+03 0.148E+01 0.355E-02 0.145E-04 0.347E-07 0.399E-03 0.160E-02 0.360E-02 0.999E-02 0.399E-01 0.160E+00 0.359E+00 0.997E+00 0.394E+01
0.259E+02 0.333E+01 0.547E-02 0.280E-05
  240.0000 0.234E+01 0.000E+00 0.000E+00 0.162E-01 0.162E-01 0.234E+01 0.000E+00 0.220E+05 0.873E+05 0.194E+06 0.499E+06 0.111E+07 0.364E+06 0.625E+05
0.398E+04 0.728E+02 0.117E+00 0.101E-03 0.162E-06 0.140E-09 0.514E-03 0.206E-02 0.463E-02 0.129E-01 0.514E-01 0.206E+00 0.463E+00 0.128E+01 0.507E+01
0.324E+02 0.274E+01 0.200E-02 0.402E-06
  300.0000 0.236E+01 0.000E+00 0.000E+00 0.158E-01 0.158E-01 0.236E+01 0.000E+00 0.225E+05 0.897E+05 0.199E+06 0.515E+06 0.119E+07 0.448E+06 0.892E+05
0.704E+04 0.175E+03 0.464E+00 0.688E-03 0.181E-05 0.268E-08 0.344E+03 0.166E+03 0.105E+03 0.547E+02 0.171E+02 0.370E+01 0.182E+01 0.217E+01 0.757E+01
0.494E+02 0.600E+01 0.883E-02 0.400E-05
  360.0000 0.238E+01 0.000E+00 0.000E+00 0.154E-01 0.154E-01 0.238E+01 0.000E+00 0.312E+05 0.124E+06 0.275E+06 0.706E+06 0.152E+07 0.421E+06 0.612E+05
0.305E+04 0.393E+02 0.363E-01 0.169E-04 0.155E-07 0.722E-11 0.118E+04 0.564E+03 0.356E+03 0.184E+03 0.571E+02 0.118E+02 0.478E+01 0.366E+01 0.112E+02
0.742E+02 0.129E+02 0.384E-01 0.391E-04
  420.0000 0.243E+01 0.000E+00 0.000E+00 0.145E-01 0.145E-01 0.243E+01 0.000E+00 0.150E+06 0.321E+06 0.498E+06 0.852E+06 0.161E+07 0.110E+07 0.334E+06
0.386E+05 0.143E+04 0.672E+01 0.187E-01 0.869E-04 0.241E-06 0.102E+05 0.479E+04 0.299E+04 0.153E+04 0.468E+03 0.935E+02 0.331E+02 0.136E+02 0.266E+02
0.184E+03 0.796E+02 0.136E+01 0.105E-01
  480.0000 0.246E+01 0.000E+00 0.000E+00 0.140E-01 0.140E-01 0.246E+01 0.000E+00 0.325E+06 0.631E+06 0.889E+06 0.126E+07 0.182E+07 0.157E+07 0.687E+06
0.129E+06 0.890E+04 0.111E+03 0.903E+00 0.112E-01 0.903E-04 0.194E+06 0.606E+05 0.301E+05 0.118E+05 0.274E+04 0.470E+03 0.152E+03 0.364E+02 0.137E+02
0.673E+02 0.292E+02 0.507E+00 0.401E-02
  540.0000 0.252E+01 0.000E+00 0.000E+00 0.131E-01 0.131E-01 0.252E+01 0.000E+00 0.474E+06 0.907E+06 0.125E+07 0.170E+07 0.218E+07 0.171E+07 0.736E+06
0.137E+06 0.945E+04 0.118E+03 0.959E+00 0.118E-01 0.959E-04 0.118E+07 0.163E+06 0.512E+05 0.118E+05 0.158E+04 0.205E+03 0.613E+02 0.136E+02 0.291E+01
0.896E+01 0.395E+01 0.709E-01 0.583E-03
  600.0000 0.256E+01 0.000E+00 0.000E+00 0.125E-01 0.125E-01 0.256E+01 0.000E+00 0.593E+06 0.113E+07 0.154E+07 0.204E+07 0.245E+07 0.182E+07 0.771E+06
0.142E+06 0.983E+04 0.123E+03 0.998E+00 0.123E-01 0.998E-04 0.155E+07 0.261E+06 0.917E+05 0.241E+05 0.369E+04 0.512E+03 0.156E+03 0.351E+02 0.811E+01
0.275E+02 0.121E+02 0.218E+00 0.179E-02
  660.0000 0.267E+01 0.000E+00 0.000E+00 0.110E-01 0.110E-01 0.267E+01 0.000E+00 0.473E+06 0.923E+06 0.131E+07 0.186E+07 0.264E+07 0.182E+07 0.589E+06
0.656E+05 0.207E+04 0.725E+01 0.145E-01 0.498E-04 0.996E-07 0.253E+07 0.739E+06 0.353E+06 0.133E+06 0.294E+05 0.493E+04 0.158E+04 0.375E+03 0.128E+03
0.598E+03 0.265E+03 0.476E+01 0.391E-01
  720.0000 0.270E+01 0.000E+00 0.000E+00 0.107E-01 0.106E-01 0.270E+01 0.000E+00 0.442E+06 0.872E+06 0.125E+07 0.181E+07 0.268E+07 0.180E+07 0.539E+06
0.522E+05 0.133E+04 0.329E+01 0.449E-02 0.109E-04 0.149E-07 0.287E+07 0.748E+06 0.333E+06 0.114E+06 0.222E+05 0.341E+04 0.107E+04 0.251E+03 0.924E+02
0.450E+03 0.199E+03 0.358E+01 0.295E-01
  780.0000 0.277E+01 0.000E+00 0.000E+00 0.989E-02 0.988E-02 0.277E+01 0.000E+00 0.102E+07 0.173E+07 0.209E+07 0.228E+07 0.250E+07 0.176E+07 0.631E+06
0.846E+05 0.354E+04 0.197E+02 0.652E-01 0.356E-03 0.118E-05 0.250E+07 0.495E+06 0.186E+06 0.504E+05 0.746E+04 0.990E+03 0.300E+03 0.732E+02 0.429E+02
0.250E+03 0.111E+03 0.199E+01 0.164E-01
```

840.0000 0.282E+01 0.000E+00 0.000E+00 0.938E-02 0.937E-02 0.282E+01 0.000E+00 0.264E+07 0.347E+07 0.331E+07 0.269E+07 0.234E+07 0.170E+07 0.693E+06
0.117E+06 0.700E+04 0.692E+02 0.433E+00 0.422E-02 0.264E-04 0.988E+07 0.867E+06 0.220E+06 0.422E+05 0.492E+04 0.603E+03 0.180E+03 0.453E+02 0.326E+02
0.200E+03 0.886E+02 0.159E+01 0.131E-01
900.0000 0.283E+01 0.000E+00 0.000E+00 0.928E-02 0.928E-02 0.283E+01 0.000E+00 0.339E+07 0.406E+07 0.363E+07 0.277E+07 0.230E+07 0.169E+07 0.705E+06
0.125E+06 0.800E+04 0.888E+02 0.630E+00 0.690E-02 0.489E-04 0.103E+08 0.867E+06 0.217E+06 0.408E+05 0.472E+04 0.578E+03 0.173E+03 0.432E+02 0.305E+02
0.186E+03 0.824E+02 0.148E+01 0.122E-01
960.0000 0.286E+01 0.000E+00 0.000E+00 0.900E-02 0.899E-02 0.286E+01 0.000E+00 0.343E+07 0.409E+07 0.365E+07 0.277E+07 0.228E+07 0.163E+07 0.665E+06
0.113E+06 0.679E+04 0.680E+02 0.432E+00 0.427E-02 0.271E-04 0.117E+08 0.864E+06 0.204E+06 0.369E+05 0.416E+04 0.505E+03 0.151E+03 0.373E+02 0.248E+02
0.150E+03 0.664E+02 0.119E+01 0.981E-02
1020.0000 0.293E+01 0.000E+00 0.000E+00 0.838E-02 0.837E-02 0.293E+01 0.000E+00 0.350E+07 0.416E+07 0.369E+07 0.277E+07 0.222E+07 0.150E+07 0.577E+06
0.887E+05 0.461E+04 0.364E+02 0.178E+00 0.139E-02 0.677E-05 0.131E+08 0.817E+06 0.172E+06 0.270E+05 0.294E+04 0.481E+03 0.196E+03 0.721E+02 0.226E+02
0.108E+02 0.311E+01 0.549E-01 0.452E-03
1080.0000 0.304E+01 0.000E+00 0.000E+00 0.751E-02 0.751E-02 0.304E+01 0.000E+00 0.296E+07 0.355E+07 0.320E+07 0.254E+07 0.234E+07 0.132E+07 0.346E+06
0.270E+05 0.497E+03 0.727E+00 0.556E-03 0.798E-06 0.610E-09 0.156E+08 0.488E+06 0.681E+05 0.627E+04 0.330E+03 0.297E+02 0.967E+01 0.300E+01 0.843E+00
0.385E+00 0.110E+00 0.195E-02 0.160E-04
1140.0000 0.308E+01 0.000E+00 0.000E+00 0.723E-02 0.722E-02 0.308E+01 0.000E+00 0.322E+07 0.385E+07 0.345E+07 0.271E+07 0.242E+07 0.128E+07 0.311E+06
0.215E+05 0.330E+03 0.359E+00 0.198E-03 0.211E-06 0.117E-09 0.150E+08 0.366E+06 0.439E+05 0.331E+04 0.132E+03 0.102E+02 0.328E+01 0.104E+01 0.298E+00
0.134E+00 0.375E-01 0.663E-03 0.545E-05
1200.0000 0.310E+01 0.000E+00 0.000E+00 0.709E-02 0.709E-02 0.310E+01 0.000E+00 0.291E+07 0.349E+07 0.315E+07 0.251E+07 0.232E+07 0.125E+07 0.302E+06
0.205E+05 0.306E+03 0.317E+00 0.167E-03 0.170E-06 0.893E-10 0.145E+08 0.311E+06 0.347E+05 0.237E+04 0.823E+02 0.587E+01 0.190E+01 0.609E+00 0.177E+00
0.821E-01 0.235E-01 0.416E-03 0.342E-05
1260.0000 0.320E+01 0.000E+00 0.000E+00 0.645E-02 0.645E-02 0.320E+01 0.000E+00 0.177E+07 0.218E+07 0.204E+07 0.180E+07 0.203E+07 0.117E+07 0.274E+06
0.171E+05 0.222E+03 0.184E+00 0.752E-04 0.609E-07 0.249E-10 0.178E+08 0.281E+06 0.438E+05 0.782E+04 0.122E+04 0.186E+03 0.587E+02 0.140E+02 0.532E+01
0.263E+02 0.117E+02 0.209E+00 0.172E-02
1320.0000 0.331E+01 0.000E+00 0.000E+00 0.584E-02 0.583E-02 0.331E+01 0.000E+00 0.173E+07 0.209E+07 0.191E+07 0.160E+07 0.170E+07 0.109E+07 0.301E+06
0.253E+05 0.515E+03 0.882E+00 0.805E-03 0.135E-05 0.123E-08 0.406E+08 0.264E+06 0.301E+05 0.424E+04 0.526E+03 0.864E+02 0.361E+02 0.157E+02 0.984E+01
0.297E+02 0.124E+02 0.223E+00 0.183E-02
1380.0000 0.340E+01 0.000E+00 0.000E+00 0.539E-02 0.539E-02 0.340E+01 0.000E+00 0.145E+07 0.172E+07 0.157E+07 0.133E+07 0.160E+07 0.123E+07 0.398E+06
0.429E+05 0.126E+04 0.393E+01 0.691E-02 0.211E-04 0.371E-07 0.248E+08 0.273E+06 0.407E+05 0.670E+04 0.827E+03 0.110E+03 0.359E+02 0.105E+02 0.599E+01
0.266E+02 0.116E+02 0.208E+00 0.171E-02
1440.0000 0.344E+01 0.000E+00 0.000E+00 0.521E-02 0.520E-02 0.344E+01 0.000E+00 0.167E+07 0.184E+07 0.164E+07 0.135E+07 0.152E+07 0.111E+07 0.348E+06
0.356E+05 0.968E+03 0.266E+01 0.407E-02 0.110E-04 0.167E-07 0.205E+08 0.288E+06 0.470E+05 0.790E+04 0.947E+03 0.119E+03 0.356E+02 0.851E+01 0.443E+01
0.249E+02 0.110E+02 0.198E+00 0.163E-02
1500.0000 0.371E+01 0.000E+00 0.000E+00 0.416E-02 0.416E-02 0.371E+01 0.000E+00 0.269E+07 0.220E+07 0.176E+07 0.126E+07 0.106E+07 0.574E+06 0.143E+06
0.102E+05 0.163E+03 0.191E+00 0.115E-03 0.131E-06 0.788E-10 0.120E+08 0.179E+06 0.265E+05 0.373E+04 0.382E+03 0.453E+02 0.134E+02 0.307E+01 0.120E+01
0.605E+01 0.268E+01 0.481E-01 0.396E-03
1560.0000 0.390E+01 0.000E+00 0.000E+00 0.359E-02 0.358E-02 0.390E+01 0.000E+00 0.310E+07 0.223E+07 0.169E+07 0.112E+07 0.808E+06 0.358E+06 0.756E+05
0.419E+04 0.464E+02 0.298E-01 0.925E-05 0.581E-08 0.180E-11 0.185E+08 0.103E+06 0.733E+04 0.486E+03 0.351E+02 0.588E+01 0.273E+01 0.125E+01 0.518E+00
0.273E+00 0.677E-01 0.118E-02 0.972E-05
1620.0000 0.399E+01 0.000E+00 0.000E+00 0.335E-02 0.335E-02 0.399E+01 0.000E+00 0.258E+07 0.193E+07 0.146E+07 0.102E+07 0.824E+06 0.295E+06 0.541E+05
0.302E+04 0.398E+02 0.361E-01 0.165E-04 0.147E-07 0.669E-11 0.282E+08 0.122E+06 0.719E+04 0.363E+03 0.195E+02 0.290E+01 0.129E+01 0.558E+00 0.208E+00
0.740E-01 0.139E-01 0.239E-03 0.196E-05
1680.0000 0.413E+01 0.000E+00 0.000E+00 0.302E-02 0.302E-02 0.413E+01 0.000E+00 0.211E+07 0.163E+07 0.126E+07 0.100E+07 0.920E+06 0.200E+06 0.307E+05
0.184E+04 0.326E+02 0.506E-01 0.419E-04 0.646E-07 0.536E-10 0.434E+08 0.111E+06 0.624E+04 0.419E+03 0.329E+02 0.430E+01 0.157E+01 0.578E+00 0.327E+00
0.103E+01 0.434E+00 0.779E-02 0.640E-04
1740.0000 0.427E+01 0.000E+00 0.000E+00 0.274E-02 0.274E-02 0.427E+01 0.000E+00 0.210E+07 0.163E+07 0.137E+07 0.140E+07 0.111E+07 0.124E+06 0.176E+05
0.122E+04 0.295E+02 0.786E-01 0.119E-03 0.316E-06 0.476E-09 0.333E+08 0.102E+06 0.567E+04 0.337E+03 0.261E+02 0.486E+01 0.234E+01 0.108E+01 0.447E+00
0.237E+00 0.533E-01 0.742E-03 0.468E-05
1800.0000 0.430E+01 0.000E+00 0.000E+00 0.268E-02 0.268E-02 0.430E+01 0.000E+00 0.218E+07 0.170E+07 0.149E+07 0.162E+07 0.115E+07 0.112E+06 0.159E+05
0.114E+04 0.295E+02 0.886E-01 0.152E-03 0.454E-06 0.779E-09 0.177E+08 0.787E+05 0.545E+04 0.393E+03 0.305E+02 0.486E+01 0.215E+01 0.935E+00 0.379E+00
0.213E+00 0.505E-01 0.725E-03 0.473E-05
1860.0000 0.438E+01 0.000E+00 0.000E+00 0.254E-02 0.254E-02 0.438E+01 0.000E+00 0.198E+07 0.153E+07 0.134E+07 0.147E+07 0.106E+07 0.105E+06 0.151E+05
0.110E+04 0.293E+02 0.914E-01 0.163E-03 0.507E-06 0.906E-09 0.117E+08 0.124E+06 0.110E+05 0.752E+03 0.416E+02 0.466E+01 0.171E+01 0.629E+00 0.238E+00
0.160E+00 0.438E-01 0.681E-03 0.485E-05
1920.0000 0.444E+01 0.000E+00 0.000E+00 0.244E-02 0.244E-02 0.444E+01 0.000E+00 0.185E+07 0.143E+07 0.125E+07 0.139E+07 0.102E+07 0.102E+06 0.148E+05
0.110E+04 0.297E+02 0.951E-01 0.175E-03 0.560E-06 0.103E-08 0.127E+08 0.124E+06 0.105E+05 0.688E+03 0.368E+02 0.407E+01 0.148E+01 0.545E+00 0.206E+00
0.142E+00 0.348E-01 0.424E-03 0.228E-05
1980.0000 0.449E+01 0.000E+00 0.000E+00 0.236E-02 0.236E-02 0.449E+01 0.000E+00 0.197E+07 0.151E+07 0.130E+07 0.136E+07 0.929E+06 0.858E+05 0.118E+05
0.807E+03 0.198E+02 0.540E-01 0.835E-04 0.228E-06 0.352E-09 0.137E+08 0.124E+06 0.101E+05 0.638E+03 0.332E+02 0.363E+01 0.132E+01 0.483E+00 0.182E+00
0.128E+00 0.286E-01 0.286E-03 0.121E-05

2040.0000 0.496E+01 0.000E+00 0.000E+00 0.175E-02 0.175E-02 0.496E+01 0.000E+00 0.193E+07 0.171E+07 0.168E+07 0.201E+07 0.115E+07 0.541E+05 0.443E+04
0.153E+03 0.146E+01 0.893E-03 0.267E-06 0.162E-09 0.486E-13 0.191E+08 0.138E+06 0.959E+04 0.520E+03 0.287E+02 0.456E+01 0.275E+01 0.206E+01 0.395E+00
0.193E-02 0.324E-05 0.930E-08 0.152E-10
2100.0000 0.501E+01 0.000E+00 0.000E+00 0.170E-02 0.170E-02 0.501E+01 0.000E+00 0.188E+07 0.167E+07 0.165E+07 0.198E+07 0.115E+07 0.556E+05 0.464E+04
0.165E+03 0.163E+01 0.106E-02 0.337E-06 0.218E-09 0.694E-13 0.117E+08 0.107E+06 0.984E+04 0.967E+03 0.894E+02 0.361E+01 0.427E+00 0.273E-01 0.643E-03
0.168E-05 0.250E-08 0.655E-11 0.971E-14
2160.0000 0.536E+01 0.000E+00 0.000E+00 0.139E-02 0.139E-02 0.536E+01 0.000E+00 0.157E+07 0.143E+07 0.145E+07 0.181E+07 0.114E+07 0.671E+05 0.646E+04
0.277E+03 0.355E+01 0.346E-02 0.173E-05 0.168E-08 0.842E-12 0.178E+08 0.162E+06 0.161E+05 0.237E+04 0.568E+03 0.619E+02 0.131E+02 0.175E+01 0.110E+00
0.136E-02 0.110E-04 0.136E-06 0.110E-08
2220.0000 0.541E+01 0.000E+00 0.000E+00 0.135E-02 0.135E-02 0.541E+01 0.000E+00 0.153E+07 0.140E+07 0.142E+07 0.178E+07 0.114E+07 0.690E+05 0.678E+04
0.299E+03 0.397E+01 0.410E-02 0.219E-05 0.226E-08 0.120E-11 0.168E+08 0.168E+06 0.181E+05 0.278E+04 0.626E+03 0.663E+02 0.140E+02 0.185E+01 0.116E+00
0.142E-02 0.115E-04 0.141E-06 0.113E-08
2280.0000 0.587E+01 0.000E+00 0.000E+00 0.106E-02 0.106E-02 0.587E+01 0.000E+00 0.548E+07 0.228E+07 0.185E+07 0.202E+07 0.967E+06 0.287E+05 0.165E+04
0.359E+02 0.180E+00 0.396E-04 0.387E-08 0.847E-12 0.827E-16 0.149E+08 0.401E+06 0.700E+05 0.114E+05 0.153E+04 0.126E+03 0.250E+02 0.315E+01 0.189E+00
0.221E-02 0.169E-04 0.197E-06 0.151E-08
2340.0000 0.620E+01 0.000E+00 0.000E+00 0.900E-03 0.900E-03 0.620E+01 0.000E+00 0.232E+07 0.291E+07 0.439E+07 0.362E+07 0.387E+06 0.133E+05 0.164E+04
0.115E+03 0.309E+01 0.999E-02 0.186E-04 0.602E-07 0.112E-09 0.401E+08 0.143E+07 0.235E+06 0.304E+05 0.286E+04 0.201E+03 0.381E+02 0.465E+01 0.271E+00
0.305E-02 0.224E-04 0.254E-06 0.187E-08
2400.0000 0.645E+01 0.000E+00 0.000E+00 0.800E-03 0.800E-03 0.645E+01 0.000E+00 0.282E+07 0.349E+07 0.446E+07 0.384E+07 0.652E+06 0.434E+05 0.807E+04
0.949E+03 0.516E+02 0.510E+00 0.323E-02 0.319E-04 0.202E-06 0.496E+08 0.167E+07 0.270E+06 0.346E+05 0.329E+04 0.240E+03 0.469E+02 0.595E+01 0.367E+00
0.451E-02 0.365E-04 0.450E-06 0.365E-08
2460.0000 0.650E+01 0.000E+00 0.000E+00 0.780E-03 0.780E-03 0.650E+01 0.000E+00 0.297E+07 0.363E+07 0.449E+07 0.388E+07 0.723E+06 0.550E+05 0.111E+05
0.145E+04 0.906E+02 0.112E+01 0.906E-02 0.112E-03 0.906E-06 0.477E+08 0.171E+07 0.288E+06 0.388E+05 0.367E+04 0.228E+03 0.391E+02 0.419E+01 0.204E+00
0.172E-02 0.918E-05 0.777E-07 0.416E-09
2520.0000 0.670E+01 0.000E+00 0.000E+00 0.710E-03 0.710E-03 0.670E+01 0.000E+00 0.434E+07 0.454E+07 0.518E+07 0.377E+07 0.446E+06 0.189E+05 0.267E+04
0.221E+03 0.751E+01 0.350E-01 0.977E-04 0.456E-06 0.127E-08 0.409E+08 0.187E+07 0.373E+06 0.617E+05 0.542E+04 0.170E+03 0.174E+02 0.940E+00 0.178E-01
0.330E-04 0.337E-07 0.629E-10 0.643E-13
2580.0000 0.720E+01 0.000E+00 0.000E+00 0.570E-03 0.570E-03 0.720E+01 0.000E+00 0.686E+07 0.640E+07 0.668E+07 0.340E+07 0.133E+06 0.131E+04 0.758E+02
0.204E+01 0.149E-01 0.611E-05 0.118E-08 0.485E-12 0.941E-16 0.587E+08 0.253E+07 0.455E+06 0.650E+05 0.543E+04 0.209E+03 0.254E+02 0.173E+01 0.449E-01
0.140E-03 0.250E-06 0.781E-09 0.140E-11
2640.0000 0.763E+01 0.000E+00 0.000E+00 0.480E-03 0.480E-03 0.763E+01 0.000E+00 0.148E+08 0.781E+07 0.587E+07 0.257E+07 0.110E+06 0.133E+04 0.878E+02
0.278E+01 0.254E-01 0.149E-04 0.425E-08 0.248E-11 0.709E-15 0.850E+08 0.326E+07 0.536E+06 0.680E+05 0.546E+04 0.250E+03 0.352E+02 0.291E+01 0.998E-01
0.482E-03 0.140E-05 0.680E-08 0.198E-10
2700.0000 0.800E+01 0.000E+00 0.000E+00 0.420E-03 0.420E-03 0.800E+01 0.000E+00 0.234E+08 0.848E+07 0.514E+07 0.206E+07 0.980E+05 0.141E+04 0.104E+03
0.380E+01 0.421E-01 0.333E-04 0.133E-07 0.105E-10 0.421E-14 0.228E+09 0.526E+07 0.676E+06 0.684E+05 0.475E+04 0.241E+03 0.375E+02 0.353E+01 0.144E+00
0.904E-03 0.351E-05 0.222E-07 0.863E-10
2760.0000 0.840E+01 0.000E+00 0.000E+00 0.360E-03 0.360E-03 0.840E+01 0.000E+00 0.222E+08 0.854E+07 0.504E+07 0.184E+07 0.783E+05 0.103E+04 0.716E+02
0.244E+01 0.246E-01 0.169E-04 0.573E-08 0.392E-11 0.133E-14 0.617E+09 0.732E+07 0.741E+06 0.643E+05 0.410E+04 0.233E+03 0.402E+02 0.434E+01 0.212E+00
0.178E-02 0.946E-05 0.795E-07 0.422E-09
2820.0000 0.950E+01 0.000E+00 0.000E+00 0.250E-03 0.250E-03 0.950E+01 0.000E+00 0.236E+08 0.929E+07 0.480E+07 0.135E+07 0.421E+05 0.424E+03 0.255E+02
0.720E+00 0.564E-02 0.258E-05 0.564E-09 0.258E-12 0.564E-16 0.498E+09 0.543E+07 0.528E+06 0.443E+05 0.264E+04 0.120E+03 0.175E+02 0.152E+01 0.546E-01
0.283E-03 0.885E-06 0.458E-08 0.143E-10
2880.0000 0.103E+02 0.000E+00 0.000E+00 0.200E-03 0.200E-03 0.103E+02 0.000E+00 0.249E+08 0.750E+07 0.328E+07 0.935E+06 0.574E+05 0.162E+04 0.185E+03
0.118E+02 0.278E+00 0.734E-03 0.109E-05 0.289E-08 0.430E-11 0.427E+09 0.438E+07 0.414E+06 0.338E+05 0.190E+04 0.734E+02 0.949E+01 0.700E+00 0.202E-01
0.736E-04 0.157E-06 0.571E-09 0.122E-11
2940.0000 0.110E+02 0.000E+00 0.000E+00 0.160E-03 0.160E-03 0.110E+02 0.000E+00 0.251E+08 0.614E+07 0.236E+07 0.658E+06 0.700E+05 0.484E+04 0.964E+03
0.125E+03 0.775E+01 0.947E-01 0.758E-03 0.925E-05 0.741E-07 0.432E+08 0.187E+07 0.306E+06 0.318E+05 0.133E+04 0.456E+02 0.602E+01 0.462E+00 0.141E-01
0.554E-04 0.128E-06 0.506E-09 0.117E-11
3000.0000 0.120E+02 0.000E+00 0.000E+00 0.120E-03 0.120E-03 0.120E+02 0.000E+00 0.128E+08 0.334E+07 0.174E+07 0.582E+06 0.269E+05 0.433E+03 0.345E+02
0.139E+01 0.177E-01 0.175E-04 0.888E-08 0.876E-11 0.445E-14 0.114E+07 0.759E+06 0.295E+06 0.370E+05 0.924E+03 0.259E+02 0.349E+01 0.283E+00 0.928E-02
0.409E-04 0.107E-06 0.470E-09 0.123E-11
3060.0000 0.130E+02 0.000E+00 0.000E+00 0.100E-03 0.100E-03 0.130E+02 0.000E+00 0.631E+07 0.154E+07 0.131E+07 0.546E+06 0.105E+05 0.386E+02 0.123E+01
0.155E-01 0.403E-04 0.322E-08 0.104E-12 0.827E-17 0.267E-21 0.124E+07 0.792E+06 0.291E+06 0.334E+05 0.815E+03 0.294E+02 0.500E+01 0.554E+00 0.281E-01
0.248E-03 0.138E-05 0.121E-07 0.677E-10

Sample Output Data—Sfluxint.dat

Detailed step-by-step electron and proton integral fluxes at indicated energies.

```
Divine IOM 5217-90-029, 02/28/90
 Energy (MeV) levels E(1) to E(13) are:
       .10       .20       .30       .50      1.00      2.00      3.00      5.00     10.00     30.00    100.00    300.00   1000.00

 INTEGRAL FLUX SPECTRA
 Each line contains the following sequence of information:
                                                                                                                                Electron_Flux
(cm^2-s)^-1                                                                                                                  Proton_Flux (cm^2-s)^-
1)
 Time(JD)   Range(Rs)  Lat(deg) WLong(deg) B(gauss) Beq(gauss)  L-shell  Blat(deg)  Se(E(1)   Se(E(2))  Se(E(3))  Se(E(4))Se(E(5))  Se(E(6))  Se(E(7))
Se(E(8))  Se(E(9))  Se(E(10)) Se(E(11)) Se(E(12)) Se(E(13)) Sp(E(1)   Sp(E(2))  Sp(E(3))  Sp(E(4))  Sp(E(5))  Sp(E(6))  Sp(E(7))  Sp(E(8))  Sp(E(9))
Sp(E(10)) Sp(E(11)) Sp(E(12)) Sp(E(13))

   60.0000 0.230E+01 0.000E+00 0.000E+00 0.171E-01 0.171E-01 0.230E+01 0.000E+00 0.118E+07 0.118E+07 0.116E+07 0.110E+07 0.677E+06 0.862E+05 0.104E+05
0.463E+03 0.549E+01 0.453E-02 0.187E-05 0.153E-08 0.635E-12 0.892E+03 0.892E+03 0.892E+03 0.892E+03 0.892E+03 0.892E+03 0.892E+03 0.891E+03 0.886E+03
0.746E+03 0.641E+02 0.563E+00 0.233E-02
  120.0000 0.232E+01 0.000E+00 0.000E+00 0.167E-01 0.166E-01 0.232E+01 0.000E+00 0.158E+07 0.157E+07 0.156E+07 0.149E+07 0.104E+07 0.223E+06 0.460E+05
0.452E+04 0.165E+03 0.822E+00 0.245E-02 0.122E-04 0.363E-07 0.145E+04 0.145E+04 0.145E+04 0.145E+04 0.145E+04 0.145E+04 0.145E+04 0.145E+04 0.144E+04
0.121E+04 0.107E+03 0.975E+00 0.422E-02
  180.0000 0.233E+01 0.000E+00 0.000E+00 0.165E-01 0.164E-01 0.233E+01 0.000E+00 0.183E+07 0.182E+07 0.181E+07 0.174E+07 0.129E+07 0.360E+06 0.968E+05
0.141E+05 0.903E+03 0.111E+02 0.886E-01 0.108E-02 0.866E-05 0.162E+04 0.162E+04 0.162E+04 0.162E+04 0.162E+04 0.162E+04 0.162E+04 0.162E+04 0.161E+04
0.132E+04 0.763E+02 0.311E+00 0.528E-03
  240.0000 0.234E+01 0.000E+00 0.000E+00 0.162E-01 0.162E-01 0.234E+01 0.000E+00 0.153E+07 0.152E+07 0.151E+07 0.144E+07 0.100E+07 0.213E+06 0.434E+05
0.420E+04 0.150E+03 0.725E+00 0.209E-02 0.100E-04 0.288E-07 0.182E+04 0.182E+04 0.182E+04 0.182E+04 0.182E+04 0.182E+04 0.182E+04 0.182E+04 0.181E+04
0.144E+04 0.546E+02 0.994E-01 0.660E-04
  300.0000 0.236E+01 0.000E+00 0.000E+00 0.158E-01 0.158E-01 0.236E+01 0.000E+00 0.172E+07 0.172E+07 0.171E+07 0.164E+07 0.118E+07 0.289E+06 0.683E+05
0.820E+04 0.399E+03 0.316E+01 0.156E-01 0.123E-03 0.607E-06 0.313E+04 0.310E+04 0.309E+04 0.308E+04 0.306E+04 0.305E+04 0.305E+04 0.305E+04 0.302E+04
0.246E+04 0.135E+03 0.493E+00 0.738E-03
  360.0000 0.238E+01 0.000E+00 0.000E+00 0.154E-01 0.154E-01 0.238E+01 0.000E+00 0.196E+07 0.196E+07 0.194E+07 0.184E+07 0.123E+07 0.223E+06 0.385E+05
0.291E+04 0.735E+02 0.203E+00 0.315E-03 0.864E-06 0.135E-08 0.536E+04 0.528E+04 0.524E+04 0.518E+04 0.513E+04 0.511E+04 0.510E+04 0.509E+04 0.506E+04
0.423E+04 0.332E+03 0.245E+01 0.825E-02
  420.0000 0.243E+01 0.000E+00 0.000E+00 0.145E-01 0.145E-01 0.243E+01 0.000E+00 0.333E+07 0.331E+07 0.327E+07 0.313E+07 0.250E+07 0.965E+06 0.312E+06
0.519E+05 0.369E+04 0.519E+02 0.481E+00 0.670E-02 0.621E-04 0.206E+05 0.199E+05 0.196E+05 0.191E+05 0.187E+05 0.185E+05 0.184E+05 0.184E+05 0.183E+05
0.163E+05 0.317E+04 0.135E+03 0.345E+01
  480.0000 0.246E+01 0.000E+00 0.000E+00 0.140E-01 0.140E-01 0.246E+01 0.000E+00 0.495E+07 0.490E+07 0.482E+07 0.461E+07 0.382E+07 0.197E+07 0.874E+06
0.227E+06 0.299E+05 0.111E+04 0.301E+02 0.112E+01 0.301E-01 0.301E+05 0.194E+05 0.151E+05 0.113E+05 0.843E+04 0.723E+04 0.696E+04 0.681E+04 0.672E+04
0.597E+04 0.117E+04 0.506E+02 0.132E+01
  540.0000 0.252E+01 0.000E+00 0.000E+00 0.131E-01 0.131E-01 0.252E+01 0.000E+00 0.568E+07 0.561E+07 0.550E+07 0.521E+07 0.422E+07 0.211E+07 0.932E+06
0.241E+06 0.317E+05 0.118E+04 0.320E+02 0.118E+01 0.320E-01 0.643E+05 0.183E+05 0.904E+04 0.399E+04 0.171E+04 0.111E+04 0.992E+03 0.933E+03 0.904E+03
0.801E+03 0.160E+03 0.715E+01 0.194E+00
  600.0000 0.256E+01 0.000E+00 0.000E+00 0.125E-01 0.125E-01 0.256E+01 0.000E+00 0.623E+07 0.614E+07 0.601E+07 0.565E+07 0.450E+07 0.222E+07 0.972E+06
0.251E+06 0.330E+05 0.123E+04 0.333E+02 0.123E+01 0.333E-01 0.100E+06 0.349E+05 0.193E+05 0.967E+04 0.474E+04 0.329E+04 0.300E+04 0.285E+04 0.277E+04
0.246E+04 0.491E+03 0.219E+02 0.597E+00
  660.0000 0.267E+01 0.000E+00 0.000E+00 0.110E-01 0.110E-01 0.267E+01 0.000E+00 0.577E+07 0.570E+07 0.559E+07 0.527E+07 0.412E+07 0.166E+07 0.541E+06
0.835E+05 0.501E+04 0.522E+02 0.348E+00 0.359E-02 0.239E-04 0.341E+06 0.205E+06 0.154E+06 0.110E+06 0.783E+05 0.657E+05 0.628E+05 0.613E+05 0.604E+05
0.537E+05 0.107E+05 0.479E+03 0.130E+02
  720.0000 0.270E+01 0.000E+00 0.000E+00 0.107E-01 0.106E-01 0.270E+01 0.000E+00 0.565E+07 0.559E+07 0.548E+07 0.517E+07 0.402E+07 0.153E+07 0.461E+06
0.618E+05 0.299E+04 0.221E+02 0.100E+00 0.731E-03 0.332E-05 0.320E+06 0.174E+06 0.124E+06 0.843E+05 0.582E+05 0.491E+05 0.471E+05 0.461E+05 0.454E+05
0.404E+05 0.808E+04 0.361E+03 0.982E+01
  780.0000 0.277E+01 0.000E+00 0.000E+00 0.989E-02 0.988E-02 0.277E+01 0.000E+00 0.604E+07 0.590E+07 0.571E+07 0.526E+07 0.407E+07 0.177E+07 0.643E+06
0.120E+06 0.953E+04 0.158E+03 0.174E+01 0.285E-01 0.315E-03 0.203E+06 0.898E+05 0.592E+05 0.394E+05 0.292E+05 0.263E+05 0.257E+05 0.254E+05 0.252E+05
0.225E+05 0.449E+04 0.201E+03 0.546E+01
  840.0000 0.282E+01 0.000E+00 0.000E+00 0.938E-02 0.937E-02 0.282E+01 0.000E+00 0.658E+07 0.626E+07 0.592E+07 0.532E+07 0.411E+07 0.197E+07 0.820E+06
0.193E+06 0.219E+05 0.646E+03 0.135E+02 0.393E+00 0.820E-02 0.418E+06 0.952E+05 0.503E+05 0.303E+05 0.226E+05 0.208E+05 0.205E+05 0.203E+05 0.201E+05
0.180E+05 0.359E+04 0.160E+03 0.437E+01
```

900.0000 0.283E+01 0.000E+00 0.000E+00 0.928E-02 0.928E-02 0.283E+01 0.000E+00 0.674E+07 0.635E+07 0.596E+07 0.533E+07 0.412E+07 0.201E+07 0.862E+06
0.212E+06 0.259E+05 0.857E+03 0.203E+02 0.665E+00 0.157E-01 0.423E+06 0.926E+05 0.480E+05 0.285E+05 0.211E+05 0.194E+05 0.191E+05 0.189E+05 0.187E+05
0.167E+05 0.334E+04 0.149E+03 0.406E+01
960.0000 0.286E+01 0.000E+00 0.000E+00 0.900E-02 0.899E-02 0.286E+01 0.000E+00 0.658E+07 0.618E+07 0.579E+07 0.516E+07 0.395E+07 0.189E+07 0.788E+06
0.186E+06 0.213E+05 0.637E+03 0.135E+02 0.400E+00 0.845E-02 0.442E+06 0.852E+05 0.418E+05 0.238E+05 0.172E+05 0.156E+05 0.154E+05 0.152E+05 0.151E+05
0.135E+05 0.269E+04 0.120E+03 0.327E+01
1020.0000 0.293E+01 0.000E+00 0.000E+00 0.838E-02 0.837E-02 0.293E+01 0.000E+00 0.622E+07 0.581E+07 0.542E+07 0.478E+07 0.359E+07 0.163E+07 0.641E+06
0.137E+06 0.136E+05 0.320E+03 0.521E+01 0.122E+00 0.198E-02 0.440E+06 0.610E+05 0.219E+05 0.752E+04 0.286E+04 0.168E+04 0.137E+04 0.113E+04 0.939E+03
0.687E+03 0.125E+03 0.553E+01 0.151E+00
1080.0000 0.304E+01 0.000E+00 0.000E+00 0.751E-02 0.751E-02 0.304E+01 0.000E+00 0.542E+07 0.508E+07 0.474E+07 0.417E+07 0.299E+07 0.101E+07 0.267E+06
0.289E+05 0.101E+04 0.440E+01 0.112E-01 0.482E-04 0.123E-06 0.389E+06 0.256E+05 0.567E+04 0.101E+04 0.173E+03 0.687E+02 0.518E+02 0.412E+02 0.335E+02
0.244E+02 0.443E+01 0.196E+00 0.534E-02
1140.0000 0.308E+01 0.000E+00 0.000E+00 0.723E-02 0.722E-02 0.308E+01 0.000E+00 0.550E+07 0.513E+07 0.476E+07 0.416E+07 0.292E+07 0.930E+06 0.228E+06
0.218E+05 0.636E+03 0.206E+01 0.379E-02 0.121E-04 0.223E-07 0.343E+06 0.174E+05 0.328E+04 0.466E+03 0.625E+02 0.236E+02 0.179E+02 0.142E+02 0.115E+02
0.834E+01 0.151E+01 0.668E-01 0.182E-02
1200.0000 0.310E+01 0.000E+00 0.000E+00 0.709E-02 0.709E-02 0.310E+01 0.000E+00 0.523E+07 0.490E+07 0.456E+07 0.400E+07 0.283E+07 0.902E+06 0.219E+06
0.206E+05 0.584E+03 0.181E+01 0.317E-02 0.967E-05 0.169E-07 0.317E+06 0.142E+05 0.246E+04 0.315E+03 0.375E+02 0.142E+02 0.108E+02 0.873E+01 0.714E+01
0.520E+01 0.945E+00 0.419E-01 0.114E-02
1260.0000 0.320E+01 0.000E+00 0.000E+00 0.645E-02 0.645E-02 0.320E+01 0.000E+00 0.434E+07 0.414E+07 0.393E+07 0.355E+07 0.261E+07 0.827E+06 0.192E+06
0.166E+05 0.409E+03 0.101E+01 0.137E-02 0.333E-05 0.454E-08 0.344E+06 0.202E+05 0.865E+04 0.493E+04 0.336E+04 0.286E+04 0.275E+04 0.269E+04 0.266E+04
0.237E+04 0.472E+03 0.211E+02 0.574E+00
1320.0000 0.331E+01 0.000E+00 0.000E+00 0.584E-02 0.583E-02 0.331E+01 0.000E+00 0.396E+07 0.376E+07 0.356E+07 0.321E+07 0.241E+07 0.869E+06 0.241E+06
0.279E+05 0.108E+04 0.550E+01 0.167E-01 0.843E-04 0.256E-06 0.607E+06 0.159E+05 0.637E+04 0.405E+04 0.328E+04 0.307E+04 0.301E+04 0.297E+04 0.291E+04
0.255E+04 0.503E+03 0.224E+02 0.611E+00
1380.0000 0.340E+01 0.000E+00 0.000E+00 0.539E-02 0.539E-02 0.340E+01 0.000E+00 0.403E+07 0.386E+07 0.370E+07 0.341E+07 0.270E+07 0.112E+07 0.360E+06
0.534E+05 0.298E+04 0.277E+02 0.162E+00 0.149E-02 0.869E-05 0.422E+06 0.187E+05 0.772E+04 0.434E+04 0.311E+04 0.279E+04 0.273E+04 0.269E+04 0.266E+04
0.236E+04 0.469E+03 0.209E+02 0.570E+00
1440.0000 0.344E+01 0.000E+00 0.000E+00 0.521E-02 0.520E-02 0.344E+01 0.000E+00 0.379E+07 0.361E+07 0.344E+07 0.314E+07 0.245E+07 0.981E+06 0.306E+06
0.431E+05 0.223E+04 0.182E+02 0.927E-01 0.750E-03 0.382E-05 0.374E+06 0.204E+05 0.839E+04 0.444E+04 0.300E+04 0.264E+04 0.257E+04 0.254E+04 0.251E+04
0.224E+04 0.448E+03 0.200E+02 0.544E+00
1500.0000 0.371E+01 0.000E+00 0.000E+00 0.416E-02 0.416E-02 0.371E+01 0.000E+00 0.259E+07 0.235E+07 0.215E+07 0.186E+07 0.130E+07 0.423E+06 0.106E+06
0.104E+05 0.319E+03 0.111E+01 0.222E-02 0.764E-05 0.153E-07 0.225E+06 0.108E+05 0.351E+04 0.143E+04 0.796E+03 0.656E+03 0.631E+03 0.618E+03 0.610E+03
0.544E+03 0.109E+03 0.485E+01 0.132E+00
1560.0000 0.390E+01 0.000E+00 0.000E+00 0.359E-02 0.358E-02 0.390E+01 0.000E+00 0.203E+07 0.177E+07 0.157E+07 0.130E+07 0.845E+06 0.236E+06 0.505E+05
0.389E+04 0.819E+02 0.157E+00 0.162E-03 0.305E-06 0.316E-09 0.276E+06 0.379E+04 0.545E+03 0.116E+03 0.475E+02 0.335E+02 0.295E+02 0.259E+02 0.220E+02
0.156E+02 0.270E+01 0.119E+00 0.324E-02
1620.0000 0.399E+01 0.000E+00 0.000E+00 0.335E-02 0.335E-02 0.399E+01 0.000E+00 0.183E+07 0.161E+07 0.144E+07 0.120E+07 0.757E+06 0.179E+06 0.359E+05
0.292E+04 0.743E+02 0.201E+00 0.305E-03 0.818E-06 0.124E-08 0.400E+06 0.408E+04 0.450E+03 0.640E+02 0.182E+02 0.109E+02 0.896E+01 0.729E+01 0.563E+01
0.347E+01 0.551E+00 0.241E-01 0.655E-03
1680.0000 0.413E+01 0.000E+00 0.000E+00 0.302E-02 0.302E-02 0.413E+01 0.000E+00 0.168E+07 0.149E+07 0.135E+07 0.113E+07 0.638E+06 0.109E+06 0.207E+05
0.192E+04 0.667E+02 0.310E+00 0.856E-03 0.396E-05 0.109E-07 0.543E+06 0.372E+04 0.541E+03 0.182E+03 0.120E+03 0.108E+03 0.105E+03 0.103E+03 0.101E+03
0.889E+02 0.176E+02 0.785E+00 0.214E-01
1740.0000 0.427E+01 0.000E+00 0.000E+00 0.274E-02 0.274E-02 0.427E+01 0.000E+00 0.183E+07 0.164E+07 0.149E+07 0.122E+07 0.538E+06 0.649E+05 0.125E+05
0.140E+04 0.671E+02 0.537E+00 0.270E-02 0.215E-04 0.108E-06 0.433E+06 0.333E+04 0.402E+03 0.874E+02 0.392E+02 0.283E+02 0.249E+02 0.218E+02 0.184E+02
0.129E+02 0.198E+01 0.696E-01 0.145E-02
1800.0000 0.430E+01 0.000E+00 0.000E+00 0.268E-02 0.268E-02 0.430E+01 0.000E+00 0.194E+07 0.175E+07 0.159E+07 0.128E+07 0.518E+06 0.585E+05 0.115E+05
0.133E+04 0.689E+02 0.619E+00 0.354E-02 0.318E-04 0.181E-06 0.249E+06 0.286E+04 0.421E+03 0.952E+02 0.377E+02 0.257E+02 0.225E+02 0.197E+02 0.168E+02
0.120E+02 0.190E+01 0.686E-01 0.148E-02
1860.0000 0.438E+01 0.000E+00 0.000E+00 0.254E-02 0.254E-02 0.438E+01 0.000E+00 0.178E+07 0.160E+07 0.146E+07 0.118E+07 0.483E+06 0.555E+05 0.110E+05
0.131E+04 0.690E+02 0.644E+00 0.384E-02 0.357E-04 0.213E-06 0.205E+06 0.506E+04 0.798E+03 0.133E+03 0.341E+02 0.199E+02 0.171E+02 0.151E+02 0.132E+02
0.996E+01 0.169E+01 0.660E-01 0.155E-02
1920.0000 0.444E+01 0.000E+00 0.000E+00 0.244E-02 0.244E-02 0.444E+01 0.000E+00 0.169E+07 0.152E+07 0.139E+07 0.113E+07 0.465E+06 0.542E+05 0.109E+05
0.131E+04 0.702E+02 0.674E+00 0.414E-02 0.397E-04 0.244E-06 0.219E+06 0.493E+04 0.743E+03 0.119E+03 0.295E+02 0.170E+02 0.146E+02 0.128E+02 0.112E+02
0.836E+01 0.125E+01 0.383E-01 0.680E-03
1980.0000 0.449E+01 0.000E+00 0.000E+00 0.236E-02 0.236E-02 0.449E+01 0.000E+00 0.161E+07 0.144E+07 0.130E+07 0.104E+07 0.408E+06 0.439E+05 0.835E+04
0.930E+03 0.452E+02 0.370E+00 0.191E-02 0.156E-04 0.805E-07 0.231E+06 0.482E+04 0.701E+03 0.108E+03 0.262E+02 0.149E+02 0.128E+02 0.112E+02 0.980E+01
0.723E+01 0.971E+00 0.243E-01 0.342E-03
2040.0000 0.496E+01 0.000E+00 0.000E+00 0.175E-02 0.175E-02 0.496E+01 0.000E+00 0.199E+07 0.181E+07 0.164E+07 0.127E+07 0.388E+06 0.211E+05 0.240E+04
0.135E+03 0.255E+01 0.467E-02 0.465E-05 0.849E-08 0.846E-11 0.308E+06 0.499E+04 0.623E+03 0.921E+02 0.257E+02 0.148E+02 0.114E+02 0.663E+01 0.114E+01
0.135E-01 0.748E-04 0.645E-06 0.352E-08

2100.0000 0.501E+01 0.000E+00 0.000E+00 0.170E-02 0.170E-02 0.501E+01 0.000E+00 0.197E+07 0.179E+07 0.163E+07 0.127E+07 0.392E+06 0.219E+05 0.254E+04
0.146E+03 0.288E+01 0.558E-02 0.593E-05 0.115E-07 0.122E-10 0.198E+06 0.450E+04 0.840E+03 0.189E+03 0.260E+02 0.169E+01 0.293E+00 0.310E-01 0.146E-02
0.115E-04 0.566E-07 0.445E-09 0.220E-11
2160.0000 0.536E+01 0.000E+00 0.000E+00 0.139E-02 0.139E-02 0.536E+01 0.000E+00 0.187E+07 0.172E+07 0.158E+07 0.125E+07 0.419E+06 0.283E+05 0.378E+04
0.263E+03 0.669E+01 0.196E-01 0.326E-04 0.951E-07 0.158E-09 0.299E+06 0.769E+04 0.204E+04 0.844E+03 0.260E+03 0.435E+02 0.134E+02 0.292E+01 0.367E+00
0.136E-01 0.367E-03 0.136E-04 0.367E-06
2220.0000 0.541E+01 0.000E+00 0.000E+00 0.135E-02 0.135E-02 0.541E+01 0.000E+00 0.186E+07 0.171E+07 0.157E+07 0.125E+07 0.423E+06 0.294E+05 0.400E+04
0.286E+03 0.756E+01 0.234E-01 0.416E-04 0.129E-06 0.229E-09 0.289E+06 0.835E+04 0.232E+04 0.948E+03 0.283E+03 0.463E+02 0.142E+02 0.309E+01 0.386E+00
0.142E-01 0.382E-03 0.141E-04 0.378E-06
2280.0000 0.587E+01 0.000E+00 0.000E+00 0.106E-02 0.106E-02 0.587E+01 0.000E+00 0.203E+07 0.169E+07 0.149E+07 0.111E+07 0.283E+06 0.965E+04 0.770E+03
0.271E+02 0.271E+00 0.178E-03 0.580E-07 0.381E-10 0.124E-13 0.343E+06 0.261E+05 0.858E+04 0.279E+04 0.598E+03 0.840E+02 0.245E+02 0.515E+01 0.620E+00
0.217E-01 0.553E-03 0.194E-04 0.495E-06
2340.0000 0.620E+01 0.000E+00 0.000E+00 0.900E-03 0.900E-03 0.620E+01 0.000E+00 0.233E+07 0.210E+07 0.173E+07 0.856E+06 0.103E+06 0.638E+04 0.117E+04
0.136E+03 0.732E+01 0.710E-01 0.441E-03 0.428E-05 0.266E-07 0.104E+07 0.858E+05 0.240E+05 0.607E+04 0.103E+04 0.130E+03 0.367E+02 0.749E+01 0.878E+00
0.297E-01 0.728E-03 0.247E-04 0.606E-06
2400.0000 0.645E+01 0.000E+00 0.000E+00 0.800E-03 0.800E-03 0.645E+01 0.000E+00 0.275E+07 0.245E+07 0.205E+07 0.116E+07 0.228E+06 0.275E+05 0.759E+04
0.148E+04 0.161E+03 0.478E+01 0.101E+00 0.299E-02 0.632E-04 0.126E+07 0.991E+05 0.275E+05 0.695E+04 0.120E+04 0.159E+03 0.463E+02 0.985E+01 0.122E+01
0.451E-01 0.122E-02 0.450E-04 0.122E-05
2460.0000 0.650E+01 0.000E+00 0.000E+00 0.780E-03 0.780E-03 0.650E+01 0.000E+00 0.287E+07 0.254E+07 0.213E+07 0.124E+07 0.270E+06 0.372E+05 0.111E+05
0.241E+04 0.302E+03 0.112E+02 0.302E+00 0.112E-01 0.302E-03 0.124E+07 0.105E+06 0.301E+05 0.777E+04 0.125E+04 0.136E+03 0.348E+02 0.623E+01 0.608E+00
0.154E-01 0.275E-03 0.697E-05 0.124E-06
2520.0000 0.670E+01 0.000E+00 0.000E+00 0.710E-03 0.710E-03 0.670E+01 0.000E+00 0.280E+07 0.237E+07 0.188E+07 0.930E+06 0.128E+06 0.986E+04 0.207E+04
0.285E+03 0.193E+02 0.270E+00 0.251E-02 0.352E-04 0.327E-06 0.117E+07 0.131E+06 0.435E+05 0.121E+05 0.144E+04 0.736E+02 0.111E+02 0.995E+00 0.376E-01
0.210E-03 0.715E-06 0.400E-08 0.136E-10
2580.0000 0.720E+01 0.000E+00 0.000E+00 0.570E-03 0.570E-03 0.720E+01 0.000E+00 0.289E+07 0.226E+07 0.159E+07 0.540E+06 0.244E+05 0.435E+03 0.375E+02
0.167E+01 0.244E-01 0.300E-04 0.194E-07 0.239E-10 0.154E-13 0.165E+07 0.162E+06 0.485E+05 0.123E+05 0.154E+04 0.997E+02 0.179E+02 0.202E+01 0.106E+00
0.985E-03 0.589E-05 0.551E-07 0.329E-09
2640.0000 0.763E+01 0.000E+00 0.000E+00 0.480E-03 0.480E-03 0.763E+01 0.000E+00 0.298E+07 0.193E+07 0.126E+07 0.416E+06 0.213E+05 0.467E+03 0.458E+02
0.241E+01 0.440E-01 0.771E-04 0.735E-07 0.129E-09 0.123E-12 0.229E+07 0.194E+06 0.533E+05 0.125E+05 0.164E+04 0.130E+03 0.272E+02 0.376E+01 0.259E+00
0.375E-02 0.364E-04 0.530E-06 0.514E-08
2700.0000 0.800E+01 0.000E+00 0.000E+00 0.420E-03 0.420E-03 0.800E+01 0.000E+00 0.308E+07 0.169E+07 0.104E+07 0.343E+06 0.198E+05 0.521E+03 0.570E+02
0.346E+01 0.765E-01 0.182E-03 0.242E-06 0.575E-09 0.765E-12 0.509E+07 0.265E+06 0.586E+05 0.117E+05 0.147E+04 0.134E+03 0.311E+02 0.487E+01 0.397E+00
0.751E-02 0.973E-04 0.184E-05 0.239E-07
2760.0000 0.840E+01 0.000E+00 0.000E+00 0.360E-03 0.360E-03 0.840E+01 0.000E+00 0.297E+07 0.160E+07 0.947E+06 0.293E+06 0.154E+05 0.369E+03 0.383E+02
0.217E+01 0.437E-01 0.898E-04 0.102E-06 0.209E-09 0.237E-12 0.111E+08 0.320E+06 0.588E+05 0.106E+05 0.132E+04 0.140E+03 0.359E+02 0.647E+01 0.633E+00
0.159E-01 0.282E-03 0.712E-05 0.126E-06
2820.0000 0.950E+01 0.000E+00 0.000E+00 0.250E-03 0.250E-03 0.950E+01 0.000E+00 0.292E+07 0.141E+07 0.745E+06 0.191E+06 0.772E+04 0.143E+03 0.128E+02
0.601E+00 0.940E-02 0.129E-04 0.940E-08 0.129E-10 0.940E-14 0.877E+07 0.232E+06 0.410E+05 0.704E+04 0.779E+03 0.640E+02 0.139E+02 0.200E+01 0.144E+00
0.224E-02 0.233E-04 0.363E-06 0.379E-08
2880.0000 0.103E+02 0.000E+00 0.000E+00 0.200E-03 0.200E-03 0.103E+02 0.000E+00 0.244E+07 0.103E+07 0.533E+06 0.164E+06 0.142E+05 0.745E+03 0.126E+03
0.134E+02 0.632E+00 0.500E-02 0.248E-04 0.197E-06 0.977E-09 0.739E+07 0.184E+06 0.316E+05 0.525E+04 0.530E+03 0.363E+02 0.694E+01 0.851E+00 0.492E-01
0.537E-03 0.381E-05 0.417E-07 0.296E-09
2940.0000 0.110E+02 0.000E+00 0.000E+00 0.160E-03 0.160E-03 0.110E+02 0.000E+00 0.209E+07 0.787E+06 0.403E+06 0.147E+06 0.247E+05 0.324E+04 0.963E+03
0.207E+03 0.258E+02 0.944E+00 0.252E-01 0.922E-03 0.246E-04 0.122E+07 0.108E+06 0.266E+05 0.448E+04 0.348E+03 0.228E+02 0.449E+01 0.572E+00 0.348E-01
0.412E-03 0.318E-05 0.375E-07 0.290E-09
3000.0000 0.120E+02 0.000E+00 0.000E+00 0.120E-03 0.120E-03 0.120E+02 0.000E+00 0.119E+07 0.548E+06 0.309E+06 0.943E+05 0.560E+04 0.165E+03 0.196E+02
0.131E+01 0.334E-01 0.989E-04 0.167E-06 0.496E-09 0.839E-12 0.180E+06 0.792E+05 0.290E+05 0.441E+04 0.218E+03 0.131E+02 0.267E+01 0.360E+00 0.236E-01
0.312E-03 0.271E-05 0.358E-07 0.312E-09
3060.0000 0.130E+02 0.000E+00 0.000E+00 0.100E-03 0.100E-03 0.130E+02 0.000E+00 0.678E+06 0.402E+06 0.262E+06 0.710E+05 0.155E+04 0.103E+02 0.489E+00
0.102E-01 0.531E-04 0.127E-07 0.137E-11 0.327E-15 0.351E-19 0.187E+06 0.786E+05 0.274E+05 0.391E+04 0.209E+03 0.175E+02 0.453E+01 0.840E+00 0.851E-01
0.225E-02 0.418E-04 0.110E-05 0.205E-07

JET PROPULSION LABORATORY

INTEROFFICE MEMORANDUM
5217-90-029

1990 February 28

TO: A. R. Hoffman (301-466)

FROM: Neil Divine (301-460)

SUBJECT: Numerical Models for Electron and Proton Distributions in Saturn's Radiation Belts

SUMMARY

Published data from charged particle experiments aboard three spacecraft during their flybys at Saturn have been used to generate numerical models for the radiation belts between 2.3 and 13 Saturn radii. The models describe the electron distributions at energies between 0.04 and 10 MeV and the proton distributions at energies between 0.14 and 80 MeV. They are intended to predict particle intensity, flux and fluence for the Cassini orbiter. Review comments on the models will be solicited.

—Neil Divine

1. INTRODUCTION

An extensive data set describing the distributions of energetic electrons and ions in Saturn's radiation belts has become available following three spacecraft flybys in 1979, 1980, and 1981. These data are presented in numerous articles in the research literature (see Sec. 2 below) and are summarized by Van Allen, 1984 (reference VA84, introducing the citation scheme employed in this memorandum). The following sections describe numerical models for the distributions based on a selection of published profiles within the data set. The present models are intended to replace those derived from rather limited, and to some extent preliminary, subsets of the data, as described in DI80, EV87a, and EV87b.

Table 1 specifies values for several Saturn quantities used with the models. The five magnetic field coefficients represent the zonal harmonic model (Z_3); all other coefficients are set equal to zero in this description of the magnetic field from CO84 (based on numerical fits to magnetic field data from the flyby spacecraft). In the equations (1 through 3) of this reference, a is equal to 1.0 R_S (Table 1), and the longitudes ϕ and ψ are both measured positive east from the prime meridian of the planet, including prograde rotation with rate ω (Table 1). Although the internal terms (proportional to g_1^0, g_2^0, and g_3^0) are axisymmetric in this representation, the external ones (proportional to G_1^0 and G_1^1) are not (because $G_1^1 \neq 0$). For a given position with respect to Saturn, the magnetic shell parameter L is obtained by evaluating the magnetic field vector $\vec{B}$ at the point, tracing the field line to the magnetic equator (where B_e is the minimum value of $|\vec{B}|$ along the line) and beyond to a location where $|\vec{B}|$ has the same value as at the initial point, evaluating the adiabatic invariant I as an integral along the field line (RO70, p. 48, eq. 2.38), and using a series expansion approximation to obtain L (RO70, pp. 154-155, where k_o is the same as g_1^0 in Table 1 here). Appendix A provides additional detail for the properties of the magnetic field description and of charged particle motion in the radiation belts.

2. FLYBY SPACECRAFT AND THE DATA PROFILES

Table 2 specifies Keplerian elements and other data for the trajectories of the three Saturn flyby spacecraft. The references cited in the last row of Table 2 are the sources for all the entries except the longitudes, which were estimated from Figures 2 and 3 of CO84 (pp. 358-359; note that these are west longitudes). Calculation of the flyby trajectories using Keplerian orbits about Saturn (as a point mass), including both planetary rotation and the magnetic field description above (Sec. 1, last para.) yield satisfactory agreement (to within about 0.05 in L) with the magnetic coordinates (and times) shown in Figure 1, for $L<9$. Attempts to simplify this process (e.g., by omitting the external field harmonics) yielded significantly degraded agreement (e.g., discrepancies near 0.2 in L). The trajectory characterizations in the following paragraphs use the entries in Tables 1 and 2 (not those from the other references or from Fig. 1).

The Pioneer 11 trajectory at Saturn was nearly equatorial, and included a minimum L=1.43 (maximim B=0.0801 G). The charged particle instrumentation aboard Pioneer 11 consists of four subsystems, namely the Geiger Tube Telescope (GTT, provided by the Univ. of Iowa), Charged Particle Telescope (CPT, Univ. of Chicago), Trapped Radiation Detector (TRD, Univ. of California at San Diego), and Cosmic Ray Telescope (CRT, Goddard Space Flight Center and Univ. of New Hampshire). These four instruments were completed prior to the 1973 launch and occupy fixed orientations aboard a spin-stabilized spacecraft intended primarily for data acquisition at its Jupiter flyby.

The Voyager 1 trajectory at Saturn was highly inclined, and included about two hours at nearly constant L (5.9±0.1) inbound, maximum B=0.011 G, and minimum L=4.36. The charged particle instrumentation aboard both Voyager 1 and 2 consists of two subsystems, namely the Low-Energy Charged Particle Experiment (LECP, provided by Applied Physics Laboratory, Johns Hopkins Univ.) and the Cosmic Ray Subsystem (CRS, Goddard Space Flight Center). These instruments were completed prior to the 1977 launch and occupy either fixed (CRS) or commandable rotating orientations (LECP) aboard three-axis-stabilized spacecraft intended for data acquisition at both Jupiter and Saturn.

The Voyager 2 trajectory at Saturn was moderately inclined, and included maximum B=0.012 G and minimum L=2.77. There were also pairs of magnetic coordinates (B, L) matched twice along the Voyager trajectories, namely (0.007, 4.43), (0.0036, 4.47), (0.0029, 6.06), (0.0017, 6.55) and (0.001, 8.45); these points (see crossings in Fig. 1) enable checks for the reproducibility of the data (as in KR83, p. 8888, Fig. 17 and 18).

Tables 3 and 4 list those profiles which have been selected from the published data (acquired during these three flybys) and used in the present electron and proton models respectively. The extensive notes accompanying these tables suggest some of the diversity and subtlety of the results. Appendix B includes a discussion of species identification for some of the profiles in Tables 3 and 4, whereas Appendix C includes summaries of the selection criteria for these profiles and of the procedures used for their processing in the models.

The histograms in Figures 2 and 3 display the coverage of the selected profiles in magnetic field and energy threshold at each of several values for L, namely those chosen for use as fitting points in the models (see App. C for a discussion of the procedures used). Even within the ranges spanned by the profiles the distribution of the data is quite uneven, as restricted by the spacecraft trajectories and by the detector thresholds, dynamic ranges, and backgrounds.

3. ALGEBRAIC FORMULATION OF THE MODELS

The basic independent variables used in these models are magnetic shell parameter L, local magnetic field strength B, pitch angle α, and (electron or proton) kinetic energy E. The form chosen to match the data (Sec. 2 and Tables 3 and 4) resembles that used in DG83 (eq. 7 through 9) and takes the integral intensity I (in $cm^{-2}s^{-1}sr^{-1}$, for particles having energy $>E$) as its basic dependent variable. The dependence of I on E is given by

$$\log I = A_0 - A_1(\log E) + \left(\frac{A_1 - A_2}{2}\right)\log\left(\frac{E^2 + E_2^2}{1 + E_2^2}\right) + \left(\frac{A_2 - A_3}{3}\right)\log\left(\frac{E^3 + E_3^3}{1 + E_3^3}\right) \quad . \qquad (1)$$

Differentiation of equation (1) with respect to energy leads to the differential intensity i (sample units $cm^{-2}s^{-1}sr^{-1}MeV^{-1}$) in the form

$$i = -\frac{dI}{dE} = \frac{I}{E}\left[A_1 + \frac{A_2 - A_1}{1 + (E_2/E)^2} + \frac{A_3 - A_2}{1 + (E_3/E)^3}\right] \quad . \qquad (2)$$

The dependence of I and i on α and B is given by

$$A_n = \frac{B_e}{B}(\sin\alpha)^2(a_n - b_n) + b_n \qquad (3)$$

for subscript $n = 0$, 1, 2, and 3 (see eq. 1 and 2). The dependence of I and i on L is achieved by taking each of the ten parameters a_n, b_n, E_2 and E_3 as linear in L between values specified at several fit points in L.

Examination of equations (1) through (3) reveals the following interpretations (illustrating the roles of the ten model parameters) at a given value of L:

(1) the spectra resemble power law segments in which I is proportional to $E^{-\gamma}$, where the integral exponent $\gamma = -d(\log I)/d(\log E)$ has the value A_1 for kinetic energy $E << E_2$, the value A_2 for $E_2 << E << E_3$, and the value A_3 for $E >> E_3$ (here γ equals the quantity in brackets in eq. 2);

(2) the coefficients A_n vary from a_n for pitch angle α=90 deg at the magnetic equator ($B = B_e$) to b_n for pitch angle α=0 at any $B \geq B_e$, and to b_n for any pitch angle $\alpha \leq$90 deg at high magnetic latitude ($B_e/B = 0$);

(3) at energy E=1 MeV, and at the magnetic equator ($B = B_e$), two parameters can be identified as $a_o = \log I_\perp$ and as $b_o = \log I_\parallel$, where subscripts distinguish intensities perpendicular to (α=90 deg) and parallel to (α=0) the magnetic field $\vec{B}$; and

(4) at high magnetic latitude ($B_e/B = 0$), the intensity I is isotropic (independent of pitch angle α) and has the same value as $I_\parallel$ at the equator.

In this formulation the kinetic energy E and the transition energy parameters E_2 and E_3 all have units MeV, and A_o, a_o and b_o are evaluated so as to yield I in the units $cm^{-2}s^{-1}sr^{-1}$.

As a subsidiary dependent variable consider the integral, omnidirectional flux J, as given by

$$J = \int_{4\pi} d\Omega\, I = 4\pi \int_0^{\pi/2} d\alpha\, (\sin\alpha)\, I = 4\pi \int_0^1 d\mu\, I \quad , \tag{4}$$

where the last equality uses the pitch angle cosine, $\mu=(\cos\alpha)$. The corresponding differential, omnidirectional flux is given by

$$j = -\frac{dJ}{dE} = 4\pi \int_0^1 d\mu\, i \quad . \tag{5}$$

Some additional quantities of interest which may be computed from the model are introduced in Appendix A.

To understand the response of a detector in the presence of the charged particle distributions, consider the general expression

$$R = \sum \int_{4\pi} d\Omega \int_0^\infty dE\, Q_D \sigma_D\, i \quad . \tag{6}$$

Here the sum proceeds over the particle species (each having local differential intensity i, as in eq. 2), the solid angle integral proceeds over all directions as seen from the detector (subscript D), and Q_D is some quantity induced in the detector per incident particle. The cross-section σ_D may depend not only on direction of particle arrival and on its kinetic energy (i depends on these two as well, of course), but also on detector discrimination level. Analysis of the TRD data from Pioneer 11 (as presented in FM80) includes examples in which a single detector is used with three discrimination levels (channels), as well as an example in which Q_D is charge (leading to R as a current, as contrasted with the more common Q_D=1 leading to R as a countrate). For the present model we assume that additional complications (not reflected in eq. 6) such as dead-time correction and coincidence or anti-coincidence discrimination (pp. 8933-8934 of SM83 provide a thorough sample discussion) are absent or already accounted for in the published data profiles (e.g., those in Tables 3 and 4) for R.

The present models employ considerable further simplification of equation (6) based on the approximations (in common use among the spacecraft investigators) that

(1) only a single species contributes significantly to R at a given time,

(2) average values (independent of direction) may be used for Q_D and σ_D, regardless of any anisotropies in i, and

(3) constant values may be used for Q_D and σ_D above some discrimination threshold and between particle kinetic energies E_a and E_b, with σ_D=0 elsewhere.

With these approximations equation (6) becomes

$$R = Q_D \sigma_D (J_a - J_b) \quad , \tag{7}$$

where subscripts a and b imply evaluation of equation (4) for omni flux at the two energies E_a and E_b. Only on this basis can the conversion value R/J in column 6 of Tables 3 and 4 be taken as a constant, independent of the local particle distributions, for a given profile (detector and channel). The conversion value is dimensionless when the response R (eq. 7) is a flux, and has units cm^2, sr^{-1}, $sr^{-1}MeV^{-1}$, or cm^2C whenever the response R is countrate, integral intensity, differential intensity, or current (examples for each may be found in the notes to Tables 3 and 4).

4. NUMERICAL EVALUATION OF THE MODELS

Table 5 specifies the parameter values adopted at 27 values of L for the electron model. Figures 4 and 5 illustrate the dependence on L of the electron integral intensity and omni flux as evaluated using the parameter values (Table 5) in equations (1), (3) and (4). Figures 6 and 7 illustrate the dependences on pitch angle, on magnetic field strength, and on energy of the electron intensity and flux.

Table 6 specifies the parameter values adopted at 29 values of L for the proton model. Figures 8 through 11 illustrate the proton model dependences (cf. Fig. 4 through 7 for the electrons).

The parameter values which appear in Tables 5 and 6 were obtained by an iteration process whose goal was to best match the model-predicted responses (defined below) to the data profiles (summarized in Tables 3 and 4). The iteration uses a computer program to find the values of several variables x_i for which some single variable Y (a function of all the x_i) has a local minimum. In an iteration, as carried out independently at each of several values of L (namely those in column 1 of Tables 5 and 6), the variables x_i are the parameters a_n, b_n, E_2, and E_3 (cf. eq. 1 and 3), and the quantity Y is evaluated as described in the following paragraph.

For a specific value of L, and for one particle species (i.e., electrons or protons), several values of the observed countrate R are obtained from measurement of the profiles in Tables 3 or 4 (as described in App. C, para. 4). These countrates are here identified with subscript D, and each such value R_D is associated with a pair of energies (E_a and E_b from column 5 of Table 3 or 4), with a conversion constant (R/J from column 6 of Table 3 or 4), with a background rate (R_B from column 7 of Table 3 or 4), and with a magnetic field ratio (B_e/B) for the spacecraft trajectory and time of measurement. Corresponding to each value of R_D, we use the model parameters (a_n, b_n, etc., here playing the roles of the variables x_i in the previous para.) and the remaining quantities (previous sentence) in equations (1), (3), (4), and (7) to evaluate the model-predicted rate R_M (to evaluate R_M=R from eq. 7, we substitute the conversion R/J from column 6 of Table 3 or 4 for the product $Q_D \sigma_D$). For each trio of rates (datum R_D, model-prediction R_M, and background R_B) we compute both a residual Δ and the quantity Z using

$$\Delta = \begin{cases} \min\left[0,\ \log(R_B/R_M)\right] & \text{for } R_D < R_B \\ \log(R_D/R_M) & \text{for } R_D > R_B \end{cases} \qquad (8)$$

and

$$Z = \begin{cases} \Delta^2 & \text{for } |\Delta| \le \Delta_0 \\ \Delta_0^2\left[2-(\Delta_0/\Delta)^2\right] & \text{for } |\Delta| \ge \Delta_0 \end{cases} . \qquad (9)$$

We compute the quantity Y (previous para.) as a modified RMS (root-mean-square) residual using

$$Y = \left[(\Sigma WZ)/(\Sigma W)\right]^{1/2} . \qquad (10)$$

In equation (10) each sum proceeds over the rate trios available at the specific value of L, and W is a weighting factor used for each (with very few exceptions the level weight W=1.0 was used throughout).

The procedures of the foregoing two paragraphs represent the heart of the model development. Additional details appear in Appendix C, but we devote the remainder of this paragraph to a numerical example which illustrates the evaluation of the residual Δ (eq. 8). Consider a point along the Pioneer 11 trajectory inbound at L=2.83, for which the magnetic field model (Table 1 and eq. 11 through 13) and the spacecraft trajectory (Table 2) yield a Saturnicentric distance 2.796 R_S, latitude -0.27 deg, B=0.009536 G, and B_e=0.009520 G at time -1.951 hr from perisaturn. The data were received at Earth (using Table 2) at (16:31-1.951 hr +86.34 min)=16:00, at which time measurement of Figure 1 of VA80c (p. 5710) yields a (spin-averaged) data countrate R_D=8930 s^{-1} for P11 GTT detector B. For this profile Table 3 specifies electron energies E_a=0.56 MeV and E_b=21 MeV, conversion (R/J)=0.00127 cm^2, and background countrate R_B=0.4 s^{-1} (this estimate is from Fig. 5 of VA80a, p. 419, and is well below R_D in our example). For the electron model, using parameter values from Table 5 at L=2.83, we evaluate the four terms in equation (1) to obtain log I=(5.52+0.0+0.059+0.040)=5.619 at E_a=0.56 MeV and log I=(5.52+0.0-0.328-2.872)=2.320 at E_b=21 MeV. These intensities agree with the spectrum in Figure 6 (upper right) and, for this isotropic distribution (b_n=a_n, see eq. 3 and 4), the corresponding omni fluxes are $J=4\pi I$=5.22×10^6 $cm^{-2}s^{-1}$ at E_a=0.56 MeV and 2.62×10^3 $cm^{-2}s^{-1}$ at E_b=21 MeV, which agree with the spectrum in Figure 7 (upper right). The model-predicted rate (eq. 7) is then $R_M=(R/J)(J_a-J_b)$=6626 s^{-1} and the residual (eq. 8) is (logR_D-logR_M)=(3.95-3.82)=+0.13. The outbound countrate R_D=6390 s^{-1} (same detector, same source in VA80c) leads to a residual -0.02, and these two residuals are plotted as adjacent circles at log$E$=-0.25 and (B_e/B)=1.0 in Figure 12 (upper left).

In equation (8) the first line insures that Δ makes no contribution to Y when both R_D and R_M are smaller than the background R_B. Equation (9) insures that a peak in dZ/dx_i occurs for $|\Delta|$ near Δ_o (where x_i is any one of the up to ten parameters being iterated), so that the iteration is most effective at reducing residuals of size comparable to Δ_o (and the hopelessly large residuals are deemphasized). Parameter values were accepted for inclusion in the model when a satisfactory minimum in Y (eq. 10) was obtained, using Δ_o=0.3 (note that $|\Delta|$=0.3 corresponds to a factor $2^{\pm 1}$ in R).

Many of the rows in Tables 5 and 6 demonstrate that, for each L, no more parameter values were iterated than could be justified by the data ranges and by their contributions to the reduction of the modified RMS residual Y (eq. 10). Specifically, $b_n=a_n$ was enforced whenever it did not lead to a major increase in Y; note that this results in the isotropy of the models ($b_n=a_n$ for all $n=0, 1, 2, 3$) for $L<3$ (no data available far from the magnetic equator). Further, changes in E_2 and E_3 between adjacent values of L are avoided where possible (partly to enable log I linear in L), and they are mostly kept within the range of the data threshold energies E_a (see Fig. 2 and 3). Lastly a_3 and b_3 were kept ≥3.0, without much degrading the fits, to avoid unfounded extrapolation to high intensity (and flux) at large kinetic energy (e.g., $E>10$ MeV for electrons or $E>100$ MeV for protons) beyond the data coverage.

Figures 2 and 3 suggest (at the right) the quality of the model fits, as represented by the residuals (eq. 8) and distinguished by magnetic shell parameter L. In each case most of the points from the data profiles are matched within a factor $2^{\pm1}$ in R. The modified RMS residuals Y (eq. 10, using $\Delta_o=0.3$) for electrons range from 0.14 to 0.26 (corresponding factors for R are 1.4 to 1.8) and for protons (excepting the disaster at $L=2.52$) range from 0.11 to 0.28 (corresponding factors for R are 1.3 to 1.9).

Tables 7 and 8 also illustrate the quality of the model fits, this time distinguished by the data profiles. The range in L for which each profile is included in the model also appears in these tables, and the last column contains the standard RMS residual for each (retaining eq. 8 but disregarding eq. 9 and 10). Some profiles are consistently well matched by the models (e.g., row 1 in Table 7 and row 10 in Table 8), whereas others are consistently badly matched (e.g., rows 8 and 9 in Table 8, for which the data countrate is about 10 times larger than the model-predicted one; see last line of eq. 8). Many of the latter "bad actors" have modest ranges in L, but some appear throughout the L range of the model (e.g., row 9 in Table 7).

Figure 12 displays some sample distributions of the residuals in energy (horizontal axes), in magnetic field strength (vertical axes), and in value (symbol styles). The "bad actors" (represented by triangles) are typically well-mixed with the well-fitted points (circles), so that no easy fix is possible (if they were isolated the iteration could easily accommodate them, considering the flexibility available in eq. 1 and 3).

The residuals cited in Tables 7 and 8 and in Figures 2, 3 and 12 suggest that a reasonable uncertainty estimate for the model is $2^{\pm1}$, the same as cited for the data (and/or its calibration) by some of the spacecraft experimenters. Some profiles consistently exceed this factor in comparison with the models, but the latter are based on so large a body of data as to be quite robust with respect to even major changes in the interpretation of a few profiles.

5. POTENTIAL IMPROVEMENTS FOR THE MODELS

The present model is intended for review by the experiment teams responsible for the data cited in Table 3 and 4. Following that review it may be worthwhile to revise the model employing the criticisms and suggestions which are made. Thus some improvements which could be made now have been deferred until the later revision, as identified in the following paragraphs.

Peaks in the electron model at L=3.4, 5.87, and 6.5 (see Fig. 4) and in the proton model at L=2.43, 2.67, and 4.13 (see Fig. 8) do not have good resolution in L, suggesting that more points in L could usefully be included in the model set (first column of Tables 5 and 6). Further, for electrons in the range $5<L<7$, rapid changes occur between pancake ($I_\perp > I_\parallel$) and dumbell ($I_\perp < I_\parallel$) distributions; it would be worthwhile to check whether such is really demanded by the data, and particularly whether data along the Voyager 1 trajectory (cf. para. 3 of Sec. 2) exerts undue influence here.

Both models specify isotropic distributions for $L<3$ (cf. para. 6 of Sec. 4), but evidence for strong anisotropy can be found in the spin modulation of the Pioneer 11 data (see for example FI80, Fig. 5, and VA80a, Fig. 5). Such anisotropy could probably be introduced into the model without increasing the residuals. In addition, for protons at $L<3$, a CRAND (cosmic ray albedo neutron decay) source suggests a strongly pancake distribution (see CO89, p. 5-C-8, para. 3), just as occurs in the model for $3<L<4$ (Fig. 8 through 11). Further the CRAND spectrum would have a smaller value of the power-law exponent (see γ in Sec. 3, para. 2, item 1), as suggested in FM80 (p. 5809 has γ=0.8) and in VA83 (p. 6913 has γ=0.7 for $E>120$ MeV). Possibly these considerations should be included in the model (note, however, that $\gamma \leq 1$ leads to infinite energy density if it extends to $E \rightarrow \infty$).

For $L>10$, the field line tracing (Sec. 1, para. 2, and App. A, para. 2) leads to values of B_e which differ significantly from the ratio g_1^0/L^3. This is the source of some discrepancies in the B_e/B coverage appearing in Figures 2 and 3 at large L (they were calculated differently in different computer runs). In such cases, presumably resulting from the importance of the external terms in the field model, reconsideration should be given to the questions of stable trapping and constant intensity along the particle trajectories and drift shells. It may also be worthwhile to compute the relations between L and I (adiabiatic invariant, App. A, eq. 17) using SL74 (pp. 19-25) instead of RO70 (pp. 154-155).

Many of the spacecraft detectors are not omnidirectional, and they respond to the local particle distribution with effective cross-sections (σ_D in Sec. 3) which vary with particle energy and direction (with respect to the finite angular apertures of the detectors). Thus the response R_M which should be evaluated from the model intensity (for comparison with the data R_D) is more properly proportional to the integrals displayed in equation (6) than to the omni flux J in equation (7). Inclusion of such an improvement (to be used in the iteration for model parameter values) would require more detailed specifications for the detector calibration, for detector orientation along the three spacecraft trajectories, and/or for time resolution along the data profiles. To a large extent these data are indeed available (although not published in detail, in most cases), but their use would introduce additional complexity into the model development which may or may not be justifiable.

Peak flux and fluence spectra for the Cassini orbiter have already been computed based on the present models, as reported in DI90; these results will be replaced when improved model distributions are completed.

ACKNOWLEDGEMENT

Thanks for assistance in the model development go to W. Fillius (UCSD) for constructive criticism of a predecessor model (DI80), to R. J. Cesarone (JPL Sec. 312) for provision of elements for the Voyager flybys at Saturn (Table 2), and to W.-P. Lee (JPL Sec. 384) for careful measurement and digitization of all the published data profiles cited in Tables 3 and 4.

APPENDIX A. **MAGNETIC FIELD AND CHARGED PARTICLE MOTION**

The following paragraphs, which supplement the discussions in Section 1 (para. 2) and Section 3 (following eq. 5), represent considerable simplifications of the thorough radiation belt analyses presented in RO70, SL74, and CO84.

Using $\vec{u}_r$, $\vec{u}_\theta$, and $\vec{u}_\phi$ as unit vectors in the directions of increasing Saturnicentric distance r, colatitude θ, and east longitude ϕ, the magnetic field vector $\vec{B}$ for the present model includes only terms proportional to the five coefficients in Table 1. The results for the field components are

$$\vec{B}\cdot\vec{u}_r = g_1^0\left[2\left(\frac{R_S}{r}\right)^3(\cos\theta)\right] + g_2^0\left[\frac{3}{2}\left(\frac{R_S}{r}\right)^4(3(\cos\theta)^2-1)\right] + g_3^0\left[2\left(\frac{R_S}{r}\right)^5(5(\cos\theta)^3-3(\cos\theta))\right]$$
$$- G_1^0(\cos\theta) - G_1^1(\sin\theta)(\cos\phi) \qquad (11)$$

$$\vec{B}\cdot\vec{u}_\theta = g_1^0\left[\left(\frac{R_S}{r}\right)^3(\sin\theta)\right] + g_2^0\left[3\left(\frac{R_S}{r}\right)^4(\sin\theta)(\cos\theta)\right] + g_3^0\left[\frac{3}{2}\left(\frac{R_S}{r}\right)^5(\sin\theta)(5(\cos\theta)^2-1)\right]$$
$$+ G_1^0(\sin\theta) - G_1^1(\cos\theta)(\cos\phi) \qquad (12)$$

and $$\vec{B}\cdot\vec{u}_\phi = G_1^1(\sin\phi) \quad . \qquad (13)$$

Note that the external terms (proportional to G_1^0 and G_1^1) correspond to a field of magnitude $[(G_1^0)^2+(G_1^1)^2]^{1/2}=1.005\times10^{-4}$ G, independent of distance r. In regions in which the magnetic lines of force do not connect to this external field, energetic charged particles may be trapped, in which case their motion can be approximately separated into three components:

(1) circulation about the field line,

(2) bounce along the field line, and

(3) drift around the planet.

These motions are listed in order of increasing path length and period (decreasing frequency), and are in addition to those of the field with Saturn's rotation and orbit. For an individual particle of rest mass m_o the constants associated with the circulation are the kinetic energy E and the magnetic moment M (sample units J/T or MeV/G), as related by

$$M = \frac{p^2c^2}{2B_m(E+m_oc^2)} \quad . \qquad (14)$$

Here the momentum p and mirror point magnetic field strength B_m are given by

$$p^2c^2 = E(E + 2m_0c^2) \tag{15}$$

and

$$B_m = B(\sin\alpha)^{-2} \tag{16}$$

The constants associated with the bounce motion are B_m and the adiabatic invariant I given by

$$I = \int_{s_{m1}}^{s_{m2}} ds\,(1 - B/B_m)^{1/2} \tag{17}$$

This integral over path length proceeds along the field line between the mirror points, at each of which $B=B_m$, α=90 deg, and the momentum $\vec{p}$ is perpendicular to $\vec{B}_m$. Elsewhere the pitch angle α is in the range (0, 90 deg), having a minimum value α_e given by

$$(\sin\alpha_e) = (B_e/B_m)^{1/2} \tag{18}$$

at the magnetic equator (minimum field strength B_e between s_{m1} and s_{m2} along the field line). The constant associated with the drift motion is the magnetic shell parameter L, related to I and B_e as discussed in Section 1 (para. 2).

For collisionless steady state distributions, the phase space density g (sample SI units (J s)$^{-3}$) for a given species of identical particles is constant along the trajectory of every individual particle. For present purposes we approximate this relationship using instead equal differential intensity (cf. eq. 2)

$$i = p^2 g \tag{19}$$

at corresponding pitch angles (cf. eq. 16 and 18) everywhere along those field lines traversed by the guiding center of the particle circulation. This approximation allows us to describe the distribution everywhere in the stable trapping region by specifying only the distribution in energy E and pitch angle α_e at the magnetic equator and at each value of L, as in paragraph 1 of Section 3.

APPENDIX B. SPECIES IDENTIFICATION AND OTHER DETECTOR ISSUES

For some detectors the responses and profiles observed in Saturn's radiation belts imply that the particle species being recorded differs from that anticipated based on experience in the Jupiter flybys. The literature includes several discussions of species identification issues (see following paragraphs). Many profiles which might otherwise have been used in the models have been ignored because these discussions bring their species identification into question, or suggest that it's variable. For the present models, all profiles attributed to ions in the original literature are used as if due to protons alone; note that MD80 (p. 5827) and SI80 (p. 5738 and p. 5744, Fig. 16) claim that protons are the dominant ion species in diverse regions of Saturn's radiation belts (for a contrasting view, see KR83, pp. 8884 to 8885).

Appendix B (pp. 5692 to 5693) of VA80b attributes the GTT countrates A and B exclusively to electrons, but C, D, and G to protons (unlike the situation at Jupiter), as reflected in Tables 3 and 4. Exceptions occur for troughs in the C and D countrates, and for the peaks in the G countrate inside L=4, so these latter features are not used in the model. Confirmation for the conversions of the proton rates corresponding to thresholds E>80 MeV (first 11 rows of Table 4) is provided by the fact that near L=2.7 an equatorial flux J=2.6×10^4 cm^{-2}s^{-1} (VA84, p. 286) yields the C and D peaks well, whereas J=2.0×10^4 cm^{-2}s^{-1} reproduces the TRD detector M peaks (with the conversions in Table 4). The TRD detector M profile ratios confirm that their rates respond to the same species as for GTT C and D (protons in the peaks, not in the troughs), as discussed in FM80 (pp. 5804 to 5805). One profile from MD80 (p. 5825, Fig. 21, curve C) resembles those just discussed but was not used in the model because no absolute conversion is cited and the response is to a mixture of proton energies.

Similarly P11 CPT profiles (for electrons, 7 to 17 MeV) from SI80a (pp. 413 and 414, Fig. 3 and 5B) and from SI80b (p. 5742, Fig. 13) have not been included in the electron model, considering challenges in VA80c (p. 5716) and CO89 (p. 5-C-9, para. 3). This last reference contains numerous other discussions of particle and energy identifications which have mostly been heeded in the present models. An exception is made in that the model does use P11 CPT proton data (0.5 to 1.8 MeV, several rows near the bottom of Table 4) which are also challenged by CO89 (p. 5-C-10, bottom), with the result that these data are *not* well matched (see residuals in Table 8). The model also uses V02 LECP electron data from VA84 (p. 307, Fig. 20) in spite of a challenge to its validity (HO89, p. 5-D-12, last para.) inside 4 R_S; these data consistently exceed the model predictions in this region.

Three published spectra were used to help confirm the profile conversions (R/J in Tables 3 and 4). For electrons, a spectrum at L=9.56 (VA84, p. 308, Fig. 21) was found to be consistent with the conversions used for countrates read from four V02 LECP profiles listed in Table 3 (from VA84, p. 307, Fig. 20). For protons, a spectrum at 7.81 R_S (MD80, p. 5816, Fig. 4) was found to be consistent with the conversion used for differential intensities from three P11 CRT profiles listed in Table 4 (from MD80, p. 5815, Fig. 3, and from TR80, p. 422, Fig. 1). However, also for protons, a spectrum at L=7.15 (VA84, p. 297, Fig. 11) did not seem to be consistent with conversions intended for countrates from two V01 LECP profiles (KR83, p. 8877, Fig. 6, curve 2 from top, and HA83, p. 8908, Fig. 3a, top curve), so these two profiles were *not* used in the model.

Adjustments to the scale of the published profiles were made in two cases, both for electrons, one of them described in note [*j*] to Table 3. The other concerns the P11 TRD CDC data (Table 3, row 4), for which the original current scale (FM80, p. 5804, Fig. 1) appears to increase downwards; the intensity profile (FI80, p. 427, Fig. 2A) and the geometric factor 7.3×10^{-14} A cm^{2}s sr (FM80, p. 5805, Table 1) suggest that the 10^{-7} A tic mark on the current scale is correct (the others should represent 10^{-9} and 10^{-11} A). The conversion adopted in Table 3 (R/J=6.3×10^{-15} A cm^{2}s) is the ratio $(4\pi \text{ sr})^{-1}[10^{-7.82} \text{ A}][1.9\times10^{5} \text{ cm}^{-2}\text{s}^{-1}\text{sr}^{-1}]^{-1}$, where the quantities in brackets are the peak inbound current (FM80, p. 5804, Fig. 1) and the peak inbound integral intensity (FI80, p. 427, Fig. 2A).

APPENDIX C. **PROCESSES OF MODEL DEVELOPMENT**

The following paragraphs detail various aspects of the model development, particularly including the selection, measurement, and filtration of the data profiles (cf. Sec. 2 and Tables 3 and 4) and the iteration of the model parameter values (cf. Sec. 4, para. 3 and 4).

To choose from among the many data profiles considered for possible inclusion in the model, a selection process was used based roughly on the following considerations:

(1) unpublished data were not sought, on the assumption that the published data may be the most secure, in terms of careful reduction and analysis;

(2) figures which display the spacecraft data as spectra or as phase space densities were not used, on the assumption that most values therein are already represented in the profiles of countrate, flux, or intensity (but spectra were used to confirm conversions in some cases);

(3) data were used only when an unambiguous, constant conversion between the profile quantity and flux (in absolute units, here $cm^{-2}s^{-1}$) could be determined from accompanying, published information (see eq. 7);

(4) consistent with item (3), very noisy data, and data requiring variable countrate corrections (e.g., for dead-time), were mostly avoided; and

(5) the same, identifiable species (e.g., electrons or protons), at constant threshold energy (again see eq. 7), is responsible for that portion of the profile used in the model.

With respect to consideration (5), a brief discussion of species identification within the data set appears in Appendix B. As a result of these ideas, a total of 239 profiles identified in the literature for potential use in the models was narrowed down to the 31 cited for electrons in Table 3 and the 32 cited for protons in Table 4.

In addition to the use of countrate, flux, or intensity (detector current in one case) as the profile quantity, the several sources display data variously as functions of Earth-received time, spacecraft time, distance from Saturn, or magnetic shell parameter L. In most cases, profiles along the inbound and outbound trajectory legs are distinctly displayed. For some detectors or channels, more than one published profile applies (e.g., rows 3 through 5 in Table 4), in which case the model uses profile points only from that source having the greatest resolution in time (or distance or L) available at each trajectory point (see note [a] to Tables 3 and 4). Unit weight was assigned to each detector or channel, with the very few exceptions cited in the notes to Tables 3 and 4.

Positions (X and Y in cm, using as origin the lower left corner of the figure frame) were measured for enough points along each profile to capture all the maxima, minima, gaps, and other important features (plateaus, shoulders, etc.). These positions were then converted linearly to the quantities with which the figure scales were labelled (commonly log R for the profile quantity), and the resulting digitized data were stored in computer files. The data from these files were replotted (by machine) on the same scales as the originals to enable visual verification that the original profiles were satisfactorily represented by the digitized data files. These files were then compared with others describing the three spacecraft trajectories (as generated from the elements in Table 2) to extract those values of L at which the profiles have maxima, minima, and end-points. Coincidence in L of the maxima and minima from the diverse profiles was generally satisfactory, enabling a selection of suitable values of L for use in the models (column 1 of Tables 5 and 6). Then, at each such value of L, using the times and distances in the spacecraft trajectory files, values were interpolated from the profile data files yielding a data point log R_D (e.g., countrate, flux or intensity) for each of several detectors (identified by local magnetic field B, energies E_a and E_b, and conversion R/J).

The iteration for model parameter values was completed independently at each value of L, using the considerations in Section 4 (para. 3 and 4). Additional features incorporated in the interactive computer program used for the iteration included

(1) control over which parameters to iterate in a given attempt, and within what range of values, as well as allowing any b_n value to be slaved to a_n when desirable (see eq. 3);

(2) capability to start with a pure power law (by taking E_2 and E_3 respectively much smaller and much larger than the range of energies E_a and E_b in the data set) and to retain the values so obtained for a_2 and b_2 (see Sec. 3, para. 2, item 1);

(3) occasional, temporary reweighting of the data to ensure that small residuals were maintained for some key countrates during parameter variation (however, the level weighting cited in the text was always reintroduced at the end); and

(4) progressive reduction of Δ_o from some large value (in which case eq. 9 and 10 yield Y as a standard RMS residual) to 0.3 (see end of para. following eq. 10), such that the "hopeless" data points are successively deemphasized in the iteration (allowing concentration on those having $|\Delta|$ near Δ_o, as being most amenable to further residual reduction).

With regard to feature (4) above (cf. eq. 8 through 10), note that $\Delta=\infty$ leads only to $Z=2\Delta_o^2$ or to $Z^{1/2}=0.424$ when $\Delta_o=0.3$; cf. the value $Y=0.35$ for protons at $L=2.52$ (Fig. 3, last column), which represents by far the least satisfactory result in the model iteration process.

Table 1. Parameter values for Saturn used in the model calculations.

QUANTITY	VALUE	SOURCE
Radius	R_S=6.033×10^7 m	CO84, p. 354
Gravitation	GM_S=3.794×10^{16} m^3/s^2	CE89
Rotation	ω=810.76 deg/day	CO84, p. 360
Magnetic field coefficients	g_1^0=0.21535 G	CO84,p. 363, Table II
	g_2^0=0.01642 G	
	g_3^0=0.02743 G	
	G_1^0=-0.0001 G	
	G_1^1=-0.00001 G	

Table 2. Circumstances of the flybys for three spacecraft at Saturn. The Pioneer 11 data are from various sources in the Science issue which includes VA80a (and note 6 on p. 421 includes the one-way-light-time 86.34 min, Saturn-to-Earth, used for profile data interpretation).

Spacecraft		Pioneer 11	Voyager 1	Voyager 2
Perisaturn	date	1979 Sept. 1	1980 Nov. 12	1981 Aug. 26
	day of year	244	318	238
	spacecraft time (UT)	16:31:00	23:45:43	03:24:05
	distance, r_1 (R_S)	1.3497	3.0522	2.67075
	argument, ω_1 (deg)	-88.7	-75.7	153.2
	west longitude, ℓ_1 (deg)	162.1	179.9	322.9
Ascending node	west longitude, ℓ_Ω (deg)	139	265	150
Eccentricity	e	1.1148	2.1078	1.48587
Inclination	i (deg)	6.55	41.17	29.51
Source		See caption	CE80, CE89	WO81, CE89

Table 3. Identification of data profiles used for the Saturn electron model. Detailed notes appear on the following page.

SPACECRAFT, SUBSYSTEM [a]	REFERENCE, PAGE	FIGURE, LINE [b]	CHANNEL	ENERGIES E_a, E_b (MeV) [c]	CONVERSION R/J (cm^2) [d]	BACK-GROUND $\log R_B$ [e]	NOTES
V02 LECP	KR82, 573	2C, 2	EAB10	10, 20	1.03(-3)	-2.0	[f]
P11 CPT	SI80b, 5749	21c, 1	ECD	3.4	1.00	4.2	[g]
	SI80b, 5742	13, 4	ECD	3.4	1.00	4.2	[g]
P11 TRD	FM80, 5804	1ab, 4	CDC	2.0	6.3(-15)	0.0	[h]
P11 CPT	SI80b, 5740	11, 2	MT	2.0, 7.0	3.42(-2)	-1.6	[i]
V02 LECP	KR82, 573	2C, 1	ESA0	1.5	9.55(-4)	0.0	[j]
P11 CRT	MD80, 5824	18, 4		1.1, 2.0	0.088	1.0	[k]
	TR80, 422	2, 3		1.1, 2.0	0.088	1.0	[k]
V02 LECP	VA84, 307	20, 5	Eγ08-Eγ09	0.853, 1.2	1.35(-5)	-1.5	[l]
P11 CRT	MD80, 5824	18, 3		0.8, 1.1	0.265	2.0	[k]
	TR80, 422	2, 2		0.8, 1.1	0.265	2.0	[k]
P11 GTT	VA80a, 419	5, 2	B	0.56, 21	1.27(-3)	-0.4	[m]
	VA80c, 5710	1, 2	B	0.56, 21	1.27(-3)	-0.4	[m]
	VA84, 300	14, 2	B	0.56, 21	0.08	2.0	[n]
V02 LECP	VA84, 307	20, 4	Eγ07-Eγ08	0.48, 0.853	2.79(-4)	1.0	[l]
P11 TRD	FI80, 429	5, 1	E1	0.45	1.64(-3)	0.2	[o]
	FM80, 5804	1ab, 3	E3	0.46	4.54(-4)	0.0	[p]
P11 CRT	MD80, 5824	18, 2		0.43, 0.8	0.215	2.0	[k]
V02 LECP	VA84, 307	20, 3	Eγ06-Eγ07	0.252, 0.48	6.45(-4)	1.7	[l]
	AR83, 8899	12, 1	Eγ06-Eγ07	0.252, 0.48	6.45(-4)	0.5	[f]
V01 LECP	KR81, 226	1A, 2	Eβ05	0.2, 0.5	1.59(-4)	-1.0	[f]
P11 CRT	MD80, 5824	18, 1		0.16, 0.43	0.295	3.0	[k]
	TR80, 422	2, 1		0.1, 0.43	0.241	3.0	[k]
P11 TRD	FI80, 427	2C, 2	E1-1.25E2	0.16, 0.25	0.856	4.0	[q]
V01 LECP	CH85, 508	2, 3&4	Eβ04	0.14, 0.2	4.77(-4)	-0.5	[f]
	KR83, 8877	6, 5	Eβ04	0.13, 0.2	4.77(-4)	-1.0	[f]
V02 LECP	VA84, 307	20, 2	Eβ04	0.112, 0.183	3.1(-4)	1.0	[l]
	AR83, 8899	11, 2	Eβ04	0.112, 0.183	3.1(-4)	1.0	[f]
P11 GTT	VA80a, 419	5, 1	A	0.04, 21	1.37(-3)	-0.3	[m]
	VA80c, 5710	1, 1	A	0.04, 21	1.37(-3)	-0.3	[m]
	VA84, 300	13, 1&2	A	0.04, 21	0.08	2.7	[n]

NOTES TO TABLE 3:

[a] The profiles appear in order of decreasing threshold energy E_a (see column 5, note [c]); a profile lacking an entry in column 1 is used in the model only for trajectory points at which no value for countrate R (note [d]) is available from the profile immediately above.

[b] Second entry in this column is the curve placement, counting down from the top of the figure cited.

[c] Where two entries appear, the response (next column) is assumed constant between them, and zero elsewhere; a single entry represents the smaller (threshold E_a) of these two energies, and the other (E_b) is assumed infinite.

[d] Units cm^{-2} assumes R is a countrate (units s^{-1}); exceptions are cited in the notes, and the entry in this column is always the ratio of the profile quantity R (countrate, intensity, flux, etc.) to the local omni flux J (see text following eq. 7). Parentheses enclose powers of ten.

[e] This entry is estimated from the noise or limit of the profile in the figure, in the same units as R in the preceding column (see note [d]).

[f] Energies from profile label, conversion is εG in cm^2sr (KR83, p. 8874, Table 1) divided by 4π sr.

[g] Energy from figure label, profile is flux J, no conversion needed.

[h] Energy from source (FM80, p. 5805, Table 1), profile is current, conversion is as discussed in Appendix B (last para.).

[i] Energies from profile label, conversion is 0.43 cm^2sr (SI80b, p. 5757, Table A1) divided by 4π sr.

[j] Energy from profile label, conversion is εG=0.12 cm^2sr (KR83, p. 8874, Table 1) divided by 4π sr and by an additional factor 10 to secure agreement with a corresponding profile (KA82, p. 1144, Fig. 2, curve 3 from top) and with Pioneer 11 detectors at nearby energies.

[k] Energies from figure caption (or label), profile is differential intensity i, conversion is $(4\pi \text{ sr})^{-1}(E_b - E_a)^{-1}$.

[l] Same as note [f], but conversion also confirmed by comparison with spectrum at L=9.56, as discussed in Appendix B (para. 4).

[m] Energies from source (VA80a, p. 416, Table 1), conversion is Q from same table.

[n] Energies as in note [m], profile is integral intensity I, conversion is $(4\pi \text{ sr})^{-1}$.

[o] Energy from profile label, comversion is $(R/J)_3(R_1/R_3)$, where subscript 1 is for channel E1, subscript 3 is for channel E3, R_1 and R_3 are the peak countrates at L=2.7, and conversion $(R/J)_3$ is derived in note [p].

[p] Energy from source (FM80, p. 5805, Table 1), conversion is 0.0057 cm^2sr (same table) divided by 4π sr.

[q] Energies from source (FI80, p. 426, Table 1), profile is differential intensity i, conversion is $(4\pi \text{ sr})^{-1}(E_b - E_a)^{-1}$.

Table 4. Identification of data profiles used for the Saturn proton model. Detailed notes appear on the following page.

SPACECRAFT, SUBSYSTEM [a]	REFERENCE, PAGE	FIGURE, LINE [b]	CHANNEL	ENERGIES E_a, E_b (MeV) [c]	CONVERSION R/J (cm^2) [d]	BACK-GROUND $\log R_B$ [e]	NOTES
P11 TRD	FI80, 429	5, 3	M1	80	0.038	0.0	[f]
	FM80, 5804	1ab, 5	M3	80	0.012	-1.0	[g]
P11 GTT	VA80a, 418	4, 2&4	D	80	0.043	-0.5	[h]
	VA80c, 5710	1, 4	D	80	0.043	-0.5	[i]
	VA80a, 417	3, 2&4	D	80	0.043	-0.5	[h]
P11 GTT	VA80a, 419	5, 3	C	80	0.122	-0.3	[h]
	VA80a, 418	4, 1&3	C	80	0.122	0.0	[h]
	VA83, 6913	4, 1	C	80	0.122	0.0	[j]
	VA83, 6913	5, 1	C	80	0.122	0.0	[j]
	VA80c, 5710	1, 3	C	80	0.122	-0.3	[i]
	VA80a, 417	3, 1&3	C	80	0.122	0.0	[h]
V02 CRS	SM83, 8925	3, 2		63, 160	8.2(-4)	-3.0	[k]
V02 LECP	KR82, 573	2C, 3	PAB12	54, 87	0.004	-2.0	[l]
V02 CRS	SM83, 8925	3, 1		48, 63	5.31(-3)	-2.5	[k]
	SM83, 8924	2, 1		48, 63	1.85	0.0	[m]
P11 CPT	SI80b, 5742	14, 2	FCD	35	2.5(-5)	-1.5	[n]
V02 CRS	VO82, 579	3, 1	A	27, 160	0.08	-0.8	[o]
P11 CRT	MD80, 5815	3, 4		2.1, 3.1	0.08	-2.0	[k]
P11 CRT	MD80, 5824	19, 1		1.56, 5.1	0.08	-2.0	[o]
P11 CRT	TR80, 422	1, 3		1.1, 2.15	0.076	0.0	[p]
P11 CRT	TR80, 422	1, 2		0.75, 1.2	0.177	1.0	[p]
P11 GTT	VA80a, 417	2, 1	G	0.61, 3.41	3.5(-3)	-0.8	[h]
	VA84, 290	5, 1&2	G	0.61, 3.41	0.08	0.2	[o]
V02 LECP	VA84, 296	10, 2	PL06	0.54, 0.99	0.009	-3.0	[l]
P11 CRT	MD80, 5815	3, 2		0.53, 0.74	0.379	1.0	[p]
P11 CPT	SI80b, 5748	20A2, 1	L1$\overline{L2}$	0.5, 1.8	0.039	0.3	[q]
	SI80b, 5748	20C2, 1	L1$\overline{L2}$	0.5, 1.8	0.039	0.3	[q]
	SI80b, 5742	14, 1	L1$\overline{L2}$	0.5, 1.8	0.039	0.3	[q]
	SI80b, 5743	15, 1&2	L1$\overline{L2}$	0.5, 1.8	0.039	0.3	[q]
P11 CRT	TR80, 422	1, 1		0.2, 0.75	0.145	2.0	[k]
V01 LECP	CH85, 508	1, 3&4	PL04	0.139, 0.22	3.2(-3)	-0.5	[l]
V02 LECP	AR83, 8895	3, 2	PL04	0.137, 0.215	0.009	2.0	[l]

NOTES TO TABLE 4:

[a] The profiles appear in order of decreasing threshold energy E_a (see column 5, note [c]); a profile lacking an entry in column 1 is used in the model only for trajectory points at which no value for countrate R (note [d]) is available from the profile immediately above.

[b] Second entry in this column is the curve placement, counting down from the top of the figure cited.

[c] Where two entries appear, the response (next column) is assumed constant between them, and zero elsewhere; a single entry represents the smaller (threshold E_a) of these two energies, and the other (E_b) is assumed infinite.

[d] Units cm^{-2} assumes R is a countrate (units s^{-1}); exceptions are cited in the notes, and the entry in this column is always the ratio of the profile quantity R (countrate, intensity, flux, etc.) to the local omni flux J (see text following eq. 7). Parentheses enclose powers of ten.

[e] This entry is estimated from the noise or limit of the profile in the figure, in the same units as R in the preceding column (see note [d]).

[f] Energy from profile label, conversion is geometric factor in cm^2 (FI80, p. 426, Table 1).

[g] Energy from source (FM80, p. 5805, Table 1), conversion is geometric factor in cm^2 (same table; note disagreement with FI80, p. 426, Table 1).

[h] Energy from source (VA80a, p. 416, Table 1), conversion is Q from same table.

[i] Energy from source (VA80b, p. 5682, Table 2), conversion is Q from same table.

[j] Energy as in note [h], conversion from source (VA83, p. 6912, eq. 1).

[k] Energies from figure caption (or label), profile is differential intensity i, conversion is $(4\pi\ \mathrm{sr})^{-1}(E_b - E_a)^{-1}$.

[l] Energies from profile label, conversion is εG in $cm^2 sr$ (KR83, p. 8874, Table 1) divided by 4π sr.

[m] Energies as for preceding profile, conversion is $(4\pi\ \mathrm{sr})^{-1}(E_b - E_a)^{-1}(R_3/i_3)$ where $\log R_3 = 3.75$ and $\log i_3 = 1.21$ are peak rates from this and the preceding profile.

[n] Energy from profile label, conversion from source (SI80b, p. 5757, Table A1), weight is 2.0 to compensate for indistinguishability of the inbound and outbound profiles.

[o] Energies from figure caption, profile is integral intensity I, conversion is $(4\pi\ \mathrm{sr})^{-1}$.

[p] Same as note [k], but conversion also confirmed by comparison with spectrum at 7.81 R_S, as discussed in Appendix B (para. 4).

[q] Energies from profile label, conversion is geometric factor in $cm^2 sr$ (SI80b, p. 5757, Table A1) divided by 4π sr.

Table 5. Parameter values for the Saturn electron model. See model description accompanying equations (1) through (5).

L	a_o	a_1	a_2	a_3	b_o	b_1	b_2	b_3	E_2	E_3
2.30	4.74	0.00	0.00	6.47	4.74	0.00	0.00	6.47	0.60	1.50
2.33	5.02	0.00	0.00	4.01	5.02	0.00	0.00	4.01	0.60	1.50
2.34	4.91	0.00	0.00	4.86	4.91	0.00	0.00	4.86	0.60	1.50
2.36	4.98	0.00	0.00	4.41	4.98	0.00	0.00	4.41	0.60	1.50
2.38	5.00	0.00	0.00	5.37	5.00	0.00	0.00	5.37	0.60	1.50
2.46	5.49	0.00	0.23	3.00	5.49	0.00	0.23	3.00	0.60	2.00
2.56	5.56	0.00	0.34	3.00	5.56	0.00	0.34	3.00	0.60	2.00
2.70	5.51	0.00	0.27	4.48	5.51	0.00	0.27	4.48	0.60	2.00
2.83	5.52	0.00	0.25	3.11	5.52	0.00	0.25	3.11	0.20	2.00
2.93	5.46	0.00	0.28	3.42	5.46	0.00	0.28	3.42	0.20	2.00
3.04	5.38	0.00	0.27	4.96	5.38	0.00	0.27	4.96	0.20	2.00
3.08	5.31	0.00	0.29	5.23	5.48	0.00	0.29	5.23	0.20	2.00
3.20	5.03	0.00	0.20	5.48	5.74	0.00	0.20	5.48	0.20	2.00
3.40	5.50	0.00	0.00	4.27	4.90	0.00	0.61	4.27	0.20	2.00
3.90	4.88	0.00	0.20	5.71	4.72	0.21	0.78	5.71	0.20	2.00
4.30	4.67	0.00	0.00	4.29	4.50	0.00	0.56	4.29	0.10	1.00
4.44	4.74	0.00	0.00	4.23	4.12	0.00	0.68	4.23	0.10	1.00
4.96	3.58	0.00	0.34	5.74	5.30	0.00	0.11	5.74	0.10	1.00
5.41	3.50	0.00	0.27	5.26	5.38	0.00	0.11	5.26	0.10	1.00
5.87	4.57	0.00	0.05	6.67	3.73	1.01	0.68	6.67	0.10	1.00
6.20	3.26	0.00	0.00	4.22	4.60	0.26	0.00	4.22	0.08	0.50
6.50	3.95	0.00	0.06	3.00	4.83	0.00	0.19	3.00	0.08	0.50
7.20	3.33	0.00	0.00	6.10	3.20	0.21	0.66	6.10	0.08	0.50
8.00	3.42	0.00	0.00	5.50	2.56	0.16	2.45	5.50	0.08	0.50
9.50	3.02	0.00	0.83	6.00	2.11	0.00	2.22	6.00	0.08	0.50
11.00	3.64	0.00	1.17	3.01	1.98	0.00	3.78	3.01	0.08	0.50
13.00	2.09	2.23	0.00	7.59	2.09	2.23	0.00	7.59	0.08	0.50

Table 6. Parameter values for the Saturn proton model. See model description accompanying equations (1) through (5).

L	a_o	a_1	a_2	a_3	b_o	b_1	b_2	b_3	E_2	E_3
2.30	1.86	0.00	0.00	4.57	1.86	0.00	0.00	4.57	1.00	60.0
2.32	2.07	0.00	0.00	4.53	2.07	0.00	0.00	4.53	1.00	60.0
2.34	2.17	0.00	0.00	6.09	2.17	0.00	0.00	6.09	1.00	60.0
2.43	3.18	0.05	0.00	3.05	3.18	0.05	0.00	3.05	1.00	60.0
2.52	2.14	1.85	0.00	3.00	2.14	1.85	0.00	3.00	1.00	60.0
2.67	3.80	0.75	0.00	3.00	3.80	0.75	0.00	3.00	1.00	60.0
2.77	3.37	1.28	0.00	3.00	3.37	1.28	0.00	3.00	0.50	60.0
2.82	3.26	2.63	0.00	3.00	3.26	2.63	0.00	3.00	0.30	60.0
2.86	3.14	2.93	0.00	3.00	3.14	2.93	0.00	3.00	0.30	60.0
3.10	0.37	0.00	0.00	3.00	0.67	4.87	6.27	3.00	1.00	60.0
3.20	2.91	0.29	0.00	3.00	-0.25	6.63	0.00	3.00	1.00	60.0
3.31	2.86	0.02	0.02	3.00	0.29	8.30	0.00	3.00	0.50	60.0
3.44	2.80	0.98	0.00	3.00	0.46	7.41	0.00	3.00	0.50	60.0
3.71	2.16	1.77	0.00	3.00	0.40	7.10	0.00	3.00	0.50	60.0
3.99	-0.13	0.00	0.26	3.00	0.58	7.70	0.52	3.00	0.50	60.0
4.13	1.29	0.00	0.00	3.00	-0.10	9.00	0.15	3.00	0.50	60.0
4.27	0.63	0.46	0.29	3.22	0.16	8.55	0.00	3.22	0.50	60.0
4.38	0.61	5.05	0.20	3.12	-0.03	6.93	0.00	3.12	0.50	60.0
4.49	0.47	5.25	0.21	3.55	-0.06	7.15	0.00	3.55	0.50	60.0
5.01	0.68	1.45	0.00	4.41	-1.13	6.73	6.85	4.41	0.50	0.80
5.36	1.77	0.00	0.00	3.00	-0.98	6.78	8.25	3.00	0.50	0.80
6.20	2.32	3.32	0.00	3.08	0.10	5.51	2.99	3.08	0.50	0.80
6.45	2.40	3.34	0.00	3.00	0.06	5.81	2.66	3.00	0.50	0.80
6.70	2.46	2.59	0.52	4.72	0.30	5.83	0.12	4.72	0.50	0.80
7.63	2.46	3.55	0.25	3.85	0.81	4.90	0.61	3.85	0.50	0.80
8.40	2.31	6.28	1.73	3.35	1.07	0.48	1.73	3.35	0.30	0.80
10.30	1.90	6.52	1.81	4.11	0.74	0.00	0.85	4.11	0.30	0.80
12.00	1.24	0.00	6.35	3.94	1.24	0.00	6.35	3.94	0.30	0.80
13.00	1.22	0.00	6.72	3.31	1.22	0.00	6.72	3.31	0.30	0.80

Table 7. Summary of range in L and residuals (see eq. 8) for the Saturn electron model. See Table 3 (column 1 and note [a]) for association with the data profiles by detector.

SPACECRAFT, SUBSYSTEM	MINIMUM L	MAXIMUM L	MINIMUM Δ	MEAN Δ	MAXIMUM Δ	RMS Δ
V02 LECP	2.83	5.41	-0.16	0.01	0.14	0.09
P11 CPT	2.34	2.38	-0.21	-0.03	0.19	0.14
	2.33	5.41	-0.07	0.72	1.23	0.81
P11 TRD	2.36	6.20	-0.66	-0.09	0.17	0.20
P11 CPT	9.5	13.0	-3.23	-1.76	-0.57	2.04
V02 LECP	2.83	5.41	-1.71	-0.13	0.18	0.46
P11 CRT	2.30	11.0	-0.81	0.18	1.05	0.41
	13.0	13.0	-0.02	0.35	0.71	0.50
V02 LECP	2.83	9.50	-1.35	0.50	1.42	0.93
P11 CRT	2.30	11.0	-0.48	0.09	0.90	0.26
	13.0	13.0	-0.03	0.39	0.80	0.57
P11 GTT	2.30	2.46	-0.26	0.10	0.52	0.28
	2.70	3.40	-0.04	0.03	0.13	0.06
	2.56	13.0	-0.27	0.02	0.21	0.13
V02 LECP	2.83	9.50	0.02	0.41	0.84	0.45
P11 TRD	2.33	3.20	-1.35	-0.22	0.09	0.46
	2.70	6.20	-0.18	-0.05	0.16	0.11
P11 CRT	2.30	11.0	-0.56	-0.12	0.28	0.21
V02 LECP	2.93	9.50	-0.34	0.36	0.87	0.45
	2.83	11.0	-0.20	0.07	0.62	0.19
V01 LECP	4.44	13.0	-1.63	-0.05	0.95	0.60
P11 CRT	4.96	11.0	-0.21	0.07	0.35	0.18
	13.0	13.0	-0.15	-0.04	0.08	0.12
P11 TRD	5.41	13.0	-0.69	-0.17	0.18	0.28
V01 LECP	11.0	13.0	0.08	0.46	0.92	0.55
	4.44	9.50	-0.11	0.36	1.24	0.58
V02 LECP	2.83	9.5	-0.07	0.27	0.55	0.34
	2.83	7.20	-0.38	-0.09	0.05	0.14
P11 GTT	2.33	2.46	-0.07	0.14	0.43	0.23
	2.70	3.40	-0.20	-0.13	-0.05	0.14
	2.36	13.0	-0.46	-0.11	0.05	0.17

Table 8. Summary of range in L and residuals (see eq. 8) for the Saturn proton model. See Table 4 (column 1 and note [a]) for association with the data profiles by detector.

SPACECRAFT, SUBSYSTEM	MINIMUM L	MAXIMUM L	MINIMUM Δ	MEAN Δ	MAXIMUM Δ	RMS Δ
P11 TRD	2.43	3.31	-0.93	-0.20	0.15	0.41
	2.77	4.13	-1.71	-0.07	0.76	0.59
P11 GTT	2.43	2.82	-0.04	0.15	0.73	0.27
	2.86	3.44	-0.12	0.57	2.46	1.11
	2.30	4.27	-1.20	0.17	1.75	0.76
P11 GTT	2.30	2.43	-0.61	0.00	0.37	0.37
	2.52	2.82	0.11	0.25	0.85	0.35
	2.82	3.10	0.20	0.98	2.50	1.46
	2.86	3.10	0.21	1.40	2.58	1.83
	3.20	3.44	-0.04	0.13	0.23	0.16
	2.34	4.27	-1.06	0.51	1.98	1.01
V02 CRS	2.77	5.36	-0.82	-0.15	0.20	0.31
V02 LECP	2.77	5.01	-2.29	-0.63	0.06	0.86
V02 CRS	2.77	5.36	-1.22	-0.08	0.21	0.32
	2.82	3.10	-0.80	-0.53	-0.28	0.57
P11 CPT	2.67	3.44	-0.26	-0.16	-0.04	0.18
V02 CRS	4.13	5.36	-0.67	-0.09	0.08	0.24
P11 CRT	3.31	4.49	-0.24	-0.10	0.03	0.13
P11 CRT	2.30	5.01	-1.19	-0.13	0.13	0.36
P11 CRT	2.43	13.0	-0.38	0.27	1.32	0.46
P11 CRT	5.01	13.0	-0.35	-0.01	0.38	0.20
P11 GTT	5.36	7.63	-0.12	-0.01	0.10	0.08
	3.99	13.0	-0.22	0.10	0.51	0.21
V02 LECP	3.10	10.3	-0.50	-0.07	0.19	0.17
P11 CRT	3.31	5.01	-0.07	0.56	1.17	0.69
P11 CPT	2.43	2.67	-1.49	-0.91	0.0	1.12
	2.67	2.67	-1.30	-1.30	-1.30	1.30
	3.10	4.49	-1.02	-0.27	-0.03	0.44
	4.38	13.0	-0.46	-0.14	0.24	0.21
P11 CRT	2.43	13.0	-0.44	0.12	1.40	0.37
V01 LECP	10.3	13.0	-1.02	-0.32	0.00	0.48
V02 LECP	2.82	7.63	-0.14	0.00	0.25	0.10

Figure 1. Trajectories of Saturn flyby spacecraft in magnetic coordinates (reproduced from Fig. 1c of KR83). The Pioneer 11 trajectory closely follows the curve labelled $|B_{eq}|$ inwards to L=1.43 and B=0.0801 G, whereas the Voyager 1 and 2 trajectories follow the dashed and solid curves, respectively. See field model and trajectory entries in Tables 1 and 2.

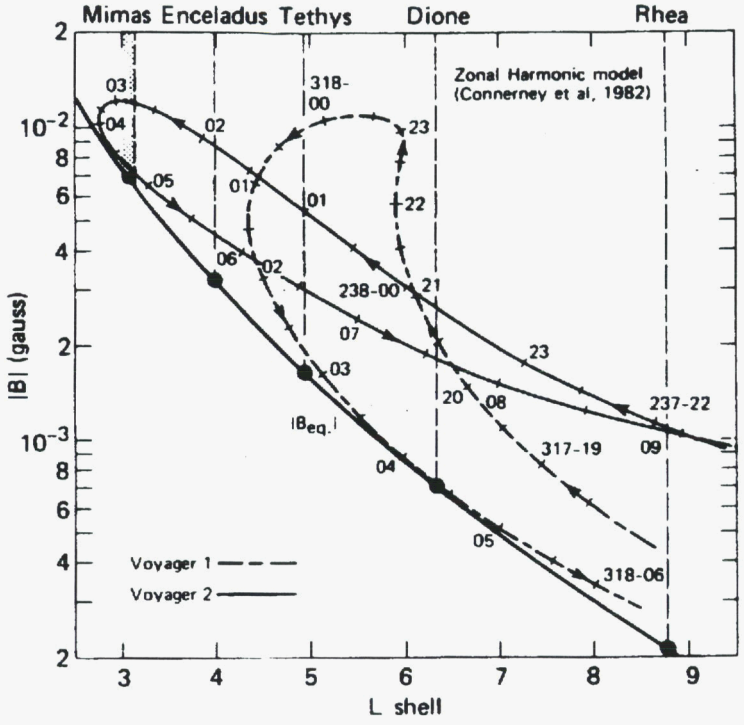

Figure 2. Coverage of the data for the Saturn electron model as a function of L. At the left, the histogram encloses values of magnetic field ratio B_e/B spanned by the data. In the center, the histogram encloses values of the threshold energy (E_a in Table 3) spanned by the data (dashed lines are E_2 and E_3 from Table 5). At the right three columns specify the number of data points used, and those having residuals limited by the factors $4^{\pm 1}$ and $2^{\pm 1}$. The last column displays the modified RMS residual at each L (see eq. 10, using Δ_o=0.3).

MAG. SHELL PARAMETER L	TOTAL POINTS	POINTS $\lvert\Delta\rvert$<0.6	POINTS $\lvert\Delta\rvert$<0.3	MODIFIED RMS RESIDUAL Y
2.30	4	4	4	0.18
2.33	8	6	6	0.22
2.34	10	8	8	0.19
2.36	12	12	12	0.14
2.38	13	13	10	0.20
2.46	11	10	9	0.23
2.56	13	12	10	0.20
2.70	16	14	14	0.19
2.83	26	23	21	0.20
2.93	26	23	20	0.21
3.04	26	23	20	0.22
3.08	26	23	20	0.22
3.20	26	22	20	0.22
3.40	26	23	19	0.23
3.90	24	21	19	0.21
4.30	24	20	18	0.21
4.44	29	26	21	0.21
4.96	27	25	18	0.24
5.41	30	24	19	0.26
5.87	29	24	22	0.23
6.20	25	20	17	0.25
6.50	23	18	17	0.24
7.20	23	20	16	0.24
8.00	22	18	17	0.22
9.50	22	19	17	0.23
11.0	19	15	12	0.25
13.0	16	11	11	0.25

Figure 3. Coverage of the data for the Saturn proton model as a function of L. At the left, the histogram encloses values of magnetic field ratio B_e/B spanned by the data. In the center, the histogram encloses values of the threshold energy (E_a in Table 4) spanned by the data (dashed lines are E_2 and E_3 from Table 6). At the right three columns specify the number of data points used, and those having residuals limited by the factors $4^{\pm 1}$ and $2^{\pm 1}$. The last column displays the modified RMS residual at each L (see eq. 10, using Δ_o=0.3).

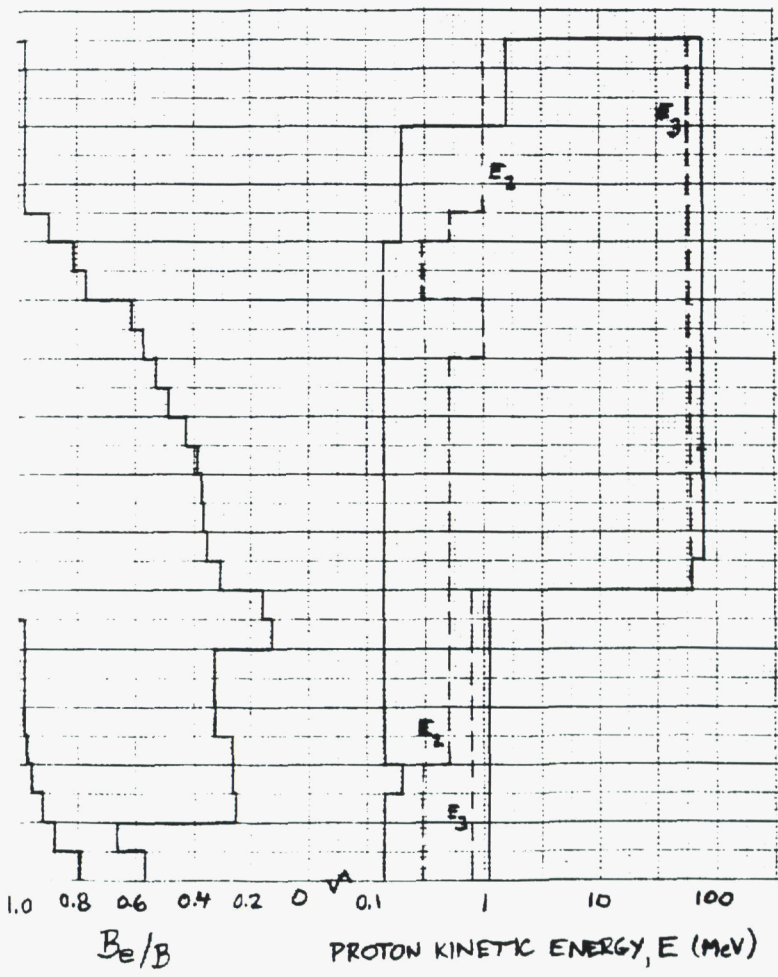

MAG. SHELL PARAMETER L	TOTAL POINTS	POINTS $\|\Delta\|<0.6$	POINTS $\|\Delta\|<0.3$	MODIFIED RMS RESIDUAL Y
2.30	3	3	3	0.11
2.32	4	4	2	0.25
2.34	5	4	4	0.23
2.43	10	6	6	0.28
2.52	12	4	4	0.35
2.67	15	11	11	0.25
2.77	21	19	16	0.23
2.82	23	19	17	0.24
2.86	23	21	18	0.23
3.10	22	14	14	0.26
3.20	23	15	14	0.28
3.31	27	25	23	0.19
3.44	26	25	23	0.17
3.71	24	23	20	0.20
3.99	25	18	18	0.23
4.13	27	22	18	0.23
4.27	23	19	18	0.20
4.38	24	23	20	0.18
4.49	24	23	21	0.17
5.01	22	19	18	0.19
5.36	20	19	18	0.16
6.20	14	14	14	0.17
6.45	14	14	13	0.18
6.70	14	14	12	0.21
7.63	14	14	12	0.18
8.40	12	12	11	0.15
10.3	14	14	13	0.16
12.0	12	12	12	0.15
13.0	12	11	10	0.24

Figure 4. Integral intensity for the Saturn electron model at three energy thresholds. As evaluated at the magnetic equator, the perpendicular and parallel intensities $I_{\perp}$ and $I_{\parallel}$ are represented respectively by the solid and dashed lines. Note that the curves for E=1.0 MeV reproduce the values for a_o and b_o in Table 5 (cf. eq. 1 and 3). The horizontal axis changes scale at L=5.

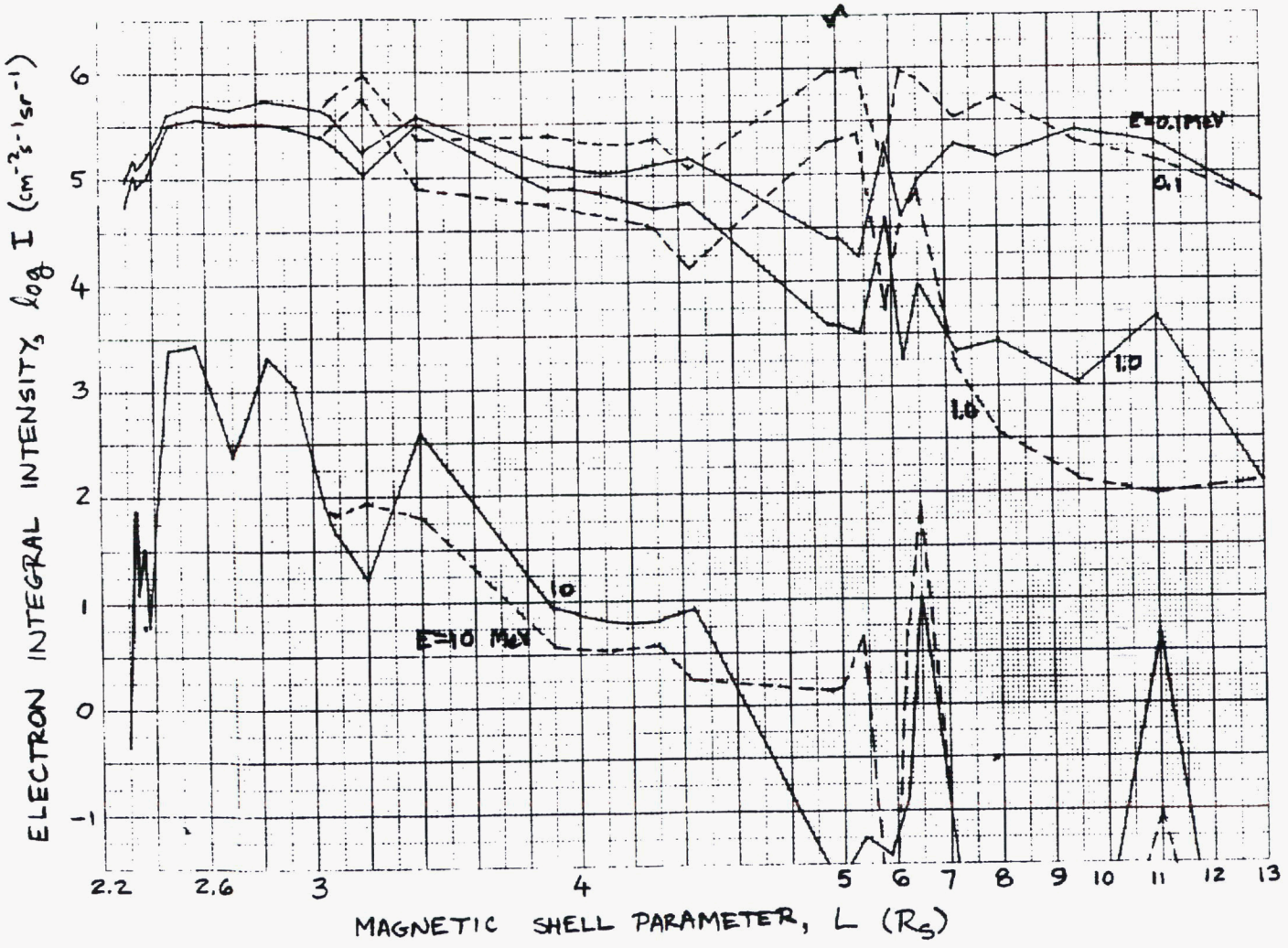

Figure 5. Integral omnidirectional flux for the Saturn electron model at three energy thresholds. The fluxes at the magnetic equator (B_e/B=1.0) and at high magnetic latitude (B_e/B=0) are represented respectively by the solid and dashed lines. The horizontal axis changes scale at L=5.

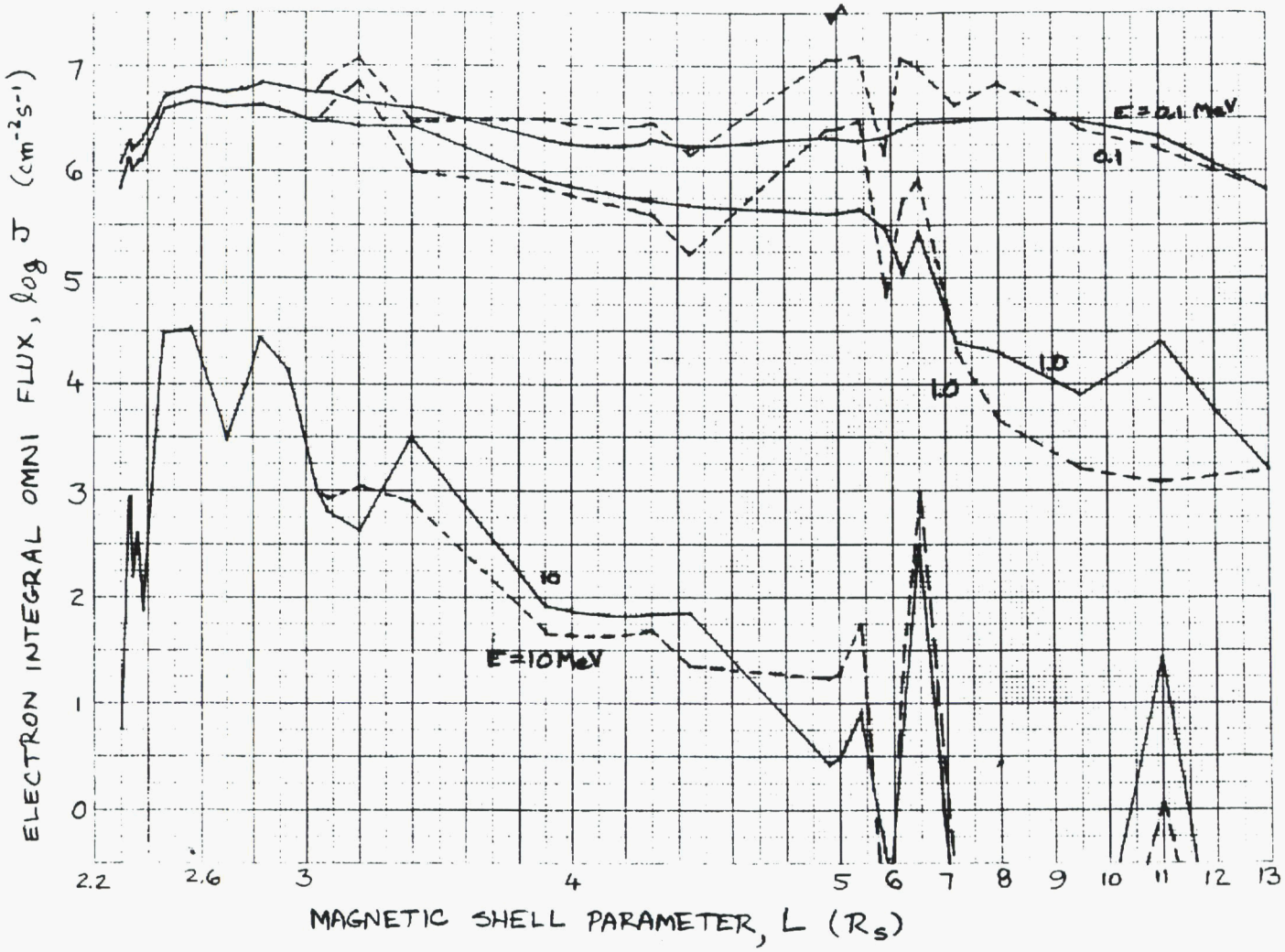

Figure 6. Integral intensity for the Saturn electron model at three sample values of L (numbers adjacent to the curves). On the left the dependences on pitch angle α are shown for energy thresholds of 0.1, 1.0, and 10 MeV (solid, dashed, and solid lines) at each L. On the right spectra are shown for $I_{\perp}$ (solid lines) and for $I_{\parallel}$ (dashed lines) at each L ($I_{\perp}$ and $I_{\parallel}$ are equal for the isotropic distribution at L=2.83).

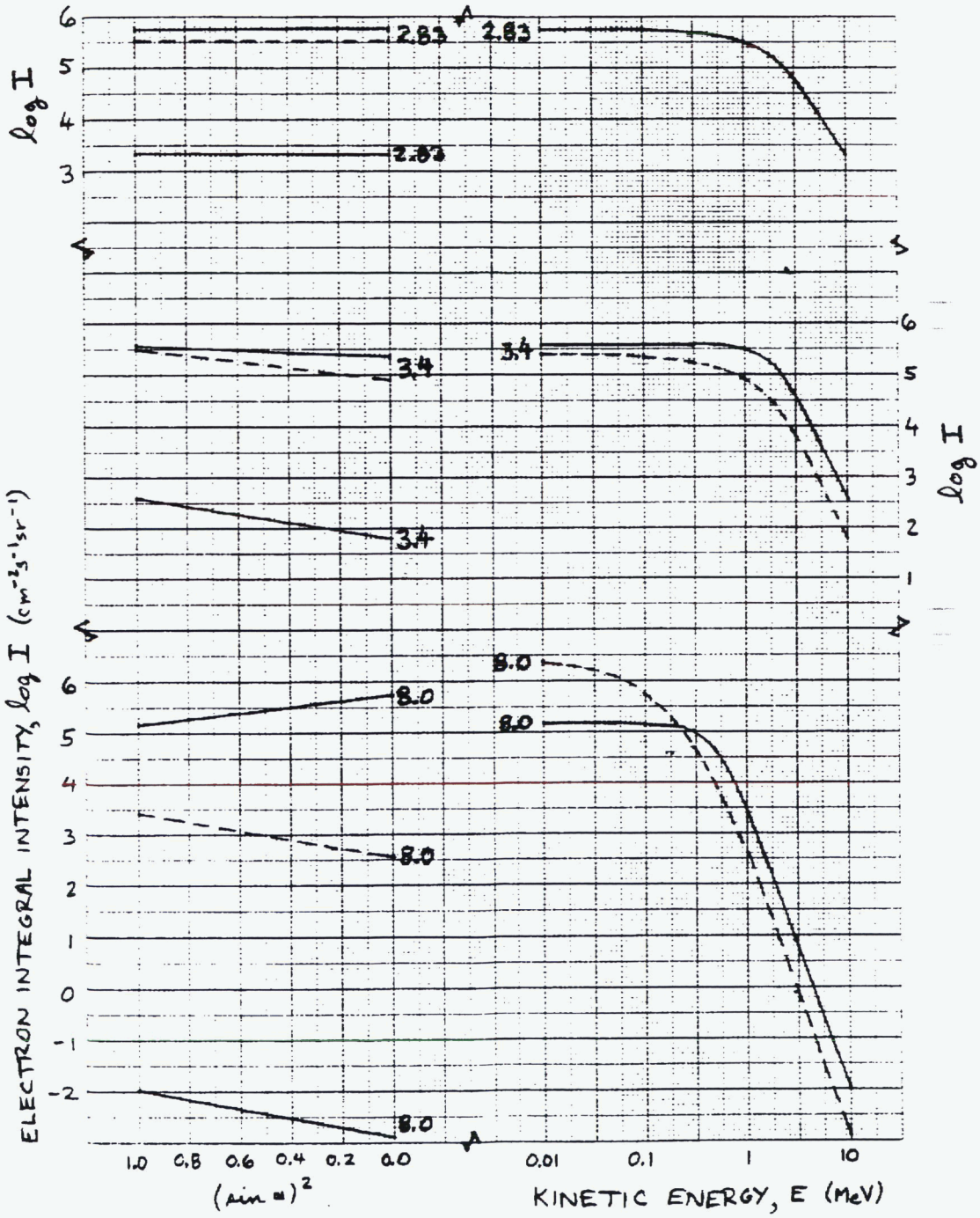

Figure 7. Integral omnidirectional flux for the Saturn electron model at three sample values of L (numbers adjacent to the curves). On the left the dependences on local magnetic field strength B are shown for energy thresholds of 0.1, 1.0, and 10 MeV (solid, dashed, and solid lines) at each L. On the right spectra are shown for the magnetic equator (B_e/B=1.0, solid lines) and for high magnetic latitude (B_e/B=0, dashed lines) at each L.

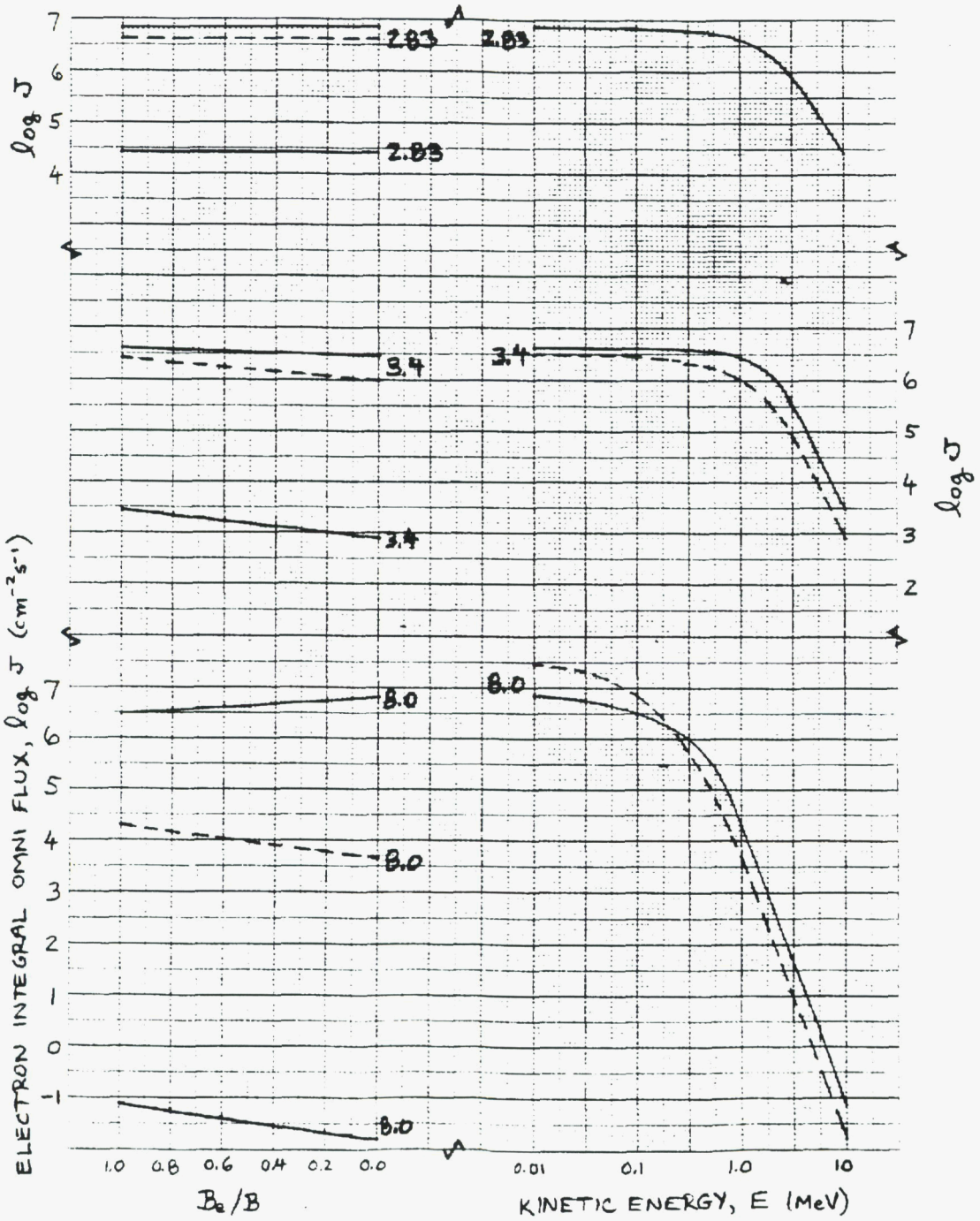

Figure 8. Integral intensity for the Saturn proton model at three energy thresholds. As evaluated at the magnetic equator, the perpendicular and parallel intensities $I_{\perp}$ and $I_{||}$ are represented respectively by the solid and dashed lines. Note that the curves for E=1.0 MeV reproduce the values for a_o and b_o in Table 6 (cf. eq. 1 and 3). The horizontal axis changes scale at L=5.

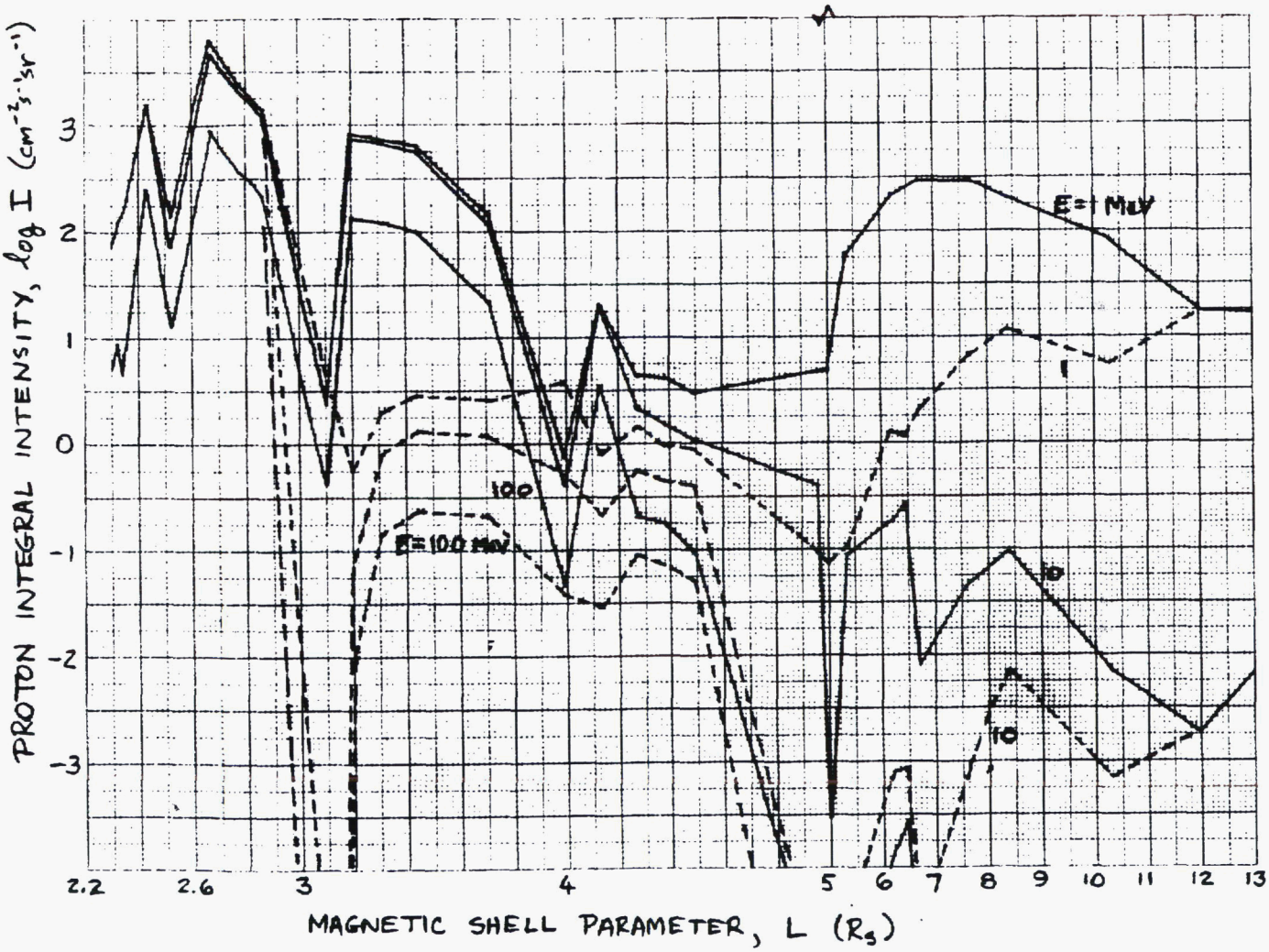

Figure 9. Integral omnidirectional flux for the Saturn proton model at three energy thresholds. The fluxes at the magnetic equator (B_e/B =1.0) and at high magnetic latitude (B_e/B =0) are represented respectively by the solid and dashed lines. The horizontal axis changes scale at L=5.

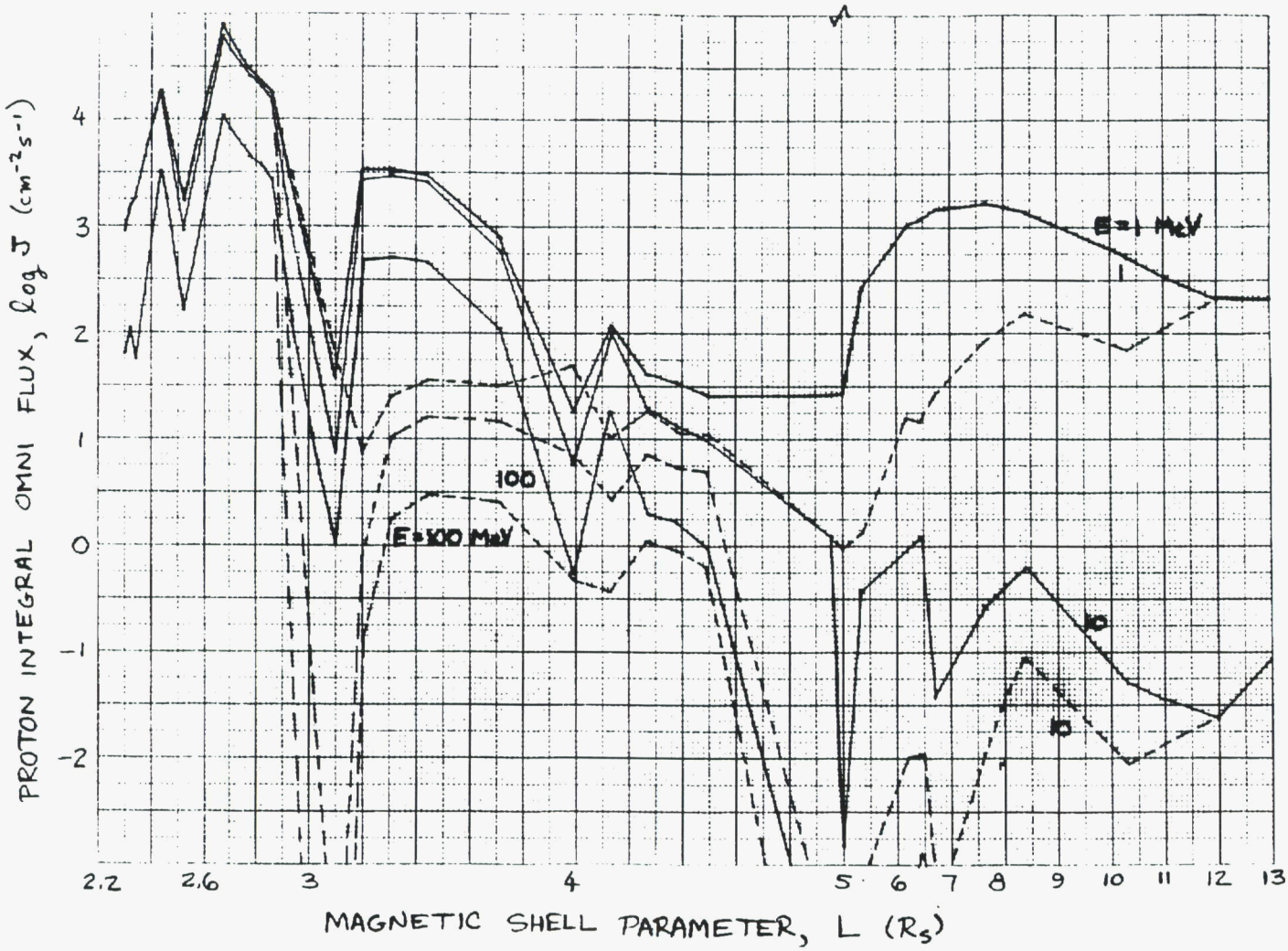

Figure 10. Integral intensity for the Saturn proton model at three sample values of L (numbers adjacent to the curves). On the left the dependences on pitch angle α are shown for energy thresholds of 1, 10, and 100 MeV (solid, dashed, and solid lines) at each L. On the right spectra are shown for $I_{\perp}$ (solid lines) and for $I_{\parallel}$ (dashed lines) at each L ($I_{\perp}$ and $I_{\parallel}$ are equal for the isotropic distribution at L=2.67).

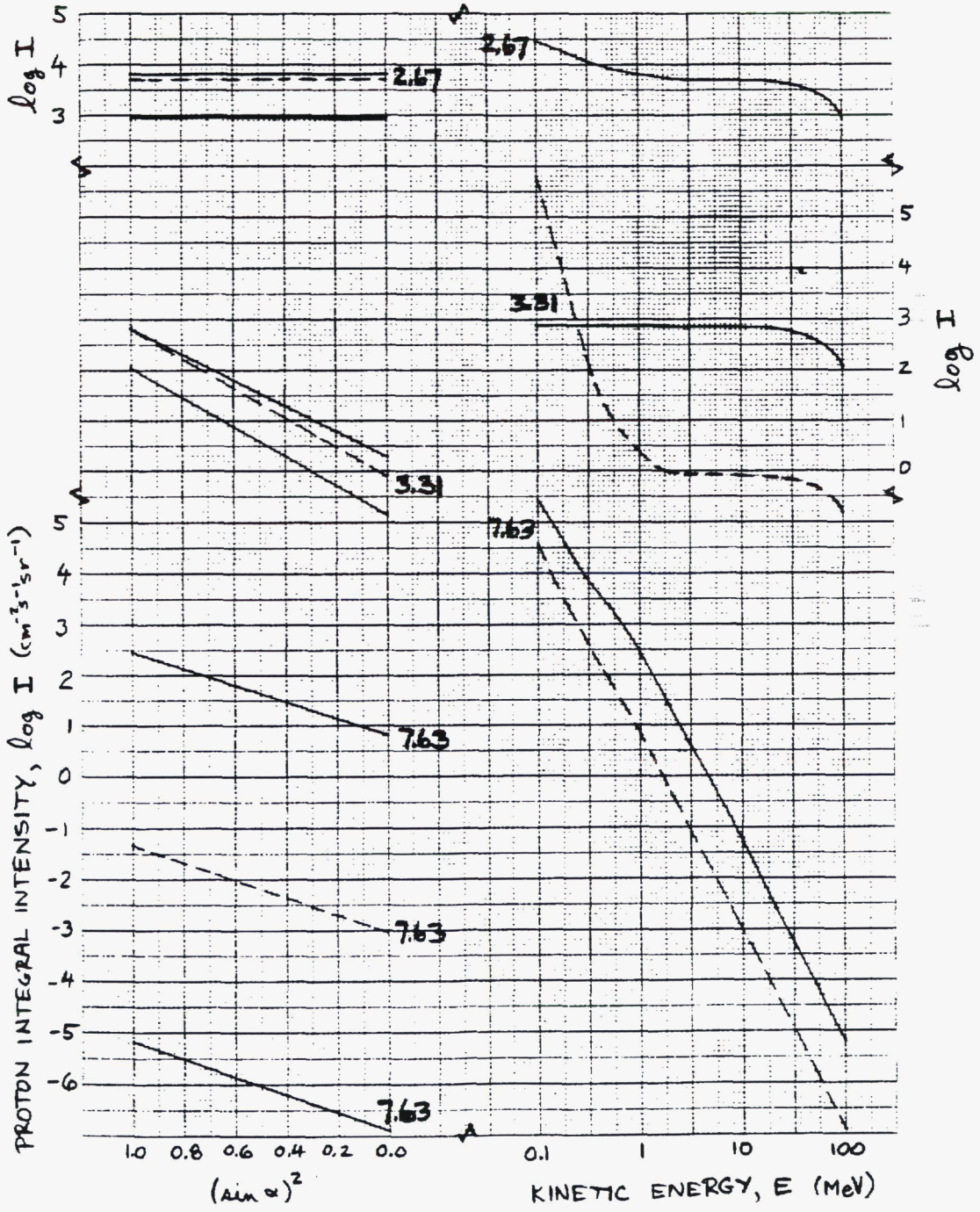

Figure 11. Integral omnidirectional flux for the Saturn proton model at three sample values of L (numbers adjacent to the curves). On the left the dependences on local magnetic field strength B are shown for energy thresholds of 1, 10, and 100 MeV (solid, dashed, and solid lines) at each L. On the right spectra are shown for the magnetic equator (B_e/B =1.0, solid lines) and for high magnetic latitude (B_e/B =0, dashed lines) at each L.

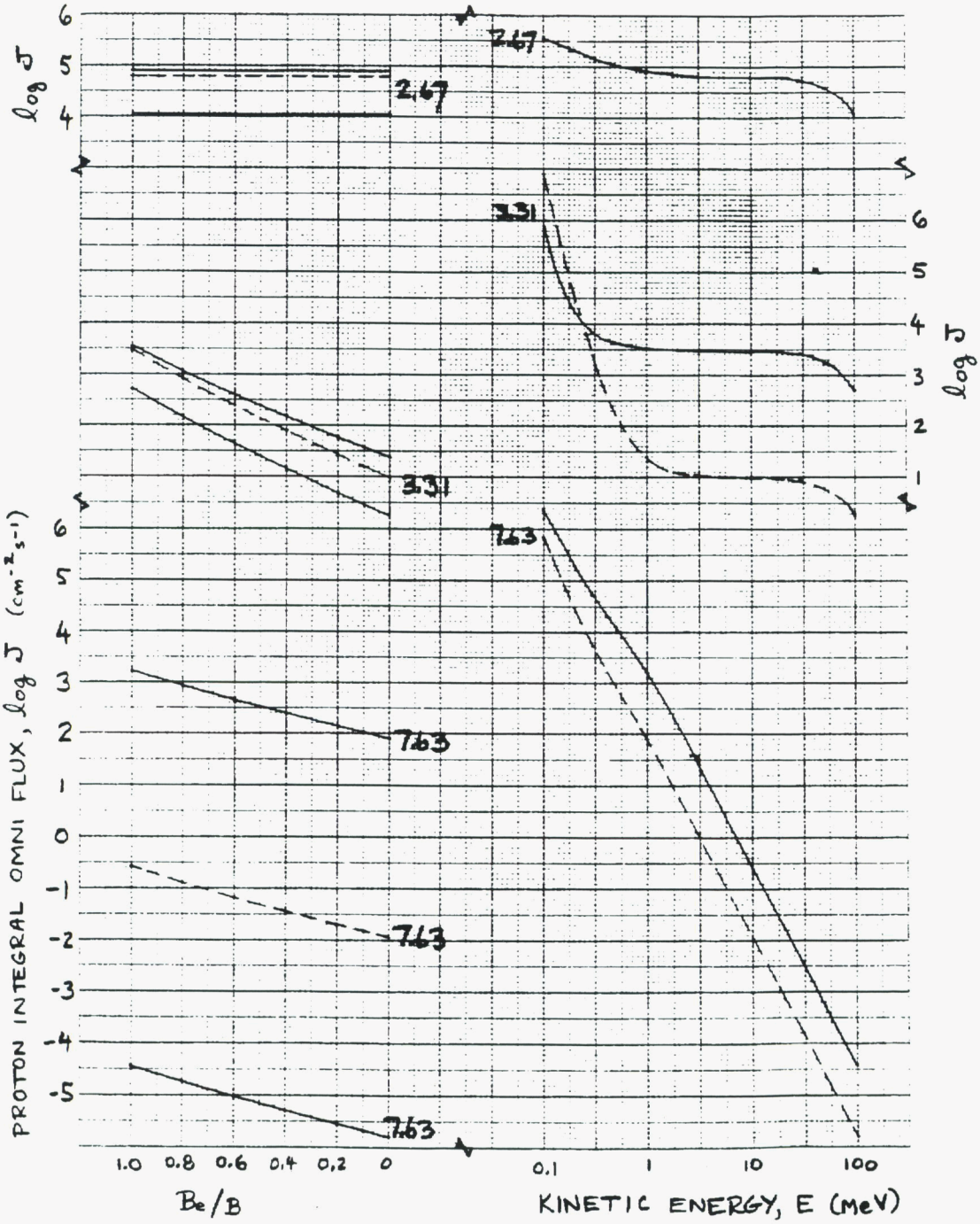

Figure 12. Coverage of the data in magnetic field strength B and threshold energy (see E_a in Tables 3 and 4) for the electron (left panels) and proton (right panels) models at three values of L for each. The residuals are distinguished by values of Δ (cf. eq. 8) in the ranges <-0.6 (symbol ▼), -0.6 to -0.3 (symbol ▽), -0.3 to 0.3 (symbol o), 0.3 to 0.6 (symbol Δ), and >0.6 (symbol ▲).

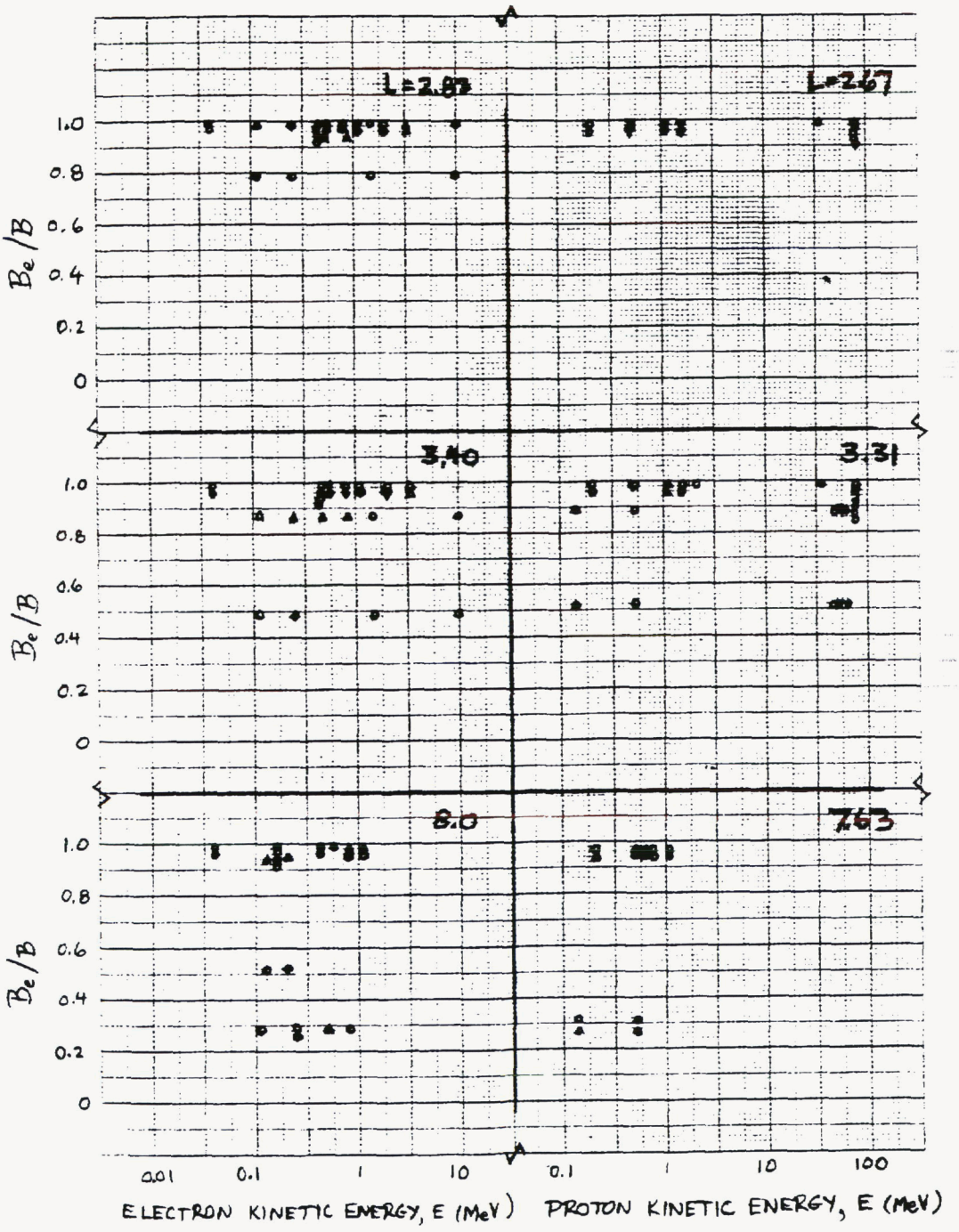

REFERENCES

AR83 Armstrong, T. P., et al., 1983 Nov. 1: "Voyager Observations of Saturnian Ion and Electron Phase Space Densities", J. Geophys. Res., Vol. 88, No. A11, pp. 8893-8904.

CE80 Cesarone, R. J., et al., 1980 Oct. 9: "Voyager 1 Saturn Encounter Trajectory Information", JPL IOM Voyager-NAV-80-196.

CE89 Cesarone, R. J., 1989: private communication.

CH85 Cheng, A. F., et al., 1985 Oct. 10: "Does Saturn Have Rings Outside 10 R_S?", Nature, Vol. 317, pp. 508-509.

CO84 Connerney, J. E. P., et al., 1984: "Magnetic Field Models", in *Saturn* (T. Gehrels and M. S. Matthews, Editors, Univ. of Arizona Press, Tucson), pp. 354-377.

CO89 Cooper, J. F., 1989 Oct. 10: "A Critical Review of Charged Particle Astronomy at Saturn: The Evidence for Co-Orbiting Material in the Inner Satellite System", pp. 5-C-1 to 5-C-35 in Vol. XIII: Physical Models, Cassini Mission: Saturn Orbiter Proposal Information Package, JPL D-6464.

DI80 Divine, Neil, 1980 May 8: "Saturn Radiation Belt Models and Predicted Electron Flux and Fluence for Voyager", JPL IOM 3576-80-93.

DI90 Divine, Neil, 1990 Feb. 12: "Saturn Energetic Electron and Proton Spectra for Cassini", JPL IOM 5217-90-023.

DG83 Divine, N., and H. B. Garrett, 1983 Sept. 1: "Charged Particle Distributions in Jupiter's Magnetosphere", J. Geophys. Res., Vol. 88, No. A9, pp. 6889-6903.

EV87a Evans, R., 1987 Jan. 22: "Saturn Proton Radiation Hazard for a Mariner Mark II Spacecraft", JPL IOM 5137-87-20.

EV87b Evans, R., 1987 Feb 6: "Jupiter and Saturn Single Event Upset Hazard for a Mariner Mark II Spacecraft", JPL IOM 5137-87-35.

FI80 Fillius, W., et al., 1980 Jan. 25: "Trapped Radiation Belts of Saturn: First Look", Science, Vol. 207, No. 4429, pp. 425-431.

FM80 Fillius, W., and C. McIlwain, 1980 Nov. 1: "Very Energetic Protons in Saturn's Radiation Belt", J. Geophys. Res., Vol. 85, No. A11, pp. 5803-5811.

HA83 Hamilton, D. C., et al., 1983 Nov. 1: "Energetic Atomic and Molecular Ions in Saturn's Magnetosphere", J. Geophys. Res., Vol. 88, No. A11, pp. 8905-8922.

HO89 Hood, L. L., 1989 Oct. 10: "Investigation of the Saturn Dust Environment from the Analysis of Energetic Charged Particle Measurements", pp. 5-D-1 to 5-D-30 in Vol. XIII: Physical Models, Cassini Mission: Saturn Orbiter Proposal Information Package, JPL D-6464.

KA82 Krimigis, S. M., and T. P. Armstrong, 1982 Oct.: "Two-Component Proton Spectra in the Inner Saturnian Magnetosphere", Geophys. Res. Letters, Vol. 9, No. 10, pp. 1143-1146.

KR81 Krimigis, S. M., et al., 1981 April 10: "Low-Energy Charged Particles in Saturn's Magnetosphere: Results from Voyager 1", Science, Vol. 212, No. 4491, pp. 225-231.

KR82 Krimigis, S. M., et al., 1982 Jan. 29: "Low-Energy Hot Plasma and Particles in Saturn's Magnetosphere", Science, Vol. 215, No. 4532, pp. 571-577.

KR83 Krimigis, S. M., et al., 1983 Nov. 1: "General Characteristics of Hot Plasma and Energetic Particles in the Saturnian Magnetosphere: Results from the Voyager Spacecraft", J. Geophys. Res., Vol. 88, No. A11, pp. 8871-8892.

MD80 McDonald, F. B., et al., 1980 Nov. 1: "If You've Seen One Magnetosphere, You Haven't Seen Them All: Energetic Particle Observations in the Saturn Magnetosphere", J. Geophys. Res., Vol. 85, No. A11, pp. 5813-5830.

MS80 McKibben, R. B., and J. A. Simpson, 1980 Nov. 1: "Charged Particle Diffusion and Acceleration in Saturn's Radiation Belts", J. Geophys. Res., Vol. 85, No. A11, pp. 5773-5783.

RO70 Roederer, J. G., 1970: *Dynamics of Geomagnetically Trapped Radiation*, Springer-Verlag, Berlin, 166 pp.

SL74 Schulz, M., and L. J. Lanzerotti, 1974: *Particle Diffusion in the Radiation Belts*, Springer-Verlag, Berlin, 215 pp.

SM83 Schardt, A. W., and F. B. McDonald, 1983 Nov. 1: "The Flux and Source of Energetic Protons in Saturn's Inner Magnetosphere", J. Geophys. Res., Vol. 88, No. A11, pp. 8923-8935.

SI80a Simpson, J. A., et al., 1980 Jan. 25: "Saturnian Trapped Radiation and Its Absorption by Satellites and Rings: The First Results from Pioneer 11", Science, Vol. 207, No. 4429, pp. 411-415.

SI80b Simpson, J. A., et al., 1980 Nov. 1: "The Trapped Radiations of Saturn and Their Absorption by Satellites and Rings", J. Geophys. Res., Vol. 85, No. A11, pp. 5731-5762.

TR80 Trainor, J. H., et al., 1980 Jan. 25: "Observations of Energetic Ions and Electrons in Saturn's Magnetosphere", Science, Vol. 207, No. 4429, pp. 421-425.

VA80a Van Allen, J. A., et al., 1980 Jan. 25: "Saturn's Magnetosphere, Rings, and Inner Satellites", Science, Vol. 207, No. 4429, pp. 415-421.

VA80b Van Allen, J. A., et al., 1980 Nov. 1: "Sources and Sinks of Energetic Electrons and Protons in Saturn's Magnetosphere", J. Geophys. Res., Vol. 85, No. A11, pp.

5679-5694.

VA80c Van Allen, J. A., et al., 1980 Nov. 1: "The Energetic Charged Particle Absorption Signature of Mimas", J. Geophys. Res., Vol. 85, No. A11, pp. 5709-5718.

VA83 Van Allen, J. A., 1983 Sept. 1: "Absorption of Energetic Protons by Saturn's Ring G", J. Geophys. Res., Vol. 88, No. A9, pp. 6911-6918.

VA84 Van Allen, J. A., 1984: "Energetic Particles in the Inner Magnetosphere of Saturn", in *Saturn* (T. Gehrels and M. S. Matthews, Editors, Univ. of Arizona Press, Tucson), pp. 281-317.

VO82 Vogt, R. E., et al. 1982 Jan. 29: "Energetic Charged Particles in Saturn's Magnetosphere: Voyager 2 Results", Science, Vol. 215, No. 4532, pp. 577-582.

WO81 Wolff, D. M., et al., 1981 June 23: "Voyager 2 Saturn Encounter Trajectory Information", JPL IOM Voyager-NAV-81-118.

cc:

J. B. Barengoltz	89-1
L. E. Baughman	301-466
R. J. Cesarone	264-211
M. D. Cherng	301-460
R. E. Diehl	301-140H
L. I. Dorsky	185-105
R. F. Draper	171-247
R. E. Evans	179-225a
W. G. Fawcett	171-247
S. B. Gabriel	301-460
H. B. Garrett	301-456
T. E. Gindorf	301-456
L. J. Horn	183-501
C. E. Kohlhase	171-247
W.-P. Lee	168-427
E. J. Marian	301-456
P. A. Robinson	301-460
D. S. Stetson	301-165

APPENDIX VII. Review RFA Comments

COMMENT #1

Reviewer: Chris Paranicas
Organization: Applied Physics Laboratory
Topic: Energetic charged particle fluxes

Concern:

Updating the Saturn radiation model.
Some Voyager channel fluxes have been corrected since the encounters. For example, PL04 is a total ion channel on Voyager but likely has been contaminated with electrons close to the planet. This means the previously reported PL04 rates are too high.

Recommendation:

Use the Cassini Low Energy Magnetospheric Measurement (LEMMS) measurements to improve the ion fluxes close to Saturn.

As an additional action, it is worthwhile to compare the model predictions to the pure proton channel (channel 1) on the Voyagers near Saturn.

COMMENT #2:

Reviewer: W. Kent Tobiska
Organization: Space Environment Technologies
Topic: Standardization of Divine Model

Concern:

While many concerns and improvements to the Divine Model have been identified, it is likely that, due to programmatic constraints, this model will become widely used for engineering applications. This implies "standardization" of the model. Concerns are:

1) How to ensure a reliable reference model for computational usage (published references, accessible code)?
2) How are uncertainties (formal) and "weather" to be characterized?
3) What is the model update strategy?

Recommendation:

1) Use JPL code as a reference code once validated. Publish beyond JPL IOM in peer-reviewed literature.
2) Clearly explain formal uncertainties in the model and how to account for space weather phenomena such as magnetospheric time variability and local time effects.
3) Describe an update strategy—proposed or actual.

COMMENT #3:

Reviewer: Tom Armstrong
Organization: Fundamental Technology, Inc.
Topic: Reconciliation with Cassini SOI

Concern:

SATRAD should be compared with Cassini SOI observations of MIMI, CAPS, and Magnetometer.

Recommendation:

1) Obtain data (calibrated) and prepare graphs.
2) Evaluate the results

COMMENT #4:

Reviewer: Tom Armstrong
Organization: Fundamental Technology, Inc.
Topic: Inclusion of PDS Archive Data

Concern:

Much more complete observations than used by Divine originally are available and should be used. Emphasize the 2-4 R_s region.

Recommendation:

1) URL of V1 and V2 Saturn PDS data available from Tom Armstrong.

COMMENT #5:

Reviewer: Tom Armstrong
Organization: Fundamental Technology, Inc.
Topic: Magnetic Field Models

Concern:

1) Account for magnetopause currents.

Recommendation:

1) Consider using Engle and Beard spherical harmonic expansions.

COMMENT #6:

Reviewer: Jack Connerney (Apr 22, 2004)
Organization: NASA Goddard Space Flight Center
Topic: Saturn Magnetic Field Models

Concern:

1) Does Saturn Z3 model in "Magnetic Fields of the Outer Planets" include external terms?

Z3 is the best one can do for internal field. You're right, I didn't mention the external field coefficients, in the Z3 paper, they're not very useful in characterizing the external field for magnetospheric field line geometry. For that I'd direct you to a ring current model.

2) The magnetic field goes to 0 around 6-10 R_s and the field line tracing routine wanders off to infinity if it passes this region.

The external field is something like 8-10 nT, as I recall, on average and on axis. You will get in trouble when the equatorial Z3 field in the theta direction approaches this value. But you ought to get well beyond 6 R_s before this happens (21,535/r**3), so if you have trouble inside of, say, 10 R_s, something is wrong; look to external field coefficient normalization, or something that would alter the relative magnitude of internal/external terms.

3) Has any further work has been done with the Saturn field since Z3 and SPV; in particular are there any field models that use "ring currents" instead of the external harmonic terms?

We did a ring current model early on, just like the Jovian magnetodisc model, and it works well to describe the field in the region where axisymmetry is OK - i.e., well within a magnetopause stand-off distance. You have code at JPL to do the calculation, just substitute the Saturn coefficients in the magnetodisc code.

For further information, see the following references:

"Zonal harmonic model of Saturn's magnetic field from Voyager 1 and 2 observations," J. E. P. Connerney, N. F. Ness, and M. H. Acuna, *Nature*, 298, 44 - 46, 1982.

"Currents in Saturn's magnetosphere," J. E. P. Connerney, M. H. Acuna, and N. F. Ness,

J. Geophys. Res., 88, 8779 - 8789, 1983.

If you want to code it up, see the Jupiter paper
"Modeling the Jovian current sheet and inner magnetosphere," J. E. P. Connerney, M. H. Acuna, and N. F. Ness, *J. Geophys. Res.*, 86, 8370 - 8384, 1981.

COMMENT #7:

Reviewer: John F. Cooper (15 March 2005)
Organization: NASA Goddard Space Flight Center
Topic: Data concerns with the Divine Model

Concern:

My previous comments are now 15 years old and I have not spent much time revisiting these data since then, with a few exceptions as noted below.

(1) I have long given up on the idea that LECP might be responding to a mono-energetic electron spectrum as suggested originally from the satellite filter model of Van Allen. My work on drift shell modeling for energetic electrons, to be reported at the Spring American Geophysical Union meeting, shows that such spectral features would be rapidly dispersed. The morphology of local time asymmetry is apparent in various Pioneer and Voyager electron data sets, and presence of these signatures in "nominal" proton or ion channels may suggest that these channels are responding to electron background within the inner magnetosphere. In general one should pay close attention to potentially anomalous morphology in counting rate data before such data are converted to fluxes . . ..

(2) I remain concerned about potentially or actually anomalous responses of the Pioneer and Voyager particle instruments to the high-energy proton environment of the inner magnetosphere. This was very clear in the University of Chicago instrument L1NL2 > 0.5 MeV proton channel on Pioneer 11 and could be a concern elsewhere as possibly in the LECP high-energy electron channel > 10 MeV. Since MeV electrons are a critical issue for radiation hazards to spacecraft systems, you should certainly address this issue.

(3) The LECP group gained much experience in correction of ion channels for electron background from Voyager measurements at Uranus and Neptune, and they have since said in publications that the earlier findings of heavy ions in the inner magnetosphere were erroneous due to this background. I note, however, that Uranus and Neptune did not have significant high energy proton components, so corrections inwards of Enceladus, where Voyager Cosmic Ray Subsystem last detected these protons, may still be uncertain.

(4) It is crucial for the high-energy proton data to correctly map in B and L, since there is a northward dipole offset and this shows up very well in apparent radial offsets of inbound and outbound data if the mapping is not computed correctly. Assume that the high-energy proton

drift shells are longitudinally symmetric but that lower-energy electron and ion drift shells may not be. There can be both temporal and local time variations for the latter.

I assume that you are setting the stage in this review for a model upgrade with all the new data from Cassini, although this mission did not have ALL the instruments really needed to fully characterize the high-energy particle environment of the inner magnetosphere. In particular, new data from a high-energy electron spectrometer would have been of great value to you now. So some uncertainties will remain.

COMMENT #8:

Reviewer: John F. Cooper (29 March 2005)
Organization: NASA Goddard Space Flight Center
Topic: Data concerns with the Divine Model

Concern:

My main comment re Chicago Pioneer 11 data would be that the "0.5-10 MeV proton" (L1NL2) and "7-17 MeV electron" (D5ND67) channels from the Simpson instrument appear by my previous analyses to have mixed nominal and high-energy (>30 MeV) proton responses in the inner magnetosphere inwards of Mimas and outwards from the outer edge of the A ring, so these channels should not be given much weight in that region. I would also be suspicious of the > 10 MeV electron rate from Voyager LECP in that region for the same reason. In this region, I would attribute inbound-outbound differences from the more equatorial Pioneer 11 data to local time asymmetry associated with drift resonance effects rather than to temporal variations. If the local time asymmetry is driven by a dusk-to-dawn electric field, then one would expect higher energetic electron intensities in the dusk-centered hemisphere, as compared to strong longitudinal symmetry for the high-energy protons as mapped in the offset-dipole system.

Finally, the region under the rings is probably well represented by the time-averaged proton, electron, neutron, and gamma ray spectra in the Cooper et al. (1985) paper from the 1979 Pioneer 11 data.

If this is possible, I certainly would like to request access to the Pioneer-Voyager Saturn model in support of my joint work with Ed Sittler (GSFC) and Bob Johnson (Univeristy of Virginia) of the Cassini Plasma Spectrometer (CAPS) team on magnetospheric interactions with rings and moons as sources of plasma and neutral molecules for the magnetosphere. To the extent that this work also involves work with Cassini plasma and energetic particle data, I would be happy to contribute to a new Cassini-based model.

APPENDIX VIII. Acronyms and Abbreviations

APL	Applied Physics Laboratory [the Johns Hopkins University]
CTS	counts per second
ESA	European Space Agency
FT	Fundamental Technologies , Inc.
GIRE	Galileo Interim Radiation Electron
GSFC	NASA Goddard Space Flight Center
JHU	Johns Hopkins University
KU	University of Kansas
LECP	Low Energy Charged Particle Instrument
MIMI	Magnetospheric Imaging Instrument
MeV	million electron volts [unit of energy]
NAIF	(NASA) Navigation and Ancillary Information Facility
PDS	Planetary Data System
RFA	Request for Action [form]
R_j	Jupiter radius [71,400 km]
R_s	Saturn radius [60,400 km]
SATRAD	Saturn Radiation Model
SET	Space Environment Technologies
SOI	Saturn Orbit Insertion
UT	Universal Time

REPORT DOCUMENTATION PAGE

Form Approved
OMB No. 0704-0188

1. REPORT DATE *(DD-MM-YYYY)*	2. REPORT TYPE	3. DATES COVERED *(From - To)*
15-10-2005	JPL Publication	

4. TITLE AND SUBTITLE
Saturn Radiation (SATRAD) Model

5a. CONTRACT NUMBER
NAS7-03001

5b. GRANT NUMBER

5c. PROGRAM ELEMENT NUMBER

6. AUTHOR(S)
H. R. Garrett
J. M. Ratliff
R. W. Evans

5d. PROJECT NUMBER

5e. TASK NUMBER

5f. WORK UNIT NUMBER

7. PERFORMING ORGANIZATION NAME(S) AND ADDRESS(ES)
Jet Propulsion Laboratory
California Institute of Technology
4800 Oak Grove Drive
Pasadena, CA 91009

8. PERFORMING ORGANIZATION REPORT NUMBER
JPL Publication 05-9

9. SPONSORING/MONITORING AGENCY NAME(S) AND ADDRESS(ES)
National Aeronautics and Space Administration
Washington, DC 20546-0001

10. SPONSORING/MONITOR'S ACRONYM(S)

11. SPONSORING/MONITORING REPORT NUMBER

12. DISTRIBUTION/AVAILABILITY STATEMENT
Unclassified—Unlimited

Subject Category 93

Availability: NASA CASI (301) 621-0390 Distribution: Nonstandard

13. SUPPLEMENTARY NOTES

14. ABSTRACT

The Saturnian radiation belts have not received as much attention as the Jovian radiation belts because they are not nearly as intense—the famous Saturnian particle rings tend to deplete the belts near where their peak would occur. As a result, there has not been a systematic development of engineering models of the Saturnian radiation environment for mission design. A primary exception is that of Divine (1990). That study used published data from several charged particle experiments aboard the Pioneer 11, Voyager 1, and Voyager 2 spacecraft during their flybys at Saturn to generate numerical models for the electron and proton radiation belts between 2.3 and 13 Saturn radii. The Divine Saturn radiation model described the electron distributions at energies between 0.04 and 10 MeV and the proton distributions at energies between 0.14 and 80 MeV. The model was intended to predict particle intensity, flux, and fluence for the Cassini orbiter. Divine carried out hand calculations using the model but never formally developed a computer program that could be used for general mission analyses. This report seeks to fill that void by formally developing a FORTRAN version of the model that can be used as a computer design tool for missions to Saturn that require estimates of the radiation environment around the planet. The results of that effort and the program listings are presented here along with comparisons with the original estimates carried out by Divine. In addition, Pioneer and Voyager data were scanned in from the original references and compared with the FORTRAN model's predictions. The results were statistically analyzed in a manner consistent with Divine's approach to provide estimates of the ability of the model to reproduce the original data. Results of a formal review of the model by a panel of experts are also presented. Their recommendations for further tests, analyses, and extensions to the model are discussed

15. SUBJECT TERMS Saturn, radiation models, radiation belts, Cassini spacecraft, high energy electrons, trapped particles, space radiation					
16. SECURITY CLASSIFICATION OF:			17. LIMITATION OF ABSTRACT	18. NUMBER OF PAGES	19a. NAME OF RESPONSIBLE PERSON STI Help Desk at help@sti.nasa.gov
a. REPORT U	b. ABSTRACT U	c. THIS PAGE U	UU	92	19b. TELEPHONE NUMBER (Include area code) (301) 621-0390

JPL 2659 R 10/03 W

Standard Form 298 (Rev. 8-98)
Prescribed by ANSI Std. Z39-18

NASA Supplementary Instructions To Complete SF 298 (Rev. 8-98 version)

NASA uses this inter-governmental form that does not allow customization. Look for special notes (NOTE) if NASA's procedures differ slightly from other agencies.

Block 1 NOTE: NASA uses month and year (February 2003) on the covers and title pages of its documents. However, this OMB form is coded for block 1 to accept data in the following format: day, month, and year (ex.: day (23), month (02), year (2003) or 23-02-2003, which means February 23, 2003. For this block, use the actual date of publication (on the cover and title page) and add 01 for the day. Example is March 2003 on the cover and title page, and 01-03-03 for block 1.

Block 2: Technical Paper, Technical Memorandum, etc.

Block 3: Optional for NASA

Block 4: Insert title and subtitle (if applicable)

Block 5a: Complete if have the information

b: Complete if have the information

c: Optional for NASA

d: Optional for NASA; if have a cooperative agreement number, insert it here

e: Optional for NASA

f: Required. Use funding number (WU, RTOP, or UPN)

Block 6: Complete (ex.: Smith, John J. and Brown, William R.)

Block 7: NASA Center (ex.: NASA Langley Research Center)
City, State, Zip code (ex.: Hampton, Virginia 23681-2199)
You can also enter contractor's or grantee's organization name here, below your NASA center, if they are the performing organization for your center

Block 8: Center tracking number (ex.: L-17689)

Block 9: National Aeronautics and Space Administration
Washington, DC 20546-0001

Block 10: NASA

Block 11: ex.: NASA/TM-2003-123456

Block 12: ex.:
Unclassified – Unlimited
Subject Category http://www.sti.nasa.gov/subjcat.pdf
Availability: NASA CASI (301) 621-0390
Distribution: (Standard or Nonstandard)
If restricted/limited, also put restriction/limitation on cover and title page

Block 13: (ex.: Smith and Brown, Langley Research Center. An electronic version can be found at http:// _____ , etc.)

Block 14: Self-explanatory

Block 15: Use terms from the NASA Thesaurus http://www.sti.nasa.gov/thesfrm1.htm,
Subject Division and Categories Fact Sheet http://www.sti.nasa.gov/subjcat.pdf,
or Machine-Aided Indexing tool http://www.sti.nasa.gov/nasaonly/webmai/

Block 16a,b,c:	Complete all three
Block 17:	UU (unclassified/unlimited) or SAR (same as report)
Block 18:	Self-explanatory
Block 19a:	STI Help Desk at email: help@sti.nasa.gov
Block 19b:	STI Help Desk at: (301) 621-0390